

**NEW INSIGHTS INTO THE STRATUM CORNEUM LIPID
MEMBRANE ORGANISATION
AN X-RAY AND NEUTRON SCATTERING STUDY**

Dissertation

zur Erlangung des akademischen Grades

Doctor rerum naturalium (Dr. rer. nat.)

vorgelegt der

Mathematisch-Naturwissenschaftlich-Technischen Fakultät
(mathematisch-naturwissenschaftlicher Bereich)
der Martin-Luther-Universität Halle-Wittenberg

von Frau Mgr. Jarmila Zbytovská

geboren am 17. 9. 1976 in Prag (Tschechische Republik)

Gutachter:

1. Prof. Dr. Dr. Reinhard Neubert
2. Prof. Dr. Siegfried Wartewig
3. Doc. RNDr. Pavel Doležal CSc.

Halle (Saale), den 20. 10. 2006

urn:nbn:de:gbv:3-000012474

[<http://nbn-resolving.de/urn/resolver.pl?urn=nbn%3Ade%3Agbv%3A3-000012474>]

CONTENTS

LIST OF ABBREVIATIONS	IV
LIST OF SYMBOLS	V
1 INTRODUCTION	1
2 CURRENT KNOWLEDGE STATUS OF THE STRATUM CORNEUM STRUCTURE AND TRANSDERMAL PERMEATION ENHANCEMENT	4
2.1 The organization of the mammalian skin	4
2.2 The stratum corneum	5
2.2.1 The origin of the SC lipids	5
2.2.2 The lipid composition within the SC	6
2.2.3 The organization of the SC lipid matrix	8
2.3 Drug penetration routes through the skin	10
2.4 Modes of actions of permeation enhancers	10
3 BASIC PRINCIPLES OF EXPERIMENTAL TECHNIQUES EMPLOYED	12
3.1 Differential scanning calorimetry	12
3.2 Infrared and Raman spectroscopy	13
3.2.1 Conformationally sensitive bands of hydrocarbon chains	13
3.3 Scattering techniques	15
3.3.1 X-ray diffraction on lipids	16
3.3.2 Small angle neutron scattering	18
3.3.3 Small angle neutron scattering on ULVs	20
3.3.4 Neutron diffraction on oriented multilamellar samples	22
3.3.5 Particle size analysis via dynamic light scattering	24
4 INFLUENCE OF PHYTOSPHINGOSINE-TYPE CERAMIDES ON THE STRUCTURE OF DMPC MEMBRANE	26
4.1 Introduction	27
4.2 Material and Methods	28
4.2.1 Materials	28
4.2.2 Sample preparation	28
4.2.3 Differential scanning calorimetry	29
4.2.4 Small angle X-ray diffraction	29
4.2.5 High performance thin layer chromatography	29
4.2.6 Small angle neutron scattering	30
4.2.7 Dynamic light scattering	30

4.3	Results	31
4.3.1	Characterization of MLVs by DSC	31
4.3.2	Characterization of MLVs by small angle X-ray diffraction	33
4.3.3	Characterization of ULVs	37
4.4	Discussion	41
4.5	Conclusions	45
5	INFLUENCE OF CHOLESTEROL ON THE STRUCTURE OF STRATUM CORNEUM LIPID MODEL MEMBRANE	46
5.1	Introduction	47
5.2	Material and Methods	48
5.2.1	Material	48
5.2.2	Vesicle preparation	49
5.2.3	Vesicle characterization	49
5.2.4	Small angle X-ray diffraction	50
5.2.5	Small angle neutron scattering	51
5.2.6	Molecular modelling	51
5.3	Results	52
5.3.1	Small angle X-ray diffraction on MLVs	52
5.3.2	Characterization of ULVs	58
5.3.3	Small angle neutron scattering from ULVs	59
5.4	Discussion	61
5.5	Conclusions	65
6	THERMOTROPIC PHASE BEHAVIOUR OF A SC LIPID MODEL SYSTEM IN THE VARIATION OF CHOLESTEROL CONCENTRATION	66
6.1	Introduction	66
6.2	Methods	66
6.2.1	Material and sample preparation	66
6.2.2	Differential scanning calorimetry	66
6.2.3	Small angle X-ray diffraction	67
6.3	Results	68
6.3.1	Differential scanning calorimetry	68
6.3.2	Small angle X-ray diffraction	70
6.4	Discussion	72
6.5	Conclusion	74
7	NEUTRON DIFFRACTION ON THE SC LIPID MODEL SYSTEM	75

7.1	Introduction	75
7.2	Methods	75
7.2.1	Material	75
7.2.2	Sample preparation	75
7.2.3	Neutron diffraction measurements	76
7.3	Results	77
7.3.1	Neutron diffraction measurements from the mixtures with various CHOL concentrations	77
7.3.2	Neutron scattering length density profiles of the SC lipid model membrane	79
7.4	Discussion	84
7.5	Conclusions	85
8	INFLUENCE OF PERMEATION MODULATORS ON THE BEHAVIOUR OF A SC LIPID MODEL MIXTURE	87
8.1	Introduction	87
8.2	Methods	88
8.2.1	Material	88
8.2.2	Sample preparation	89
8.2.3	SAXD measurements	89
8.3	Results and discussion	89
8.3.1	Influence of urea on the SC lipid system	89
8.3.2	Influence of oleic acid on the SC lipid system	91
8.3.3	Influence of 12G12 on the SC lipid system	93
8.4	Conclusions	95
9	SUMMARY AND PERSPECTIVES	97
10	ZUSAMMENFASSUNG UND AUSBLICK	99
	REFERENCES	103
	Appendix A	
	Appendix B	
	Appendix C	

List of Abbreviations

AMD	automated multiple development
CCD	charge-coupled device
Cer[AP]	ceramide[AP]
Cer[NP]	ceramide[NP]
CS	cholesterol sulphate
CHOL	cholesterol
DLS	dynamic light scattering
DMPC	dimyristoylphosphatidylcholine
DSC	differential scanning calorimetry
HPTLC	high performance thin layer chromatography
IR	infrared
KHGs	keratohyalin granules
L-phase	long phase
L_{α}	liquid crystalline phase
L_{β}	gel phase
L_{β}'	ripple phase
LBs	lamellar bodies
LPP	long periodicity phase
MLVs	multilamellar vesicles
NIBS	non-invasive back-scatter
NIR	near infrared
NMR	nuclear magnetic resonance
OA	oleic acid
PA	palmitic acid
RXLI	recessive X-linked ichthyosis
S-phase	short phase
SANS	small angle neutron scattering
SAXD	small angle X-ray diffraction
SC	stratum corneum
SPP	short periodicity phase
ULVs	unilamellar vesicles
UV	ultraviolet
VIS	visible
WAXD	wide angle X-ray diffraction

List of Symbols

A	membrane area per molecule	[Å ²]
c	light velocity	[in vacuum 2.998*10 ⁸ ms ⁻¹]
D	lamellar repeat distance	[Å]
	diffusion coefficient	[m ² .s ⁻¹]
d	membrane thickness parameter derived from MSFF	[Å]
d _g	membrane thickness parameter derived from KP-plot	[Å]
d _{hkl}	distance between two parallel planes characterized by Miller indices <i>hkl</i>	[Å]
d _m	membrane thickness	[Å]
E	energy	[J]
F _h	structure factor	[a.u.]
ΔH	enthalpy	[J.mol]
h	diffraction order; reflexion	
	Planck's constant	[6.626 176*10 ⁻³⁴ J ·s]
I	intensity	[a.u.]
λ	wavelength	[Å] or [nm]
m	weight	[g]
M _w	molecular weight	[g.mol ⁻¹]
N _A	Avogadro's number	[6.022*10 ²³]
n	refractive index	
η	viscosity	[Pa.s]
ν	wave number	[cm ⁻¹]
q	scattering vector	[Å ⁻¹]
R	vesicle radius	[Å]
R _g	radius of gyration	[Å]
R _h	hydrodynamic vesicle radius	[Å]
ρ	electron/neutron length density	[cm]
Δρ _m	average excess scattering-length density per unit mass	[cm.g ⁻¹]
T	temperature	[°C]
t	time	[s]
θ	scattering angle	[°]
V	volume	[cm ³] or [l]
V _{SA}	solvent accessible volume	[Å ³]

The rest of symbols are explained in relevant Chapters.

1 Introduction

The primary function of the mammalian skin is the protection against chemical, pathogen and UV radiation. It must provide a mechanically strong structure that resists physical stress. The skin plays also a major role in thermoregulation and water balance of the body. The functions of skin as sensory, endocrine and immune organ should be mentioned as well [1,2,3,4]. The skin protection function is ensured by its unique barrier properties. First in the 1940s, it was postulated that the outermost layer of the human skin, the stratum corneum (SC) is responsible for the skin barrier function [5].

The SC consists of dead cells, the corneocytes, which are filled with protein keratin. The corneocytes are embedded in a lipid matrix with a unique composition. The SC lacks phospholipids but it is enriched in ceramides, free fatty acids, cholesterol and its derivatives. The SC lipids are organized in lipid membranes arranged into a lamellar structure. Due to the special physicochemical properties of ceramides, these membranes are extremely rigid and, therefore, very poorly permeable [6].

The necessary impermeability of the human skin represents, however, a very strong limitation for the systemic transdermal drug delivery. This administration route offers many advantages, namely the avoidance of the first pass metabolism in the liver, reduced side effects, or the opportunity to deliver the drug continuously. In order to increase absorption of a drug through the skin, a reversible decrease in its barrier function is needed.

Several physical (sonophoresis, iontophoresis, electro-osmosis, electroporation and temperature) and chemical or formulation methods have been described, which have successfully increased the drug delivery across or into the skin. Recently, the application of permeation enhancers has been most commonly used to overcome the SC lipid barrier [7].

The most of the non-irritating permeation enhancers are of amphiphilic character. They can incorporate into the SC lipid membranes in order to change the membrane structure. Thus, the membrane becomes more fluid and permeable for a drug. This effect was described for a number of substances, but only little has been known about the molecular background of the permeation enhancers' mode of action so far. In contrast, only few

enhancers such as urea were described to interact with the polar head groups of the SC lipids [8].

Some topically administrated substances (e.g. repellents, sunscreens) should reach only the superior skin layers, so that the systemic absorption connected with undesired side effects is minimized. Here, the so-called transdermal permeation retardants (reducers) can be applied [9].

Furthermore, damaged skin barrier due to a disease or trauma tends to abnormal function and increased permeability of the skin. A number of skin diseases with elevated or decreased levels of a lipid fracture in the SC lipid matrix, like for example the recessive X-linked ichthyosis, psoriasis or atopic dermatitis, have been reported [10,11,12,13,14]. Till now, however, there is only little information about the changes in the internal membrane structure of the SC lipid lamellae caused by such an abnormal lipid composition. Efforts to elucidate the physicochemical changes in the SC lipid membranes due to pathologic events can finally be helpful in finding suitable therapeutic approaches.

Currently, there are several techniques employed in the characterization of the SC lipid membranes, namely X-ray diffraction, IR- and Raman spectroscopy, dynamic light scattering, nuclear magnetic resonance, calorimetric, electron microscopic methods etc. However, each of these methods is restricted in some way.

All of the facts mentioned above encourage to look for new attitudes towards investigating the physicochemical behaviour of the SC lipid matrix on the molecular level and to describe the internal membrane arrangement.

This thesis aims to contribute to the understanding of the SC lipid organization in the given context. The purpose is to find new ways allowing to characterize the internal structure of the stratum corneum membranes in order to monitor the changes in the membranes evoked by the permeation enhancers.

Following objectives should be elaborated in the framework of this thesis:

- Development of two types of membrane models from commercially available substances: a binary system, which should help to elucidate the behaviour of ceramide molecules in a membrane and a quaternary system which should mimic the SC lipid composition.
- Characterization of the binary system by diffraction, spectroscopic and calorimetric methods. Application of small-angle neutron scattering on unilamellar vesicles in order to follow influence of ceramides on the membrane structure (Chapter 4).
- Characterization of the quaternary SC lipid model system by X-ray diffraction. Introduction of small angle-neutron scattering on unilamellar vesicles into the SC lipid research. Description of the thermotropic phase behaviour of the mentioned

system. Monitoring of cholesterol influence on the membrane structure (Chapters 5, 6).

- Introduction of neutron diffraction on organized multilayers into the research of SC lipid membranes in order to characterize the internal membrane structure and an influence of cholesterol on the membrane (Chapter 7).
- Monitoring of effects of selected permeation enhancers on the SC lipid membrane (Chapter 8).

2 Current knowledge status of the stratum corneum structure and transdermal permeation enhancement

2.1 *The organization of the mammalian skin*

The skin consists of three distinct layers [2, 8]. The **subcutis** and the **dermis**, forming the bulk of skin, are made up of adipose and connective tissue elements, respectively. The overlying, avascular **epidermis** is composed primarily of keratinocytes and is divisible into four layers, namely the stratum basale, spinosum, granulosum, and corneum [2]. These layers present different stages of the cell differentiation, termed *keratinisation*. The continuously dividing stem cells on the basal layer generate columns of keratinocytes, which finally differentiate into the flattened corneocytes (Fig. 2.1).

The innermost epidermal layer, the *stratum basale*, is a single layer of columnar basal cells that remain attached to the basement membrane via hemidesmosomes.

The next epidermal layer, the *stratum spinosum*, has a spiny appearance of its cells in histological sections due to the abundance of desmosomes. First in this layer, lamellar bodies (also called membrane coating granules, keratinosomes or Odland bodies) and increased amount of keratin filaments can be detected.

In the *stratum granulosum*, a quantitative increase in keratin synthesis occurs. The keratohyalin granules containing proteins (profillaggrin, loricrin and keratin) become progressively larger and give the name to this layer. Simultaneously, the uppermost cells in the stratum granulosum display a unique structural and functional organization of the lamellar bodies consistent with their readiness to terminally differentiate into a corneocyte, during which the lamellar bodies are secreted to the intercellular domains.

The uppermost layer of the epidermis, the SC, creates the main skin barrier.

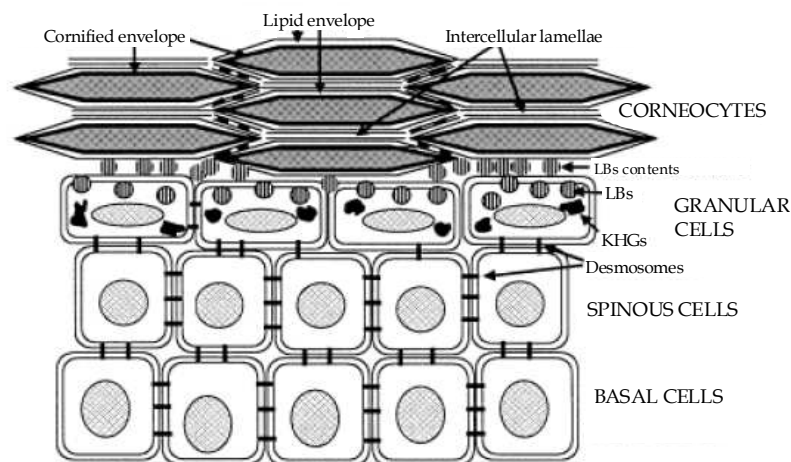


Fig. 2.1 Schematic diagram of the particular epidermal layers (according to [17]). LBs: lamellar bodies, KHGs: keratohyalin granules.

2.2 The stratum corneum

The organization of the SC can be simply described by the two-compartment ‘brick and mortar’ model. The terminally differentiated keratinocytes, the corneocytes (bricks), create a discontinuous part embedded in a continuous lipid matrix (mortar) [15]. This arrangement creates a tortuous path, through which substances have to traverse in order to cross the SC. The SC consists of approx. 18-21 cell layers. The corneocytes are flat and comprise crosslinked keratin fibres.

Two layers can be distinguished inside the SC. The *stratum compactum* is stabilized by corneodesmosomes between the cells, which confer structural stability to the SC. In the *stratum disjunctum*, the degradation of corneodesmosomes allows the process of corneocyte desquamation [2].

The corneocytes in the SC are surrounded by a cornified cell envelope formed by proteins (loricrin and involucrin). The cornified envelope is covalently bound to ω -hydroxy acid-containing ceramides of a lipid envelope [16]. Both envelopes allow the cohesiveness of corneocytes with the lipid matrix.

2.2.1 The origin of the SC lipids

As mentioned above, the SC barrier lipids originate from lamellar bodies (LBs). LBs contain stacks of lipid lamellae composed of phospholipids, cholesterol and glucosylceramides that are precursors of the SC intercellular lipids. Additionally, there are enzymes as phospholipase A2 and β -glucocerebrosidase [17]. During the epidermal

differentiation on the stratum granulosum/SC interface, the LBs are assumed to fuse with the plasma membrane of the granular cell and discharge their lipids into the intercellular space where the lipid membrane sheets fuse end-to-end together [18]. This change in structure correlates with a sequence of changes in lipid composition, i.e. from the polar lipid-enriched mixture to the non-polar one, consisting of ceramides, free sterols and free fatty acids that are present in the SC.

An alternative to this traditional conception of the SC lipid matrix origin is the ‘membrane folding model’ recently suggested by Norlén [19]. His objection to the above mentioned Landman model [18] is that the fusogenic processes require a lot of energy and do not promote the flat bilayer organization. The basic idea of the ‘membrane folding model’ is that the skin barrier formation takes place via a continuous, highly dynamic process of ‘intersection free unfolding’ of a single and coherent three dimensional structure. The transgolgi network, lamellar bodies and the SC intercellular lipids are connected in the same continuous (cubic-like) membrane structure, which transforms into a flat dimensional lamellar membrane structure at the stratum granulosum/SC interface [19].

2.2.2 The lipid composition within the SC

The major lipid classes that can be extracted from SC are ceramides, cholesterol, and fatty acids, which make up approximately 50, 25, and 10 percent of the SC lipid mass, respectively. Small amounts of cholesterol sulphate and cholesterol esters are also present [6,20]. Interestingly, phospholipids, which are the major components of biological membranes, have been found only in traces in the SC.

Cholesterol is a ubiquitous membrane component, which may either increase or decrease membrane fluidity, depending upon the proportion of cholesterol and the nature of the other membrane components. In the SC, cholesterol should provide a degree of fluidity to what otherwise be a rigid, possibly brittle membrane system [20].

Although the cholesterol sulphate amount in the SC is small, it plays an important role in the cell cohesion and herewith in the process of SC desquamation. Cholesterol esters (mainly oleate) are not bilayer forming and may serve to isolate the residual unsaturated fatty acids in order to prevent their fluidising effect on intercellular membrane domains [21].

The *free fatty acids* of the SC consist of predominantly straight chained saturated species and are derived from de novo synthesis in the epidermis [16]. They range from 16 to 30 carbons in length. The most abundant species are C22:0, C24:0, C26:0, and C28:0. The free fatty acids and cholesterol sulphate are the only ionisable lipids in the SC and may be important for bilayer formation [21].

Ceramides are structurally heterogeneous and complex group of sphingolipids containing mainly sphingosine, phytosphingosine, or 6-hydroxysphingosine amide-linked to a variety of nonhydroxy, α -hydroxy, or ω -hydroxy acids (Fig. 2.2) [16]. The fatty acid chain length of ceramides varies between 16 (ceramide 5 [AS]) and 30-40 carbons (ceramide 1 [EOS]). Furthermore, ceramide 1 [EOS], ceramide 4 [EOH], and ceramide 9 [EOP] contain mainly linoleic acid ester-linked to the ω -hydroxyacid. Currently, nine major ceramides have been detected in the SC lipid matrix [16,17,20,22].

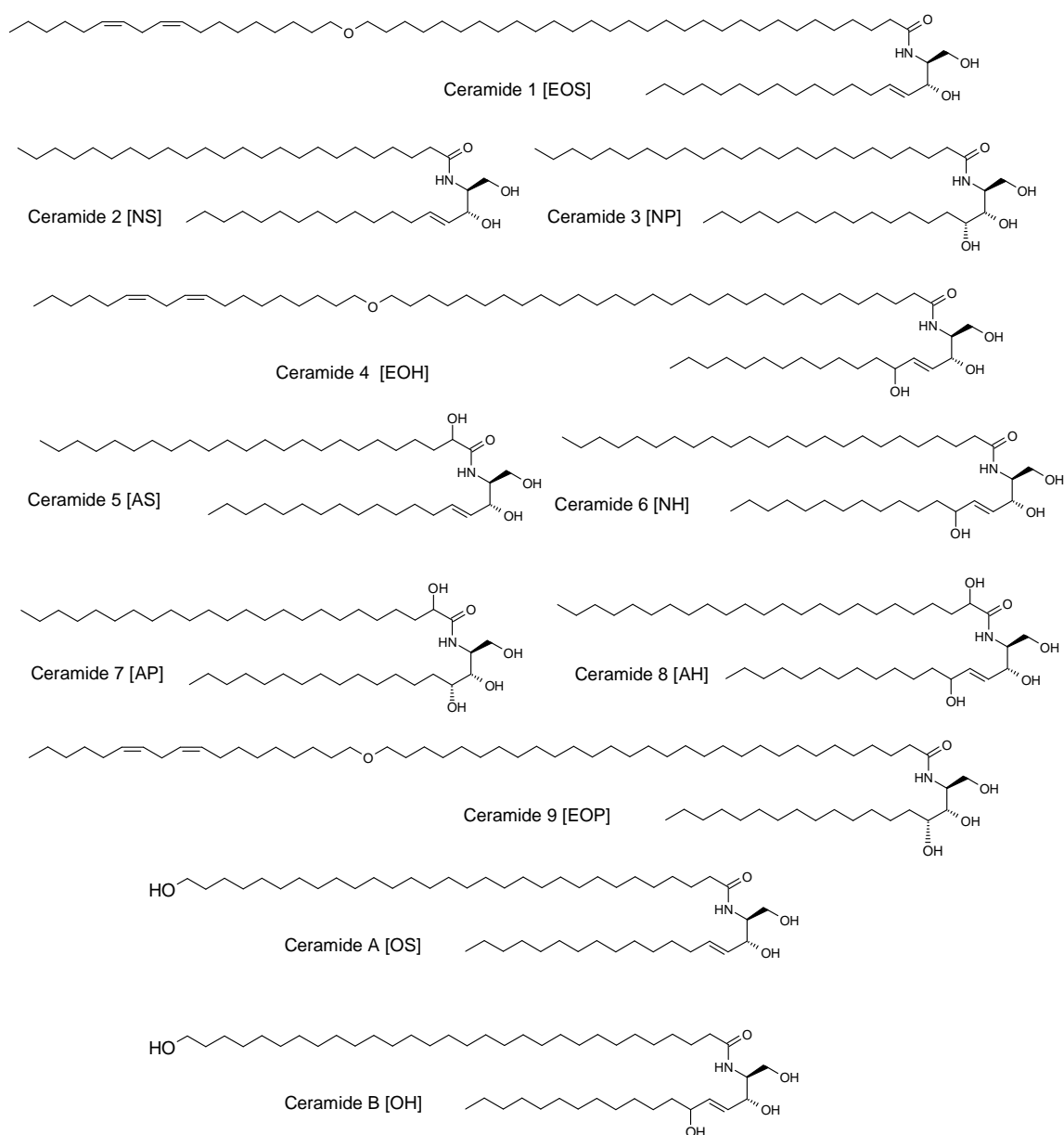


Fig. 2.2 Structures of ceramides in human SC (according to [17]). Numbers 1-8 represent the polarity of the molecule (the thin layer chromatographic mobility). Ceramide 9 [EOP] [22] has recently been found and its polarity is between ceramide 2 and 3. Ceramides A [OS] and B [OH] are the covalently bound ones in the lipid envelope. **S**: sphingosine; **P**: phytosphingosine; **H**: 6-hydroxysphingosine; **N**: nonhydroxy fatty acid; **A**: α -hydroxy fatty acid, **O**: ω -hydroxy fatty acid; **E**: esterified ω -hydroxy fatty acid.

The original nomenclature of ceramides was based on a series of numbers (1-6) according to their mobility on thin layer chromatography [23]. With the increasing number in the classification increased the polarity of the ceramide molecule. Currently, a nomenclature based on the molecular structure of ceramide [24] instead of the chromatographic fractions is preferred.

With the exception of ceramides [EOS], [EOH], and [EOP], which have a special function in the SC lipid organization, all the aliphatic chains in the ceramides as well as in the fatty acids are highly ordered and saturated. The polar head groups are relatively small, compared to e.g. phospholipids [21]. Evidently, this is a prerequisite for the excellent barrier properties of the SC.

2.2.3 The organization of the SC lipid matrix

In the 1970s, the freeze fracture electron microscopy studies have discovered that the lipids are organized in lamellae located in the intercellular spaces in the SC [25,26]; however, it was not evident in the routine transmission electron micrographs. In 1987, RuO₄ has been introduced as a post-fixation agent, instead of the more usual OsO₄, to visualize the saturated lipids in the SC. The electron microscopy studies revealed an unusual trilamellar repeat units arrangement with a broad-narrow-broad appearance and an interval dimension of 130 Å [27]. In 1988, the 130 Å periodicity has been detected in murine SC by X-ray diffraction. Furthermore, it was reported that the lipids are mainly in a crystalline phase [28]. Further X-ray diffraction studies confirmed two lamellar phases with a periodicity of about 60 Å (the short periodicity phase) and 130 Å (the long periodicity phase, LPP) in pig and human SC [29,30,31]. It has been concluded that the LPP of 130 Å is typical of the SC arrangement and crucial for the SC function. The LPP occurs in mixtures with isolated or (semi)synthetic skin lipids as well [32,33,34].

Recently, a study by Hill and Wertz [35] has revised the conception of the broad-narrow-broad arrangement of the LPP. The authors have proposed that all the three bands are of the same width. They have moreover confirmed preceding suggestions that the linoleate chains are present only in the central lamella. This results in a higher ruthenium reduction in the central LPP unit, which consequently seems to be narrower than the lateral ones.

When ceramide 1 [EOS] is absent, the phase behaviour of the SC lipids changes dramatically; namely, just a very small population of lipids forms the 130 Å lamellar phase. For this reason, it has been postulated that ceramide [EOS] plays an important role in the formation of the LPP [36]. Ceramide [EOS] is supposed to act as a molecular rivet which links the trilayer unit together and consequently dictates the broad-narrow-broad sequence in the LPP [37]. A similar role in the SC lipid matrix organization may also be played by ceramides 4 [EOH] and 9 [EOP] [38].

Simultaneously with the lamellar organization of the SC lipids, a lateral arrangement has been studied. It has been described that at physiological temperatures, the SC lipid chains are in highly ordered state [39,40,41]. The wide-angle X-ray diffraction studies confirmed a coexistence of orthorhombic and hexagonal crystalline arrangement in the SC [37,42]. Similar phase coexistence was observed also by NMR studies [43,44].

The exact determination of the LPP internal structure is crucial for our understanding of the skin barrier properties. Therefore, based on the above-summarized facts, several conceptions of the SC lipids organization, namely the domain mosaic model, the sandwich model, and the single gel phase model have been suggested.

The domain mosaic model

The domain mosaic model proposed by Forslind [45] depicts the bulk of the lipids as segregated into crystalline/gel domains effectively hindering water to be lost from the organism. The domains are bordered by the 'grain borders' with lipids in the fluid crystalline state. The fluid character of the bordering areas between the crystalline domains allows diffusion of hydrophilic and hydrophobic molecules through the barrier.

The sandwich model

While the domain mosaic model suggests the crystalline and liquid domains to be side by side in one layer, the sandwich model proposes that the domains are located in separated layers in the trilayer arrangement. A similar organization has also been suggested by other authors earlier [35,46,47]. According to this concept, the linoleate moieties of Cer[EOS], [EOH] and/or [EOP] are located in the narrow central layer of the long periodicity phase and link the three layers together. This central layer is in a liquid phase. Two regions in which the crystallinity increases gradually are located next to the central layer. The decreased mobility in the adjacent layers can be attributed to the presence of less mobile, long saturated hydrocarbon chains. The fluid phase of the central layer is assumed to be discontinuous and substances penetrating through the SC always have to pass the crystalline lipid lamellar region and partly diffuse through the less densely packed lipid regions [26,37,48].

The single gel phase model

The single gel phase model differs significantly from the previously mentioned models and proposes that the skin barrier is formed by a single coherent lamellar gel structure in the intercellular space of the SC. No phase separation, neither between liquid crystalline and gel phases nor between different crystalline phases with hexagonal and orthorhombic chain packing, respectively, is present in the barrier structure [49]. The proposed single lipid structure possesses low water content, a low degree of mobility, and low water permeability because of a close-packing of the constituent lipids. Contrary to the domain mosaic and the sandwich models, which propose that the ceramides are organized entirely in a hairpin

conformation (parallel oriented chains towards the membrane interior), the single gel phase model supposes both hairpin and splayed chain (chains point away from a central polar head group in the opposite directions) conformations of ceramides in the SC lipid matrix. This assumption is supported by other authors [50]. The pros and cons of the single gel phase model are discussed currently [51,52].

2.3 Drug penetration routes through the skin

The transdermal permeation of drugs occurs via diffusion through the *intact epidermis* and through the *skin appendages* (hair follicles and sweat glands) that form shunt pathways through the SC (transfollicular and transglandular penetration, respectively). The skin appendages, however, occupy only 0.1% of the total skin surface, and the contribution of this pathway is usually considered to be small [53].

During the diffusion through the intact epidermis, a drug must penetrate through all the epidermis layers described in Chapter 2.1 till it reaches the bloodstream in the dermis. Because of its barrier properties, the main limiting step during the transdermal absorption is crossing the SC.

Two penetration pathways across the intact SC may be identified: the *intercellular route* and the *transcellular route* through the corneocytes. In both cases, the permeant must diffuse through the intercellular lipid matrix [53,54]. Lipid bilayers exhibit strong structural heterogeneity that results in spatial variations in solute partition and diffusion coefficients [55,56]. As a result, molecules are believed to diffuse across skin following tortuous pathway within either the tail-group (for hydrophobic molecules) or head group (for hydrophilic molecules) regions, in which transport between bilayers can occur at bilayer-bilayer interfaces or other sites of structural disorganization [56]. According to this, a lipophilic and hydrophilic intercellular pathway is sometimes differentiated [8,9].

The ability of topically applied agents to interact with the intercellular lipids offers a convenient opportunity to enhance the percutaneous absorption.

2.4 Modes of actions of permeation enhancers

There are several possible modes of action of permeation enhancers. Some of the enhancers denature or modify the SC keratin conformation, which causes swelling and increases hydration. Enhancers can affect desmosomes, solubilize the permeant in the donor or modify the thermodynamic activity of the vehicle. However, most enhancers interact with the intercellular lipid domains of the SC [57,58].

In principle, permeation enhancers interacting with the intercellular lipids can be divided into two main groups, namely the small polar molecules and the amphiphilic lipid-like

molecules. Small polar molecules may break the hydrogen bonds that hold the ceramides molecules together [59]. They can extract the lipids from the SC intercellular spaces and herewith increase the SC permeability.

Amphiphilic enhancers are likely to be inserted into the lamellae, with their headgroups into the polar region and with their hydrophobic chains between the hydrophobic chains of the SC lipids. This may induce disturbance of the lipid packing, lateral fluidisation of the lamellae or phase separation within the SC lipid lamellae (Fig. 2.3). Consequently, the skin barrier resistance decreases [57].

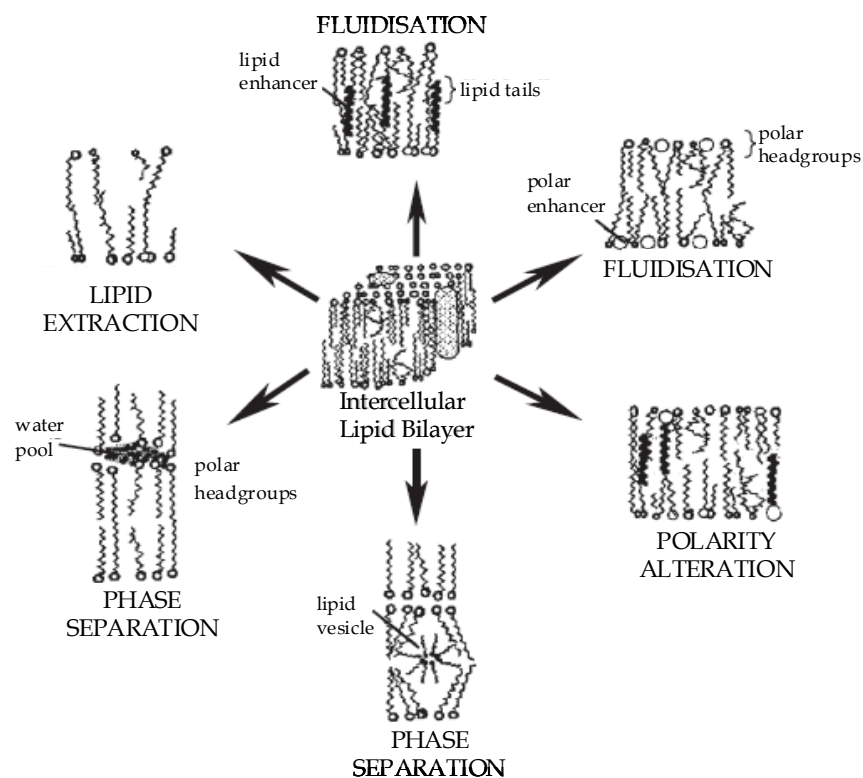


Fig. 2.3 Possible modes of actions of amphiphilic and/or small polar permeation enhancers (reproduced from [57]).

3 Basic principles of experimental techniques employed

3.1 *Differential scanning calorimetry*

Thermo-analytical measurements are used to describe temperature-induced changes of a substance, which are connected with changing energy content. In differential scanning calorimetry (DSC), a sample and a reference are exposed to the same heating regime [60]. A difference in the absorbed (endothermic reaction) or released (exothermic reaction) energy is measured as a function of temperature. A temperature characteristic for a phase transition is mostly determined as the extrapolated onset of a DSC peak. The integrated area under the peak corresponds with the transition enthalpy (ΔH), which can be given in kJ or kcal per mole or gram.

DSC is a widely used method for the characterization of the lipid phase behaviour. It provides the first information about phase changes in the lipid molecules. Typically, the largest peak in a DSC curve of a lipid represents the melting of hydrocarbon chains. However, also other phase transitions, such as transition from one crystalline packing to another or changes in the polar head group region, can be detected via DSC.

DSC is a very useful method in constructing the phase diagrams of lipid mixtures, which can give a number of information about the lipid miscibility. It has been used also in many studies on SC lipid mixtures [61] or on interactions of ceramides or other SC lipids with a permeation enhancer [62].

Of course, DSC gives only initial information about the temperature and enthalpy of a phase transition. In order to describe what exactly happens during the transition, other methods must be employed (see below). Numerous studies on the phase behaviour of SC lipids [39,63] or permeation enhancers [64] used DSC in combination with spectroscopic methods and/or X-ray diffraction.

3.2 Infrared and Raman spectroscopy

Both of these spectroscopic methods are based on the interactions of molecule vibrations with electromagnetic radiation.

In the infrared spectroscopy (IR-spectroscopy), a sample is exposed to the IR-radiation. The molecule vibrations of the substance absorb a part of the radiation that is detected then. Not every vibration can interact with the IR beams. A prerequisite is that the dipole moment of the bond changes during this interaction. Such vibrations are consequently distinct in an IR-spectrum.

On the contrary to the IR-spectroscopy, the Raman spectroscopy is based on the Raman effect which is inelastic scattering of electromagnetic radiation by a molecular system. A Raman spectrum is obtained by focusing monochromatic radiation on a sample and analysing the scattered frequency [65]. The used radiation is in the region of the UV, VIS or NIR light. The energy of this radiation causes an excitation of electrons in a virtual state. When the electrons return to their initial state, they emit a photon. In Raman scattering, the energies of the incident and scattered photons are different. The difference in energy between the incident photon and the Raman scattered photon is equal to the energy of a vibration of the scattering molecule. In order for a molecular vibration to be Raman-active, the vibration must be accompanied by a change in the polarizability of the molecule [66].

Generally, two types of molecule vibrations are to be distinguished. If the atoms participating in a vibration move in the direction of their bond, to or from each other, one can term this vibration as *stretching*. It is typical for *deformation* vibrations (δ) that the angle between two bonds changes.

3.2.1 Conformationally sensitive bands of hydrocarbon chains

Although IR- and Raman spectra of lipids are in the same region, the IR- and Raman-bands differ from each other [65]. Generally, the IR-spectroscopy can efficiently describe the polar head groups in the molecules as well as the non-covalent hydrogen bonding. On the other hand, the Raman spectroscopy is more suitable for the characterization of the non-polar parts of the molecule. In the case of lipids, the degree of the order and arrangement of the long hydrocarbon chains can be well described especially by the Raman spectroscopy (for a review see [67]).

It is well known that hydrocarbon chains in the crystalline state are in a highly ordered 'zig-zag' structure with a high number of *trans* conformers. With increasing temperature, the number of *gauche* conformers grows which is accompanied by a decrease in the chain ordering and an increase in the chain flexibility.

The region between 2800-3000 cm^{-1} in the IR- and Raman spectra contains the CH stretching vibrations and deformation vibrations overtones. The CH_2 symmetric stretching vibration ($\nu_s\text{CH}_2$) is detectable at about 2850 cm^{-1} . The position of this mode is typical of the *trans/gauche* ratio in the hydrocarbon chains according to the rule: the lower the position of the $\nu_s\text{CH}_2$ mode, the higher the content of the *trans* conformers in the chains [68,69]. For example, ceramides show a very high degree of order of the hydrocarbon chains with the position of the $\nu_s\text{CH}_2$ mode at about 2848 cm^{-1} . In the melt, the position of $\nu_s\text{CH}_2$ shifts to about 2853 cm^{-1} [40,70,71] which is the result of an increased number of *gauche* conformers in the chains leading to a higher chain flexibility. Another characteristic of the *trans* conformers content is the intensity ratio of the antisymmetric CH_2 stretching mode (at about 2920 cm^{-1} in the IR- and 2880 cm^{-1} in the Raman spectra) vs. a symmetric CH_2 stretching mode (at about 2850 cm^{-1}) or vs. a reference [39,64,71]. With a decrease in this ratio, the number of the *gauche* conformers in the chains increases.

The antisymmetric and symmetric CC stretching vibrations at about 1060 and 1130 cm^{-1} , respectively, as well as the CH_3 -rocking mode at 890 cm^{-1} and the so-called 'longitudinal accordion modes' (below 400 cm^{-1}) in the Raman spectrum are also very sensitive indicators of the *trans/gauche* ratio in the chains in a Raman spectrum [69,72].

Besides the chain order, the arrangement of the hydrocarbon chains in a crystalline subcell [73] can also be determined from the IR- and Raman spectra.

When there are two chains in a subcell (orthorhombic or monoclinic chain packing), the CH_2 scissoring deformation between 1450-1500 cm^{-1} in the Raman spectra shows a factor group splitting into three bands and the CH_2 rocking mode at about 720 cm^{-1} in the IR-spectra is split into two bands. The splitting of the CH_2 scissoring deformation into two bands and a single peak of the CH_2 rocking mode indicate only one chain in the subcell (triclinic or hexagonal chain packing) [74].

The phase behaviour of a number of SC lipids [39,40] and permeation enhancers [64,75] in a bulk phase or in water environment [76] have been described by IR- and Raman spectroscopy in the past.

A problem arises in the lipid mixtures, where the signals from the hydrocarbon chains overlap. The application of deuterated substances is a reasonable but not exactly inexpensive solution. Deuterium shifts the modes to lower wavenumbers so that it is possible to distinguish the separate modes of deuterated and non-deuterated chains in the spectrum. Some spectroscopic studies on SC lipids characterization used either a fully deuterated lipid in a mixture with a non-deuterated lipid [77,41] or a partially deuterated one, in which one of two hydrocarbon chains was deuterated [78, 79]. An interesting IR-study on the H-D exchange describing the hydrogen bonding in the ceramide head groups was published by Rerek et al. [80].

3.3 Scattering techniques

Scattering is deflection of beams of radiation due to interference of waves that interact with objects whose size is of the same order of magnitude as the wavelengths [81].

Scattering can be divided according to various aspects, but the chief criterion is the type of the radiation used. Thus, there are X-ray, neutron or light scattering techniques.

Although the X-ray, neutron, and light scatterings show a lot of similarities, the mechanism by which the incident radiation interacts with matter is considerably different. While light and X-rays are scattered by the electron cloud of an atom, the neutrons are scattered by the atomic nucleus [82,83]. Unlike neutrons, both X-ray and light are typical electromagnetic radiations. In this case, energy E and wavelength λ are related according to:

$$E = hc/\lambda \quad (3.1)$$

where c is the light velocity and h the Planck's constant.

On the other hand, neutrons have a finite mass m and their kinetic energy is related to λ according to:

$$E = h^2/2m\lambda^2 = mv^2/2 \quad (3.2)$$

where v is the neutron velocity. This difference results in the fact that the X-ray radiation possesses severalfold higher energy than neutrons [82].

A typical scattering experiment consists of sending a well-collimated beam of radiation of wavelength λ through or on a sample and of measuring the variation of the intensity (Fig. 3.1).

The scattering intensity can be then plotted as a function of the scattering angle θ or more frequently of the scattering vector q [84], which is given by the difference between the wave propagation vectors of the scattered and incident beam and is related to the scattering angle by:

$$q = |\vec{q}| = |\vec{k}_s - \vec{k}_i| = \frac{4\pi n}{\lambda} \sin \theta \quad (3.3)$$

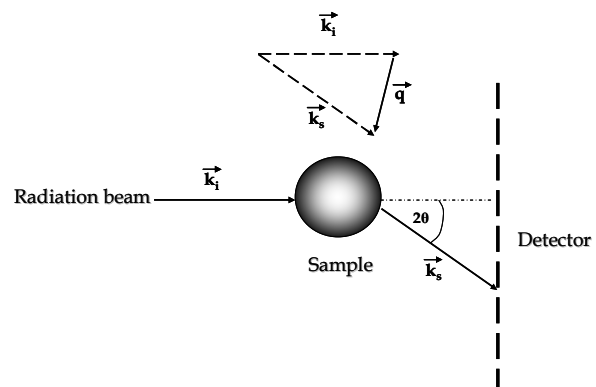


Fig. 3.1 A schematic depiction of a scattering experiment. The scattering vector is a difference between the wave propagation vectors of the final and incident beam. According to [84].

where n is the refractive index. For light in water, n is 1.33, but for X-rays and neutrons, n is very near to unity [85].

In the case when the matter scattering the radiation beams does not show a geometrical organization (e.g. particles dispersed in a homogenous medium), the waves scattered travel different distances and so they differ in their relative phases. Such scattering data can give information about the shape, size, and interactions of the individual particles.

In this context, diffraction may be regarded as a special type of scattering by which the incident beams streaming on an organized structure (e.g. crystal) are diffracted under a defined angle 2θ according to the Bragg's law (Eq. 3.4) and interference between waves scattered from the parallel planes occurs [86,87].

The most essential parameters that can be obtained from the scattering studies of lipid biomembranes are the thickness of the bilayer and the average area occupied by a lipid along the surface of the bilayer (i.e. 'the membrane density') [88].

In principal, there are two approaches to obtain these structural parameters of a bilayer. The first approach is based on diffraction of the beams from multilayer arrays (either multilamellar vesicles, MLVs, or oriented multilamellar films). The electron or neutron length density profiles can be constructed from the intensities of the diffraction peaks using Fourier transformation. The other approach to obtain the bilayer structure is based on measuring of unilamellar vesicles (ULVs). In comparison to diffraction from the multilamellar structures, the scattering from ULVs is continuous in the scattering vector q [88].

3.3.1 X-ray diffraction on lipids

X-ray diffraction is one of the basic methods in the lipid research. In the investigations of the SC lipids, the X-ray diffraction allowed elucidating a number of issues related to membrane organization (for a review see [89]). The X-ray experiments confirmed the presence of the LPP with a repeat distance of 130 Å in the SC [28] and allowed to develop the recent theory about the 'sandwich organization' of the SC lipid lamellae [36].

In principle, the method is based on the diffraction of X-ray beams from an organized structure according to the Bragg's law:

$$2d_{hkl} \sin \theta = n\lambda \quad n=1,2,3\dots \quad (3.4)$$

which describes the effect when the organized structures reflect X-ray beams at certain angles of incidence, θ (Fig. 3.2). d_{hkl} is the distance between the two parallel planes characterized by the Miller indexes hkl , λ is the wavelength of the incident X-ray beam, and n is an integer.

According to this equation, an X-ray wave amplification (interference) is possible only when the beams coincide. This happens when the left member of Eq. 3.4 equals to the wavelength λ or to its whole number multiples. In this case, a maximum in the diffraction curve appears. Because the integer n can gain more values, it is possible to receive more maxima for one d_{hkl} which represent the consequent diffraction orders [86].

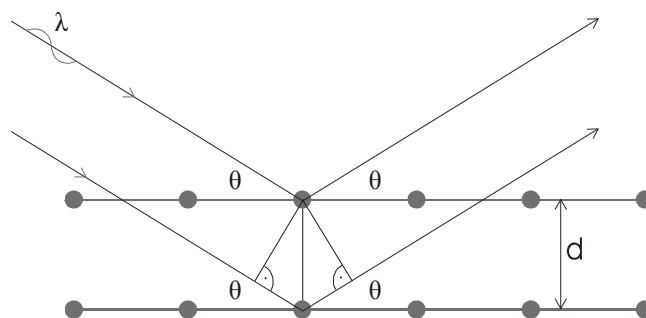


Fig. 3.2 Explanation of Bragg's law by an optical analogy to crystallographic planes reflecting X-rays (according to [86]).

In the most lipid studies, the diffraction measurements are separated into the range of *small angles* (small angle X-ray diffraction, SAXD) where 2θ is smaller than about 2° and *wide angles* (wide angle X-ray diffraction, WAXD) where 2θ is between 2 - 50° . The reason is the anisotropic behaviour of amphiphilic lipid molecules, which leads to the characteristic packing with distinct short and long spacing [90].

The long spacings arise from the periodicity in 'end-to-end' packing, are in the order of the molecular length (about 30 - 60 \AA) and can be detected only in the SAXD region. According to the position of the Bragg's reflections in the SAXD region, the reciprocal spacings of which are in characteristic ratios, a phase of the long chain organization can be assigned to the lipid system. For example, diffraction maxima in ratios of $1, 2, 3, 4, \dots$ are typical of a *lamellar phase*; in ratios of $1, \sqrt{3}, 2, \sqrt{7}, 3, \sqrt{12} \dots$ of a *hexagonal phase*; and in ratios of $1, \sqrt{2}, \sqrt{3}, 2, \sqrt{5}, \sqrt{8} \dots$ of a *cubic phase* [91,92].

In the case of multilamellar samples (MLVs or oriented multilamellar lipid films), the membranes are arranged in a lamellar phase. The so-called *lamellar repeat distance*, D (d_{hkl}), can be calculated combining equations 3.3 and 3.4:

$$D = h2\pi/q_h \quad (3.5)$$

where h is the diffraction order. The lamellar repeat distance includes the bilayer thickness and one water layer between the membranes (Fig. 3.3).

The SAXD studies of the SC lipid systems confirmed the special lamellar organization with coexisting two lamellar phases with repeat distances of about 60 and 130 \AA (the short and long periodicity phase, respectively) [29,32,33,34].

WAXD can describe the short spacings originated from the 'side-by-side' subcell packing (lateral organization) of the hydrocarbon chains. The spacings amount to values of about 3 - 5 \AA [73].

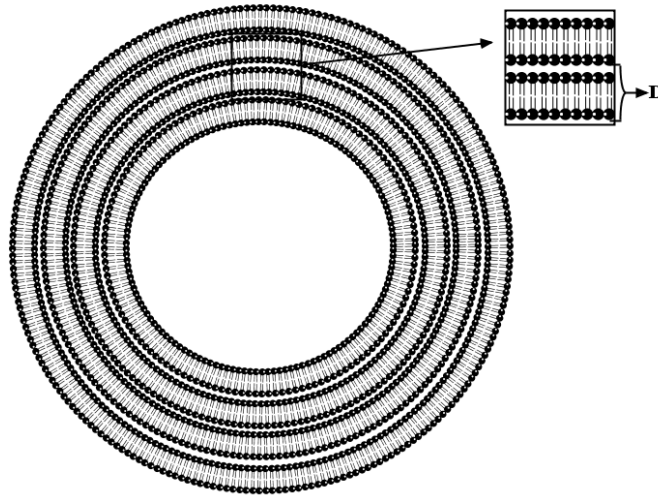


Fig. 3.3 A schematic depiction of a multilamellar vesicle. The D-value includes the bilayer thickness and one water layer between the membranes.

Ceramides themselves are often arranged in a triclinic, orthorhombic or hexagonal subcell packing [93,94]. The mixtures of SC lipids both in the native SC and in the mixtures of isolated or semisynthetic SC lipids show an orthorhombic and/or hexagonal chain packing in the state below the main phase transition. The orthorhombic packing gives two diffraction peaks in the WAXD region with the d_{hkl} -value at about 4.1 and 3.7 Å. On the contrary, the hexagonal chain packing shows only one sharp peak with the spacing of 4.1 Å. Above the main phase transition, the chains are in a liquid phase, which results in a very broad peak at approximately 4.6 Å [42].

3.3.2 Small angle neutron scattering

When a neutron beam irradiates a matter, the incident radiation is partly transmitted, partly absorbed, and partly scattered. The intensity of the scattered beam can be generally expressed by:

$$I(\lambda, \theta) = I_0(\lambda) \Delta\Omega \mu(\lambda) \tau V \frac{\partial\sigma}{\partial\Omega}(q) \quad (3.6)$$

The first three terms in Eq. 3.6 are clearly instrument-specific: I_0 is the incident flux, $\Delta\Omega$ is an instrument parameter given by the sample-to-detector distance and detector dimensions; μ is the detector efficiency. The last three terms in Eq. 3.6 are characteristic of the sample: τ is the sample transmission and V is the sample volume illuminated by the neutron beam. $\partial\sigma/\partial\Omega(q)$ is the *microscopic differential scattering cross section* which includes the complete information about the shape, size, and interactions of the scattering particles. In principal, the $\partial\sigma/\partial\Omega(q)$ is given by:

$$\frac{\partial \sigma}{\partial \Omega}(q) = C_p V_p (\Delta \rho)^2 F(q) S(q) + B_{inc} \quad (3.7)$$

where C_p is the concentration of scattering particles, V_p is the volume of one scattering particle, and B_{inc} is the incoherent background signal. $F(q)$ is the form or shape factor that describes how $\partial \sigma / \partial \Omega(q)$ is modulated by the interference effects between radiation scattered by different parts of the same scattering body. It is highly dependent on the shape of the scattering body. $S(q)$ is the interparticle structure factor, which is related to the degree of local order in the sample and interactions between the particles measured [82].

$(\Delta \rho)^2$ is the contrast which is given by the square of the difference in neutron scattering length density of the sample ρ_p and the medium ρ_m :

$$(\Delta \rho)^2 = (\rho_p - \rho_m)^2 \quad (3.8)$$

It is also notable that the product of multiplying the microscopic differential cross section by the number of particles is known as *the macroscopic differential scattering cross section* $\frac{\partial \Sigma}{\partial \Omega}(q)$ [82].

As described above, the X-rays are scattered by electrons while the neutrons by atomic nuclei. Consequently, the atomic scattering factors are considerably different. The X-ray atomic scattering factor increases with the atomic number, Z , i.e. with the number of electrons present. However, neutron scattering factors vary completely irregularly from Z from isotope to

Table 3.1 Neutron (b_{coh}) and X-ray (f_{X-ray}) scattering lengths for various elements.

Atom	b_{coh} (10^{-12} cm)	f_{X-ray} (10^{-12} cm)
H ¹	-0.374	0.28
D ² (2H)	0.667	0.28
C ¹²	0.665	1.69
N ¹⁴	0.930	1.97
O ¹⁶	0.580	2.25

isotope. The power by which the individual atoms scatter the neutron or X-ray beams is called the scattering length (b_{coh} for neutrons; f_{X-ray} for X-ray) (Table 3.1).

For neutrons, it holds true that there is so large difference in the coherent scattering length between deuterium and hydrogen that the latter is actually negative. This arises from a change of phase of the scattered wave and results in a marked difference in scattering power (contrast) between molecules including deuterium or hydrogen [95]. This is the main advantage of the neutron scattering in comparison to the X-rays and the most neutron scattering experiments are based on this phenomenon. The deuterium labelling techniques make a molecule or a part of molecule ‘visible’ for the neutrons. Using either the deuterated molecule or the environment, the signal-to-noise ratio of the measurements can increase by orders of magnitude.

3.3.3 Small angle neutron scattering on ULVs

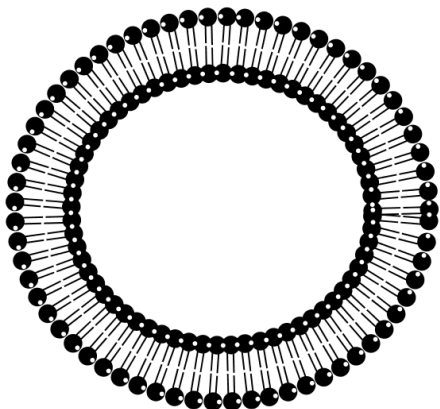


Fig. 3.4 A schematic depiction of a unilamellar vesicle.

A schematic depiction of a unilamellar vesicle (ULV) is presented in Fig. 3.4 and its typical scattering curve in Fig. 3.5a. Several approaches can be used to evaluate the SANS signal from ULVs. Either the curve can be fitted according to some of mathematical models [88,96] or the classical Guinier approximation, which gives the radius of gyration R_g from the Kratky-Porod plot [97,98,99], can be used for the data analysis.

In this thesis, the analysis of the SANS curves has been performed using the ‘model of separated form factors’ [96], and the Guinier approximation.

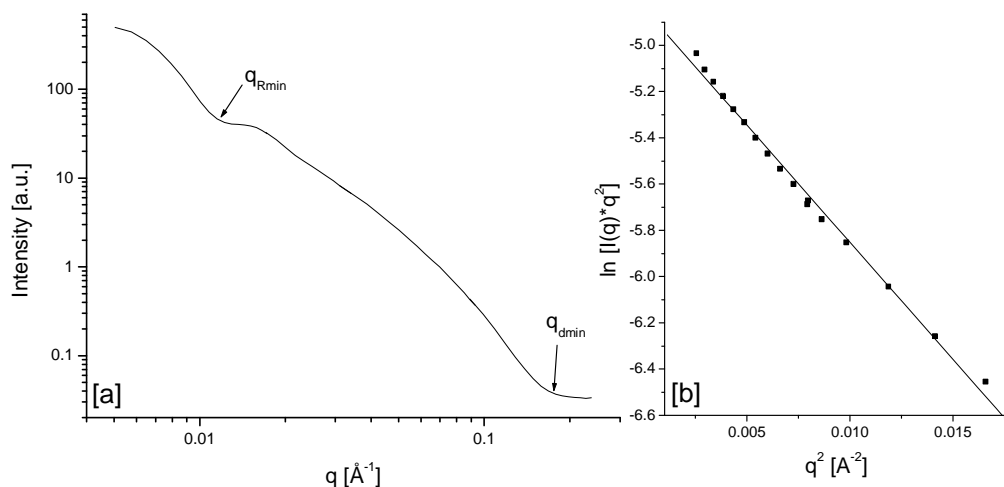


Fig. 3.5 [a] A typical SANS curve from DMPC ULVs. The arrows show the minima related to the average vesicle radius and the membrane thickness, respectively. [b] The linear area of the correspondent Kratky-Porod plot.

According to the ‘model of separated form factors’, the macroscopic scattering cross section of the monodispersed population of ULVs is given by:

$$\frac{\partial \Sigma(q)}{\partial \Omega_{mon}} = N F_s(q, R) F_b(q, d) S(q) \quad (3.9)$$

where N is the number of vesicles per unit volume, $F_s(q, R)$ is the form factor of the infinitely thin sphere with the radius R

$$F_s(q, R) = \left(4\pi \frac{R^2}{qR} \sin(qR) \right)^2 \quad (3.10)$$

$F_b(q, d)$ is the form factor of the symmetrical lipid bilayer with the thickness d , which can be expressed by

$$F_b(q, d) = \left(\frac{2\Delta\rho}{q} \sin\left(\frac{qd}{2}\right) \right)^2 \quad (3.11)$$

for the case of a bilayer with a constant scattering length density across the membrane $\rho(x) = \text{const}$. $\Delta\rho$ is the neutron contrast.

$S(q)$ is the structure factor of the vesicle population which characterizes interactions between the particles. For the systems with the concentration of 1% (w/w) of lipids in buffer, the structure factor has been found near to 1 [100].

The average vesicle radius R can be calculated from the scattering curve based on Eq. 3.10 as $R = \pi/q_{Rmin}$, where q_{Rmin} is the first minimum in the form factor of the infinitely thin sphere after averaging of the population of polydisperse vesicles [101].

The membrane thickness parameter d can be directly calculated from the position q_0 of the first minimum of the sine function in the Eq. 3.11 as $d = 2\pi/q_{dmin}$. For a membrane thickness of about 30 Å, the position of q_{dmin} is about 0.2 Å⁻¹.

The Guinier approximation offers another possibility to determine the membrane thickness parameter, d_g , which is a measure of the membrane thickness, from a scattering curve [97,98,99]. In the q -range valid for a homogeneous membrane approximation ($\pi/R < q < 1/R_g$), the scattering intensity of ULVs dispersed in heavy water can be given by

$$I(q) = 2\pi I(0) q^{-2} \exp(-q^2 R_g^2) \quad (3.12)$$

where $I(0)$ is the scattering intensity to 'zero angle' and R_g is the membrane gyration radius. In this approach, the R_g parameter is the absolute value of the slope of the Kratky-Porod plot ($\ln[I(q)q^2]$ vs q^2) (Fig. 3.5b) and the membrane thickness parameter can be calculated as

$$d_g^2 = 12R_g^2 \quad (3.13)$$

$I(0)$ cannot be measured experimentally but it can be determined by extrapolation of the Kratky-Porod plot to the zero value. The value of $I(0)$ is given by the total particle scattering length, namely, by the sum of the scattering lengths of all atoms inside the particle. Therefore, the chemical composition being known, the evaluation of $I(0)$ allows the molecular mass per unit of vesicle surface to be determined [98,102]. In the limit of

$q \rightarrow 0$, the mass of the membrane per unit of surface, M_s , can be determined by dividing the scattered intensity $I(0)$ by the total lipid concentration c and the scattering length density per unit mass, $\Delta\rho_m$, according to:

$$I(0) = M_s c \Delta\rho_m^2 \quad (3.14)$$

The membrane area per molecule, A , in centrosymmetric bilayers can be calculated by:

$$A = \frac{2}{(M_s N_A / M_w)} \quad (3.15)$$

where M_w is the average molecular weight of the lipids, M_s the determined membrane mass per unit of surface and N_A the Avogadro number.

3.3.4 Neutron diffraction on oriented multilamellar samples

As mentioned above, the scattering length density profiles of the membranes can be determined using the Fourier analysis in the X-ray and neutron diffraction studies. The profile is a function characterizing the density distribution of the scattering centres in real space and can be interpreted in terms of molecular structure. In the case of X-rays, the scattering centres are the electrons surrounding the atomic nuclei. In the case of the neutron scattering, it is the strength of the neutron-nucleus interaction (see Chapter 3.3.2).

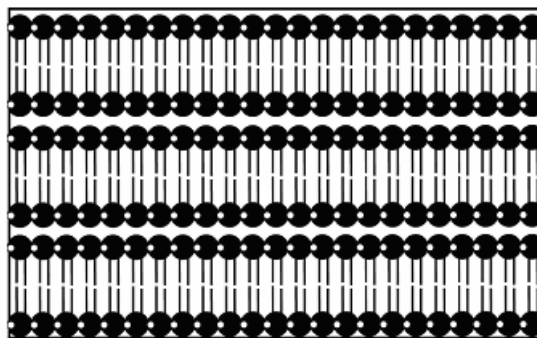


Fig. 3.6 A schematic depiction of a multilamellar lipid film.

Multilamellar films on the nearly ideally smooth quartz substrate (Fig. 3.6) show a very high degree of ordering. Thus, the diffraction signal from such samples is stronger in comparison to the signal from MLVs, and consequently, more diffraction orders can be detected.

According to the Bragg's law (Eq. 3.4), the lamellar repeat distance D can be simply determined. When at least five diffraction orders from the bilayers are successfully measured, Fourier transformation can be applied to calculate the electron or neutron length density profile of the membrane:

$$\rho(x) - \rho_w = \frac{1}{D} F_o + \frac{2}{D} \sum_{h=1}^{h_{\max}} \alpha_h F_h \cos\left(\frac{2\pi hx}{D}\right) \quad (3.16)$$

where ρ_w is the electron or neutron length density of the environment (mostly water or D₂O). For the different diffraction orders $h > 0$, α_h is the phase factor, which can assume only values of +1 or -1 for centrosymmetric bilayers. F_h is the bilayer structure factor.

The form factor accounts for the statistical distribution of electron/neutron length in the bilayer. For a homogenous centrosymmetric structure, the discrete structure factor can be obtained from the square root of the diffraction intensity I_h according to:

$$F_h = \sqrt{C_h \cdot I_h} \quad (3.17)$$

under the h^{th} diffraction peak. C_h is the Lorentz polarization corrector factor. For oriented samples, C_h is nearly proportional to h . The structure factor F_h involves an unknown scale factor so only the absolute values can be measured [103].

This problem is caused by the fact that the measurements of the intensities in diffraction patterns can only give the amplitude, and not the phase, of the structure factor. For this reason, it is impossible to obtain directly the Fourier transform of the structure factor F to determine the electron or neutron length density distributions. This phenomenon is generally known as *the phase problem* of X-ray and neutron scattering [87].

There are several methods to overcome the phase problem directly or indirectly. The neutron diffraction provides a convenient solution to determine the phases and consequently the membrane structure by using the large scattering difference between hydrogen and deuterium. The scattering contrast between different components can be adjusted by simply replacing or mixing H₂O with D₂O. A gradual H₂O/D₂O exchange permits direct observation of phase changes of particular reflections [104,105].

According to this ‘isomorphous replacement method’, when H₂O is replaced by D₂O, the even-order structure factors will increase but the odd-order structure factors will decrease algebraically. Thus, the linear plots of structure factor versus mole per cent D₂O should have positive slopes for even orders and negative slopes for odd orders [106]. The phases (the signs of the structure factor F_h) can be determined according to this rule when the absolute values of $|F_h|$ are arranged as a linear function versus the concentration of D₂O in the sample environment. Consequently, the neutron length density profiles can be calculated from equation 3.16.

Determination of electron and/or neutron length density profiles represents a novel approach in the characterisation of the SC lipid membranes and possibly of the permeation enhancers’ influence on the membranes. In a recent study, electron density profile of a membrane consisting of isolated SC lipids obtained from the X-ray diffraction data has been published. The main problem in determining the phases was solved by the ‘swelling’ process induced by varying the environment pH [107]. Neutron diffraction with the

'isomorphous replacement method' on SC lipid model membrane has been used for the first time in the SC lipid research within this dissertation.

3.3.5 Particle size analysis via dynamic light scattering

In contrast to the other methods mentioned in this Chapter, dynamic light scattering (DLS) also known as photon correlation spectroscopy (PCS) is not often used to describe the lipid phase behaviour on the molecular level. The method is applied particularly to determine the hydrodynamic radius of particles with a size between 30 and 10^3 Å and is therefore convenient to characterize the ULVs with regard to their size and stability [108]. In

principal, DLS is based on the detection of visible or UV light scattered by the non-isotropic medium. As in the case of other scattering techniques, the scattering vector, q , is the important descriptor of the properties of scattered light and is given by equation 3.3. The only difference to the X-ray and neutron scattering is that the refractive index, n , is not close to 1 and cannot be neglected in the calculations.

During the scattering process, minimum energy is absorbed. For this reason, DLS is sometimes called as *quasi-elastic light scattering*.

In contrast to static light scattering, where the scattered light intensity is detected as a function of the scattering vector q ; DLS monitors fluctuations in the scattered light

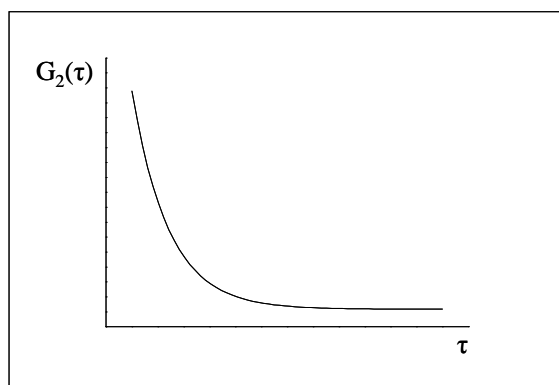


Fig. 3.8 An example of autocorrelation function of a monodisperse population.

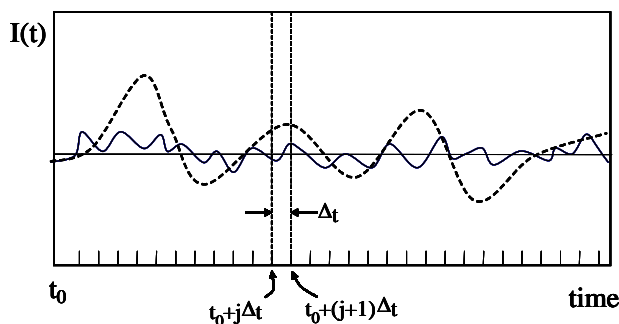


Fig. 3.7 Fluctuations in scattered light intensity in relation to particle size. The movement of large particles (dashed line) is slower than of small particles (full line). According to [111].

intensity, as a function of time, while q is constant [109]. The fluctuations arise from the random Brownian motion of the measured particles, which is related to the particle size. Small particles move faster than larger ones (Fig. 3.7).

This process can be described by the autocorrelation function $G_2(\tau)$ of the scattered intensity [110,111], which mirrors an averaged value of the

intensity registered at an arbitrary time t , $I(t)$, multiplied by the intensity registered at a time delay τ according to:

$$G_2(\tau) = \langle I(t) \cdot I(t + \tau) \rangle = \left\langle \int_{-\infty}^{\infty} I(t)I(t + \tau)dt \right\rangle \quad (3.18)$$

with $\tau = j\Delta t$ $j=0, 1, 2, \dots$

The time delay amounts to some nano- till milliseconds.

If the particles are monodisperse, the autocorrelation function of the scattered light intensity (Fig. 3.8) is a single decaying exponential:

$$G_2(\tau) = A + B \cdot e^{(-2\Gamma\tau)} \quad (3.19)$$

where A and B can be considered as instrumental factors. The decay rate Γ is related to the translational diffusion coefficient, D , by:

$$\Gamma = Dq^2 \quad (3.20)$$

For polydisperse samples, the autocorrelation function is the sum of the exponentials of each component size. In such case, various more complex algorithms can be used to analyse the distribution of the decay rates. In the presented study, the CONTIN algorithm was used [112].

Having obtained the diffusion coefficient, the hydrodynamic particle radius, R_H , can be determined by inserting D into the Stokes-Einstein Equation:

$$D = \frac{k_B T}{6\pi\eta R_H} \quad (3.21)$$

where k_B is the Boltzmann constant, T the absolute temperature, η viscosity of the solvent, and R_H the mean hydrodynamic vesicle radius.

4 Influence of phytosphingosine-type ceramides on the structure of DMPC membrane

Most parts published in: Zbytovská J, Kiselev MA, Funari SS, Garamus VM, Wartewig S, Neubert R, 2005. *Influence of phytosphingosine-type ceramides on the structure of DMPC membrane. Chem. Phys. Lipids 138 (1-2), 69-80.*

Abstract

The present paper describes the influence of the ceramides with phytosphingosine base, N-stearoylphytosphingosine (Cer[NP]) and α -hydroxy-N-stearoylphytosphingosine (Cer[AP]), on the structure and properties of multilamellar (MLVs) and unilamellar vesicles (ULVs) of dimyristoylphosphatidylcholine (DMPC). The lamellar repeat distance, D, has been measured at various temperatures using small angle X-ray diffraction. The incorporation of ceramides into the DMPC membrane causes larger D compared to pure DMPC membrane. For both ceramide types, at 32 °C, there is a linear relationship between the D value and the ceramide concentration. However, there is no such dependence at 13 or 60 °C. Unlike Cer[AP], Cer[NP] induces a new phase with a repeat distance of 38.5 Å.

The membrane thickness and the vesicle radius of ULVs in water and in sucrose solution were calculated from small angle neutron scattering curves. Phytosphingosine ceramides increase both the membrane thickness and the radius in comparison to pure DMPC ULVs. The stability of ULVs in time was studied by dynamic light scattering. Both ceramides induce an aggregation of the ULVs into micrometer sized non-multilamellar structures in pure water. Presence of sucrose in the environment averts the vesicle aggregation.

4.1 Introduction

Ceramides are unique lipids, which abound in many special functions in biological membranes. They play a crucial role in apoptosis, cell proliferation, and cell differentiation [113]. The anticancer activity of ceramides and its derivatives was confirmed in the last years [114,115]. Recently, the phenomenon of the ceramide function as a second messenger is controversially discussed. Many studies suggested that the mechanism of the ceramide effect is based on the changed membrane properties [116]. According to Kolesnick et al. [117], the observed changes in the phospholipid membranes induced by ceramides are: i) the phase separation in ceramide-rich and -poor domains [118,119] ii) the increasing order of the hydrocarbon chains in the bilayer, and iii) the facilitated transition from bilayer to non-bilayer structure [120]. It has been shown that ceramides incorporated in phospholipid membrane can cause vesicle budding [116], transbilayer lipid movement [121,122], and membrane fusion [123].

Although many studies have been published about the influence of the sphingosine- or sphinganine- type ceramides [124,122], sphingosine [125], glycosphingolipids [126] even the synthetic ceramide derivatives [127] on the phospholipid membranes (for a review see [128]), little attention has been paid to ceramides with the phytosphingosine base.

While ceramides with sphingosine base were described as potent mediators of the apoptotic response, their saturated analogues, sphinganine-ceramides, are thought to be inactive [122,124,129]. This implies the hypothesis that the presence of a double bond in the 4-5 position of the ceramide head group is essential for the biological activity [115]. Due to this, mostly the phase behaviour of sphingosine-ceramides was studied.

Ceramides with the phytosphingosine base do not possess such a double bond, however, unlike dihydroceramides a hydroxyl group is present in the position 4. In contradiction to the above-mentioned hypothesis, these ceramides were described to regulate cell growth, stress and apoptotic processes in yeast [130,131], as well as in mammalian tissues [132,133]. Hwang [134] suggests that, due to their hydroxyl group, phytosphingosine-ceramides can be even more active in the apoptotic response than ceramides of the sphingosine type. Due to these findings, it is required to study more deeply interactions between phospholipids and ceramides with the phytosphingosine base.

The present chapter describes the influence of two phytosphingosine-ceramides namely Cer[NP] (N-stearoylphytosphingosine) and Cer[AP] (α -hydroxy-N-stearoylphytosphingosine) on the structure of dimyristoylphosphatidylcholine (DMPC)

membrane. The difference between these two ceramides is in the hydroxyl group on the α -carbon of the amide-linked stearic acid, which causes an increased hydrophilicity of Cer[AP].

Because disaccharides (e. g. sucrose) can stabilize biological membranes by replacing water molecules on the membrane [135], the influence of sucrose on ULVs was studied with the purpose to enhance the stability of the vesicles.

Multilamellar and unilamellar vesicles (MLVs, ULVs, respectively) of the DMPC/ceramide systems prepared in water or in sucrose solution were studied by differential scanning calorimetry (DSC), small angle X-ray diffraction (SAXD), small angle neutron scattering (SANS), and dynamic light scattering (DLS).

4.2 *Material and Methods*

4.2.1 **Materials**

Dimyristoylphosphatidylcholine (DMPC) was a gift from Lipoid (Ludwigshafen, Germany). N-octadecanoylphytoosphingosine (N-stearoylphytoosphingosine, Cer [NP]) and α -hydroxy-N-octadecanoylphytoosphingosine (α -hydroxy-N-stearoylphytoosphingosine, Cer [AP]) were gifts from Cosmoferm (Delft, The Netherlands). Sucrose and sodium azide were purchased from Sigma-Aldrich (Taufkirchen, Germany). D₂O (99.98% deuteration) was purchased from Chemotrade (Leipzig, Germany). Water was of HPLC grade. Solvents used for the sample preparation and the TLC purposes were of HPLC grade and purchased from Merck (Darmstadt, Germany), Baker (Deventer, The Netherlands), and Roth (Karlsruhe, Germany).

4.2.2 **Sample preparation**

MLVs were prepared by the 'thin layer method' [108]. The lipids were dissolved separately in chloroform/methanol mixture 2/1. The required amounts of the solutions were mixed together and dried down using a rotary evaporator. To remove the rest of the solvent, the samples were kept for one day under vacuum. An appropriate amount of water, D₂O or 20% sucrose solution in water or in D₂O was added to the dry sample. The samples were then heated for one hour at 75 °C and mixed on a vortex every 30 min till a milky MLV suspension was formed. The ULVs were prepared from the MLV suspension by extrusion through polycarbonate filters with a pore diameter of 500 Å at 75 °C using a LiposoFast Basic extruder from Avestin (Ottawa, Canada).

4.2.3 Differential scanning calorimetry

The MLVs with 20% lipids in water (w/w) were measured in the temperature range from 10 °C to 85 °C with a differential scanning calorimeter DSC 200 (Netsch Gerätebau, Selb, Germany) with an empty cell as reference. The scan rate was 5 K min⁻¹. Transition temperatures were inferred from peak onset temperatures using the Netsch software.

The samples were prepared one day before the measurement.

4.2.4 Small angle X-ray diffraction

Small angle X-ray diffraction data were collected on the Soft Condensed Matter beamline A2 of HASYLAB at the storage ring Doris III of the Deutsches Elektronen Synchrotron (DESY). A two-dimensional CCD detector was used for data acquisition. The MLVs with 20% (w/w) lipid concentration in water were measured at three temperatures (13±1, 32±1, and 60±1 °C) in specially designed copper cells with a polyimide-foil (Kapton[®], DuPont, Luxembourg) window (50 µl in volume). The sample-to-detector distance was 585 mm and the X-ray wavelength was 1.5 Å. The acquisition time of each sample was 5 minutes. Silver behenate and rat tendon tail collagen were used for calibration. Prior to each measurement, the sample was allowed to equilibrate for 5 minutes.

The data evaluation was carried out using the FIT2D software. The scattering intensity was measured as a function of the scattering vector, q . The latter is defined as $q = (4\pi/\lambda)\sin\theta$, where 2θ is the scattering angle and λ is the X-ray wavelength. The lamellar repeat distance, D , was calculated as an average from the 1st and 2nd order of diffraction according to $D=2\pi/q_1$ for the 1st order diffraction peak and $D=4\pi/q_2$ for the 2nd diffraction peak. Assuming a Lorentzian function, the diffraction peaks were fitted to determine the exact positions.

4.2.5 High performance thin layer chromatography

High performance thin layer chromatography (HPTLC) with automated multiple development (AMD) was used to confirm the ceramide content in the extruded samples.

Sample application on a HPTLC plate (Merck, Darmstadt, Germany) has been carried out using the TLC Sampler 4 (Camag, Muttenz, Switzerland) at a dosage speed of 100 µl s⁻¹. Fifteen samples were applied on one plate at a start line 8 mm from the bottom. The development of the plates was performed using an AMD-2 apparatus (Camag). The development procedure was according to Farwanah [136]. After drying, the plates were dipped into an aqueous solution of 10% CuSO₄, 8% H₃PO₄ and 5% methanol for 20 s and

then dried at 150 °C for 20 min. Afterwards, the plates were scanned using a TLC scanner 3 (Camag). The scanning was carried out in reflectance mode at a wavelength of 546 nm. The slit dimensions were 4×0.1 mm at a scan speed of 20 mm s⁻¹ and a data resolution of 25 μm per step. Integration and quantification based on peaks areas were performed using CATS software (Camag).

4.2.6 Small angle neutron scattering

The ULVs with 1% (w/w) lipid concentration (molar content of ceramide $X_{\text{cer}}=0.11$) in D₂O and in 20% sucrose solution (with 0.02% sodium azide) in D₂O were measured at the neutron wavelength of 8.1 Å at the SANS 1 spectrometer of the Geesthacht Neutron Facility, GKSS, Germany. To obtain scattering curves in a broad q range, four sample-to-detector distances of 70.5, 180.5, 450.5, and 970.5 cm were used. The data were collected at 32 °C. The acquisition time at 70.5 cm was 1 hour, at other sample-to-detector distances 0.5 hour. For background subtraction, the scattering curve of the relevant buffer has been used, which was measured on the same way as the sample.

4.2.7 Dynamic light scattering

The hydrodynamic vesicle radius and the polydispersity of ULVs with 1% and 0.1% (w/w) lipid concentration, with the molar ceramide content of $X_{\text{cer}}=0.11$, in water and in 20% sucrose solution (with 0.02% sodium azide) in water were determined by the photon correlation spectroscopy with a particle size analyzer (Malvern HPPS-ET, Malvern Instruments, UK). A He-Ne gas laser with a laser power of 3.0 mW was the source of coherent light at the wavelength of 633 nm. An avalanche photodiode detector was arranged in the position of scattering angle of 173°. The measurements were carried out at 32 °C. No significant difference in the hydrodynamic radius and polydispersity was obtained between the samples of 0.1 and 1% lipid concentration.

For testing the stability of ULVs, the samples with 1% lipid concentration in water or sucrose solution were stored at 25 °C between the measurements.

The hydrodynamic radius and the polydispersity have been calculated from the correlation function by the CONTIN algorithm using the HPPS-Malvern program for dispersion technology and light scattering systems.

4.3 Results

4.3.1 Characterization of MLVs by DSC

4.3.1.1 System DMPC/Cer[NP]

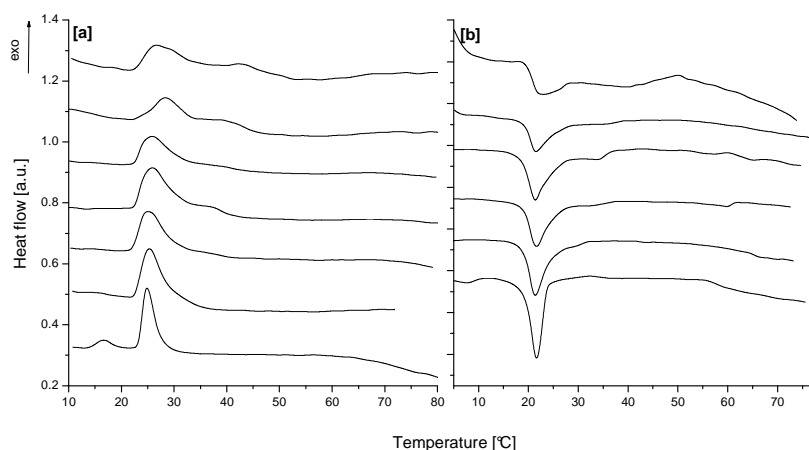


Fig. 4.1 The DSC scans of the DMPC/Cer[NP] MLVs recorded during the heating [a] and cooling [b] regime. From bottom to top: [a] $X_{\text{Cer[AP]}} = 0; 0.04; 0.066; 0.083; 0.1; 0.143; 0.25$; [b] $X_{\text{Cer[AP]}} = 0; 0.04; 0.066; 0.083; 0.1; 0.25$.

Representative DSC up- and down scans of DMPC/Cer[NP] MLVs with the Cer[NP] molar content from 0 to 0.25 are illustrated in Fig. 4.1. The pure DMPC MLVs show two phase transitions. The first one with an onset at 14.3 °C represents the transition from the gel (L_{β}) to the ripple ($L_{\beta'}$) phase. The main phase transition at which the chains transform to the liquid crystalline (L_{α}) phase is presented as a sharp peak with an onset at 23.9 °C [137]. There arise changes in the thermogram already when a minimum of Cer[NP] is present in the sample ($X_{\text{Cer[NP]}} = 0.04$). The first phase transition of the DMPC at about 14 °C is not observable anymore. The main phase transition becomes broader that the onset value is similar to that of pure DMPC but the offset value of the peak is higher (34.4 °C).

With the increasing Cer[NP] concentration in the system the main phase transition broadens. While the onset of the main phase transition remains at similar values (about 23 °C) in all the samples, the offset increases to higher temperatures (to 52.4 °C in the sample with $X_{\text{Cer[NP]}} = 0.25$). A partial phase diagram was constructed from the DSC data recorded during upscans (Fig. 4.2). This diagram seems to be of a monotectic type and indicates that both lipids are practically immiscible in the gel phase.

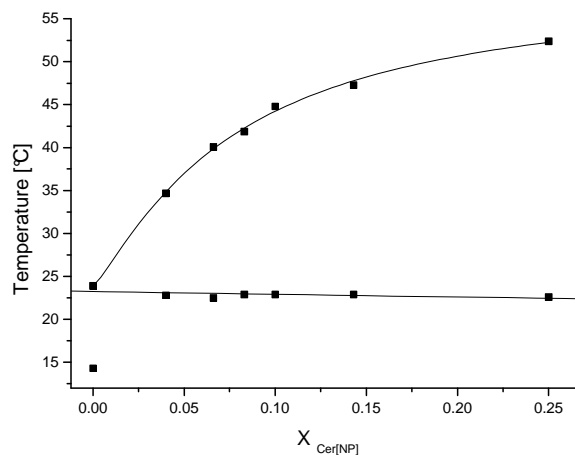


Fig. 4.2 Phase diagram of the system DMPC/Cer[NP]. The squares represent the onset and completion temperatures of the main phase transition.

4.3.1.2 System DMPC/Cer[AP]

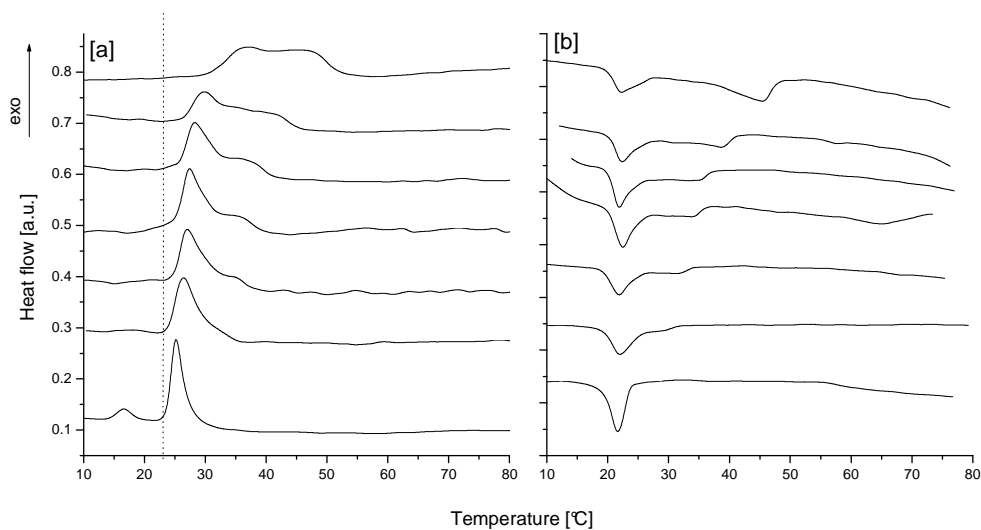


Fig. 4.3 The DSC scans of the DMPC/Cer[AP] MLVs recorded during the heating [a] and cooling [b] regime. In both figures: from bottom to top: $X_{\text{Cer[AP]}} = 0; 0.04; 0.066; 0.083; 0.1; 0.143; 0.25$. The dot line shows the shift of the main phase transition.

The heating- and cooling-DSC responses of the DMPC/Cer[AP] MLVs are shown in Fig. 4.3. Similarly to the DMPC/Cer[NP] system, no L_{β} to L_{β} phase transition is detectable in the thermogram, when a small amount of Cer[AP] is present in the DMPC membrane. The main phase transition broadens with the increasing Cer[AP] concentration in the system. The completion temperatures of the main phase transition reaches

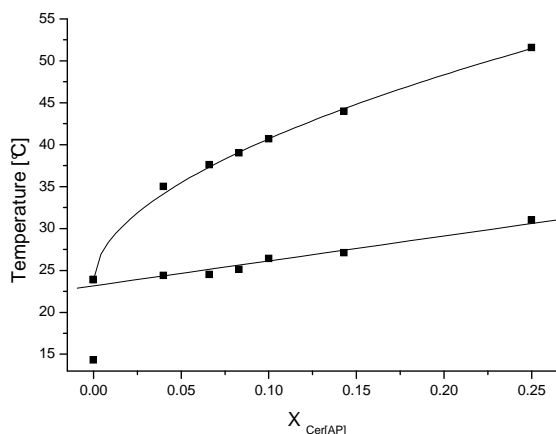


Fig. 4.4 The phase diagram of the system DMPC/Cer[AP]. The squares represent the onset and completion temperatures of the main phase transition, respectively.

51.6 °C in the sample with the highest Cer[AP] concentration ($X_{\text{Cer[AP]}} = 0.25$). Unlike the DMPC/Cer[NP] system, the onset of the main phase transition shifts to higher temperatures with the increasing Cer[AP] concentration in the system. This shift seems to have a linear tendency. The onset value of the sample with $X_{\text{Cer[AP]}} = 0.25$ amounts to 31 °C. The appropriate partial phase diagram is shown in Fig. 4.4. Also in this case, a monotectic behaviour of both lipids is presumable, however, the shift of the onset temperatures of the main phase transition to higher temperatures is somewhat atypical.

4.3.2 Characterization of MLVs by small angle X-ray diffraction

4.3.2.1 System DMPC/Cer[NP]

Fig. 4.5a, b, and c show the diffraction patterns of the DMPC/Cer[NP] MLVs with various Cer[NP] content measured at 13, 32 and 60 °C. At 13 °C, pure DMPC MLVs show two peaks, which represent the 1st and 2nd order of diffraction of a lamellar phase with a repeat distance of 62.6 ± 0.3 Å. The incorporation of Cer[NP] into the DMPC membrane weakens the intensity in particular of the first-order reflection, thus it was possible to calculate the lamellar repeat distance only from the second-order reflection. Obviously, the presence of Cer[NP] even in the lowest molar content of $X_{\text{Cer[NP]}} = 0.04$ increases the repeat distance of DMPC to 65.0 ± 0.3 Å. However, no further dependence between the repeat distance and

the ceramide concentration in the membrane was found. The repeat distance of all other samples ($X_{\text{Cer[NP]}}$ from 0.08 to 0.25) is also about 65 Å (see Fig. 4.5d).

An additional peak arises in the sample with $X_{\text{Cer[NP]}} = 0.08$. The intensity of this peak increases with further increasing content of ceramide. The position remains constant at $q = 0.166 \text{ \AA}^{-1}$ in all the samples. Moreover, the sample with $X_{\text{Cer[NP]}} = 0.25$ shows a small peak at a q value of 0.498 \AA^{-1} (see arrow in Fig. 4.6a). Both peaks were assigned to the 1st and 3rd order of a lamellar phase with a repeat distance of $37.9 \pm 0.1 \text{ \AA}$.

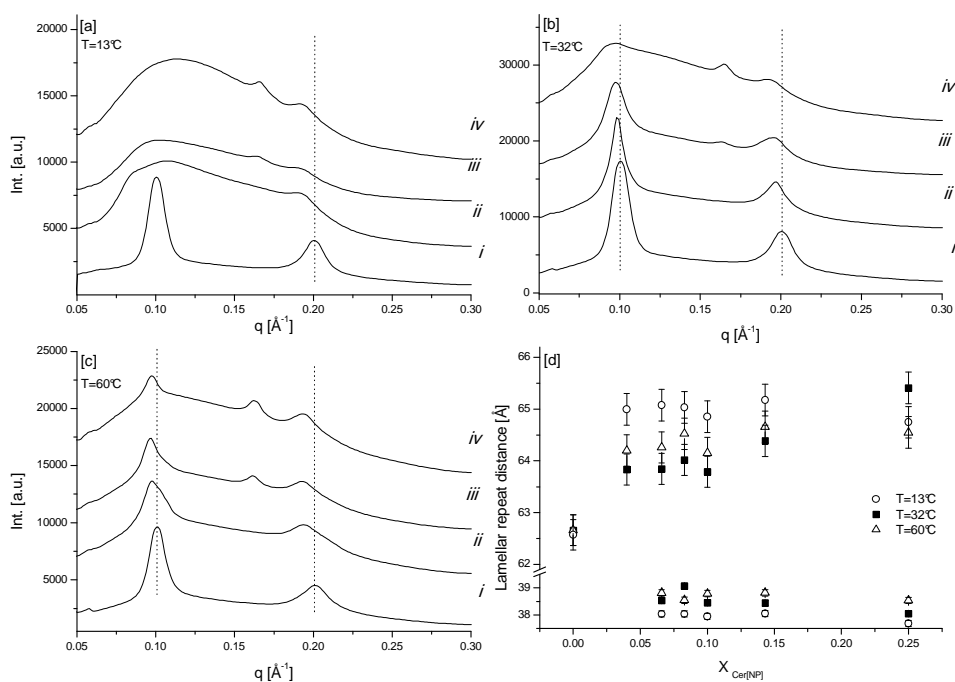


Fig. 4.5 The diffractograms of the system DMPC/Cer[NP] at [a] 13 °C, [b] 32 °C, and [c] 60 °C. From bottom to top: $X_{\text{Cer[NP]}} = (i) 0$, $(ii) 0.04$, $(iii) 0.14$, and $(iv) 0.24$. (d) Influence of the Cer[NP] content on the lamellar repeat distance at 13 °C (open circles), 32 °C (filled squares), and 60 °C (open triangles).

In contrary to 13 °C, the diffraction intensity of the system at 32 °C is much higher (Fig. 4.5b). The lamellar phase of pure DMPC shows two diffraction orders. The peak position shifts with increasing Cer[NP] concentration to lower q -values. Thus, at 32 °C, the lamellar repeat distance of the system increases with increasing ceramide concentration from $62.7 \pm 0.3 \text{ \AA}$ for pure DMPC to $65.4 \pm 0.3 \text{ \AA}$ for the sample with $X_{\text{Cer[NP]}} = 0.25$ (Fig. 4.5d).

Similarly to 13 °C, at 32 °C, a new peak emerges at 0.164 \AA^{-1} in the system with $X_{\text{Cer[NP]}} = 0.08$. The intensity of the peak increases with the increasing ceramide content, whereas the peak position remains unchanged. The sample with $X_{\text{Cer[NP]}} = 0.25$ shows a

small additional peak at 0.493 \AA^{-1} (Fig. 4.6b). The corresponding repeat distance of this phase is $38.3 \pm 0.1 \text{ \AA}$.

At $60 \text{ }^\circ\text{C}$, two diffraction orders of the ‘longer’ phase are visible in the diffractograms (Fig. 4.5c). As observed at the other temperatures, the presence of ceramide in the membrane enhances the lamellar repeat distance from $62.7 \pm 0.3 \text{ \AA}$ for pure DMPC to $64.2 \pm 0.3 \text{ \AA}$ for the sample with $X_{\text{Cer[NP]}} = 0.04$. A further increase in the ceramide concentration does not change the repeat distance (see Fig. 4.5d).

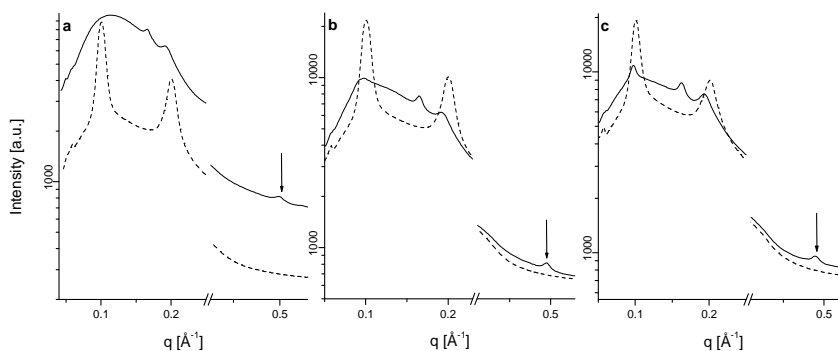


Fig. 4.6 The diffractograms of the sample with $X_{\text{Cer[NP]}} = 0.25$ (solid line) and of pure DMPC MLVs (dashed line) at [a] $13 \text{ }^\circ\text{C}$, [b] $32 \text{ }^\circ\text{C}$, and [c] $60 \text{ }^\circ\text{C}$. The arrow shows the 3rd order of diffraction of a lamellar phase with a repeat distance of about 38 \AA .

As in the other cases, at $60 \text{ }^\circ\text{C}$, another phase with the repeat distance of $38.6 \pm 0.1 \text{ \AA}$ appears in the system with $X_{\text{Cer[NP]}} = 0.08$. Increasing the ceramide content increases the intensity of the diffraction peak, while the position is stable. At this temperature, the sample with $X_{\text{Cer[NP]}} = 0.25$ shows the 3rd order reflection of this phase (Fig. 4.6c).

4.3.2.2 System DMPC/Cer[AP]

Fig. 4.7a displays the diffraction patterns of DMPC/Cer[AP] MLVs with various Cer[AP] concentrations at $13 \text{ }^\circ\text{C}$. There are two reflections for all the samples measured. The peaks represent the 1st and 2nd order of diffraction of a phase with a lamellar repeat distance of $62.6 \pm 0.3 \text{ \AA}$ for pure DMPC MLVs. Incorporating Cer[AP] into DMPC increases the repeat distance to $65.1 \pm 0.3 \text{ \AA}$ for the sample with a molar concentration of $X_{\text{Cer[AP]}} = 0.04$. This value remains unchanged up to a ceramide content of $X_{\text{Cer[AP]}} = 0.1$. Further increase in the ceramide concentration decreases the lamellar repeat distance to about 64.3 \AA (see Fig. 4.7d).

At 32 °C, there is a continuous shift in the peak position to lower q -values with increasing Cer[AP] concentration (Fig. 4.7b) indicating that the repeat distance linearly increases from 62.7 ± 0.3 Å for pure DMPC to 66.8 ± 0.3 Å for the sample with $X_{\text{Cer[AP]}} = 0.25$ Å (Fig. 4.7d).

At a temperature of 60 °C, the effect of the ceramide incorporation into the DMPC matrix is not so pronounced as was the case at the other temperatures (Fig. 4.7c). The lamellar repeat distance increases from 62.7 ± 0.3 Å for pure DMPC to about 63.8 ± 0.3 Å for the samples with $X_{\text{Cer[AP]}} = 0.04 - 0.1$. Further increase in the Cer[AP] concentration decreases the lamellar repeat distance to 63.0 ± 0.3 Å in the sample with $X_{\text{Cer[AP]}} = 0.25$ (see Fig. 4.7d).

In contrast to the DMPC/Cer[NP] system, the DMPC/Cer[AP] system investigated at all temperatures mentioned above revealed no other phase due to the presence of ceramide in the membrane.

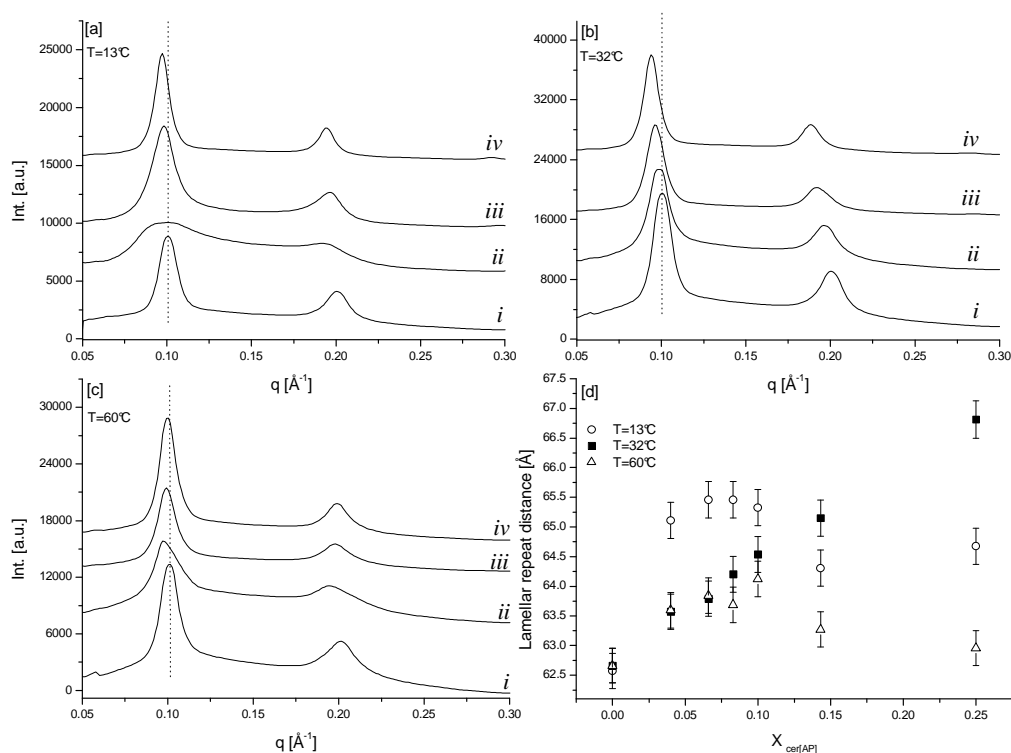


Fig. 4.7 The X-ray diffraction patterns of the system DMPC/Cer[AP] at [a] 13, [b] 32, and [c] 60 °C. From bottom to top: $X_{\text{Cer[AP]}} = (i) 0, (ii) 0.04, (iii) 0.14,$ and $(iv) 0.24$. (d) Influence of the Cer[AP] content on the lamellar repeat distance at 13 °C (open circles), 32 °C (filled squares), and 60 °C (open triangles).

4.3.3 Characterization of ULVs

4.3.3.1 Determination of ceramide content after extrusion by HPTLC

The content of ceramide in the ULV samples was quantified using HPTLC. No difference was found in the Cer[AP] amount between the extruded and the non-extruded sample. On the other hand, a loss of Cer[NP] was observed due to the extrusion. The highest possible molar concentration of Cer[NP] in the DMPC matrix of the ULVs amounts to 0.11. Samples of this concentration were used for the SANS experiments.

4.3.3.2 SANS measurements of ULVs

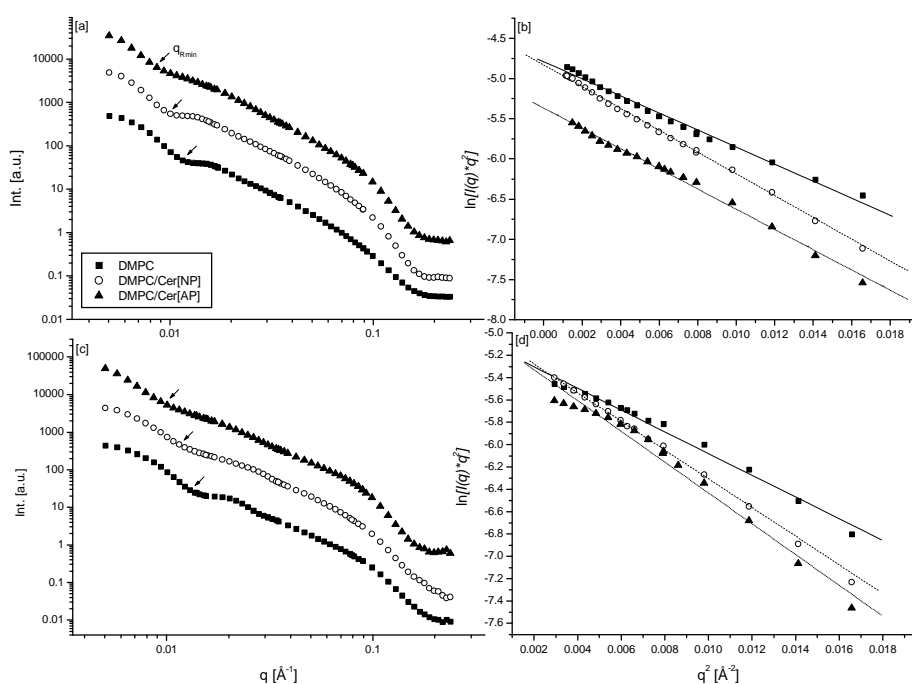


Fig. 4.8 [a] The neutron scattering curves from pure DMPC, DMPC/Cer[NP], and DMPC/Cer[AP] 1% ULVs in D₂O extruded through 500 Å filter. [b] The corresponding Kratky-Porod plots of the scattering curves from [a]. [c] The scattering curves from pure DMPC, DMPC/Cer[NP], and DMPC/Cer[AP] 1% ULVs in 20% sucrose solution in D₂O extruded through 500 Å filter. [d] The corresponding Kratky-Porod plots of the scattering curves from [c]. In all figures: pure DMPC - filled squares, DMPC/Cer[NP] - open circles, and DMPC/Cer[AP] - filled triangles. The arrows in Figs. 4.8 a and c show the minimum of the vesicle radius (q_{Rmin}) in each curve.

The SANS curves of pure DMPC, DMPC/Cer[NP], and DMPC/Cer[AP] ULVs in D₂O and in 20% sucrose in D₂O are shown in Fig. 4.8a and c, respectively. According to the ‘model of separated form factors’, a minimum typical of the average vesicle radius (q_{Rmin}) is observable in the curves (see arrows in Fig. 4.8a, c). In both environments, ceramides evoke a shift in q_{Rmin} to lower q values. The R-values derived from this experiment are summarized in Table 4.1.

The average radii determined with an accuracy of 20% for pure DMPC vesicles in D₂O and in 20% sucrose solution in D₂O are 251 Å and 217 Å, respectively. The presence of Cer[NP] increases the vesicle radius in both D₂O and sucrose solution to 302 Å and 251 Å, respectively. Likewise, in the DMPC/Cer[AP] system, the vesicle radii are larger in both environments. The R-values amount to 365 Å in D₂O and 324 Å in sucrose solution. Note that, in all systems, the vesicle radii of the samples in D₂O are larger than the radii of the samples in the sucrose solution by about 15%. The minimum at q_{Rmin} is flatter in the samples with ceramides than that in pure DMPC.

Table 4.1 Parameters of ULVs derived from SANS and DLS. (d_g is the membrane thickness parameter, R the vesicle radius, and R_h the hydrodynamic radius of the vesicle)

Method applied	SANS	SANS	DLS	DLS
Sample (ULVs, 1% lipid concentration)	d_g [Å]	R [Å]	R_h [Å]	Polydispersity [%]
DMPC in D ₂ O/H ₂ O	35.7±0.7	251±50	335±7	18
DMPC in 20% sucrose solution in D ₂ O/H ₂ O	34.2±0.7	217±43	413±8	28
DMPC/Cer[NP] in D ₂ O/H ₂ O	40.3±0.8	302±60	451±9	36
DMPC/Cer[NP] in 20% sucrose solution in D ₂ O/H ₂ O	39.3±0.8	251±50	346±7	29
DMPC/Cer[AP] in D ₂ O/H ₂ O	38.9±0.8	365±73	1443±80 (average) 2 populations: 422±23 11500±5741	62
DMPC/Cer[AP] in 20% sucrose solution in D ₂ O/H ₂ O	40.7±0.8	324±65	462±9	42

The minimum related to the membrane thickness (q_{dmin}) is not observable in the present SANS curves. Therefore, the Guinier analysis has been chosen for the evaluation of the membrane thickness parameter.

The Kratky-Porod plots of the SANS curves are shown in Fig. 4.8b and d. The membrane thickness parameters, d_g , were calculated from the slopes of the plots according to Eq. 3.13 and are listed in Table 4.1. The d_g value of pure DMPC membrane is $35.7 \pm 0.7 \text{ \AA}$ in D_2O and $34.2 \pm 0.7 \text{ \AA}$ in 20% sucrose D_2O solution, which are smaller in comparison to both DMPC/ceramide systems. The membrane thickness parameter of the DMPC/Cer[AP] ULVs amounts to $40.3 \pm 0.8 \text{ \AA}$ in D_2O and $39.3 \pm 0.8 \text{ \AA}$ in sucrose D_2O solution. The membrane thickness parameter of the DMPC/Cer[NP] system is $38.9 \pm 0.8 \text{ \AA}$ in D_2O and $40.7 \pm 0.8 \text{ \AA}$ in sucrose D_2O solution.

4.3.3.3 Size and stability of ULVs measured by DLS

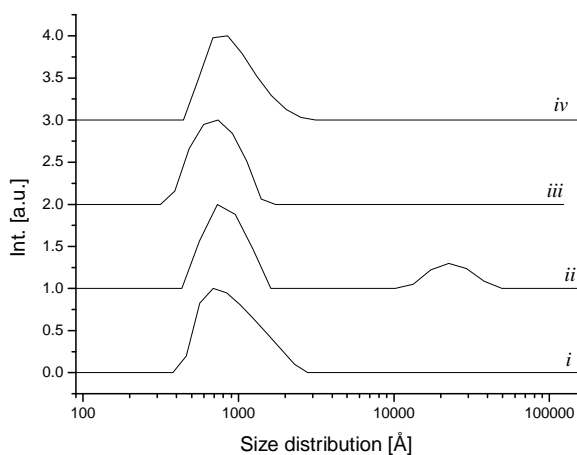


Fig. 4.9 The size distribution of extruded systems. From bottom to top: (i) DMPC/Cer[NP] in water, (ii) DMPC/Cer[AP] in water, (iii) DMPC/Cer[NP] in 20% sucrose solution, (iv) DMPC/Cer[AP] in 20% sucrose solution. All samples: 1% (w/w) lipids in water.

evokes changes in R_h and in polydispersity. The size distributions of the DMPC/ceramide samples are shown in Fig. 4.9.

The DMPC/Cer[NP] system shows a monomodal population with an R_h of 451 \AA in water and 346 \AA in 20% sucrose solution. Unlike the pure DMPC vesicles, the hydrodynamic radius in sucrose solution is smaller than in water.

The hydrodynamic radii, R_h , and the polydispersity of the ULVs measured at $32 \text{ }^\circ\text{C}$ immediately after the extrusion are summarized in Table 4.1. The DMPC ULVs in water show a monomodal population with an R_h of 335 \AA and 18% polydispersity. In 20% sucrose solution, the R_h value of the pure DMPC sample is 413 \AA and the polydispersity 28%. The hydrodynamic radius of the sample in sucrose is higher than that of the sample in pure water. Incorporation of ceramides into the membrane

The DMPC/Cer[AP] system in water shows two populations. The first one has a particle radius of 422 Å and the other population is in the micrometer range. The ULVs of the DMPC/Cer[AP] system in 20% sucrose solution are monomodal with an R_h -value of 462 Å and a polydispersity of 42%.

The stability in time of the ULVs has been studied. The average hydrodynamic radius measured over a period of 30 days is shown in Fig. 4.10. During this time period, the hydrodynamic radius of pure DMPC ULVs in H₂O and in 20% sucrose solution does not change significantly. However, the polydispersity of these samples increased from 18% to 44% in water and from 24% to 43% in the sucrose solution.

Unlike pure DMPC, the DMPC/Cer[NP] ULVs in water show a rapid increase in the hydrodynamic radius to the micrometer range on the 14th day of the measurement. While the vesicle population with the hydrodynamic radius of 420 Å is still present in the sample, a new population with a hydrodynamic radius in a micrometer range evolves at this time.

The DMPC/Cer[NP] vesicles in the 20% sucrose solution show a slight increase in the hydrodynamic radius during the measurement time from 346 Å to 418 Å. The polydispersity of this sample increased from 29% to 42%, too.

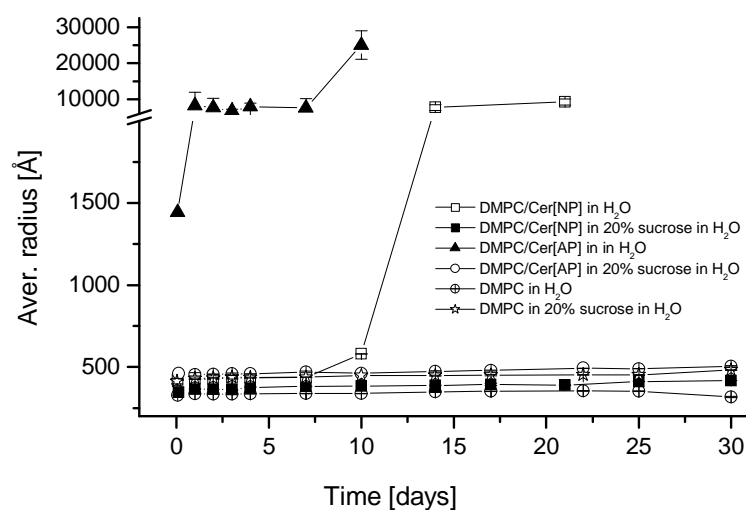


Fig. 4.10 The average hydrodynamic radius of 1% (w/w) ULVs in H₂O and in 20% sucrose solution measured in a time period of 30 days. Legend: DMPC/Cer[NP] in H₂O-white squares, DMPC/Cer[NP] in 20% sucrose solution-filled squares, DMPC/Cer[AP] in H₂O-filled triangles, DMPC/Cer[AP] in 20% sucrose solution-open circles, DMPC in H₂O-white circles with cross, DMPC in 20% sucrose solution-asterisks.

The DMPC/Cer[AP] system in 20% sucrose solution shows also a small increase in the hydrodynamic radius from 462 Å measured immediately after the extrusion to 504 Å at the end of the experiment. The same system in water shows a very high average hydrodynamic radius (1443 Å) already immediately after the extrusion. One day later, the radius increases about five times and in the next days remains constant. In this sample, with the increasing time, the population of small particles declines to the detriment of the population in the micrometer range. On the 10th day of the experiment, the population of small particles is no more detectable.

4.4 Discussion

The typically monotectic phase behaviour of the DMPC/Cer[NP] system indicates that both lipids are immiscible in the gel phase and interactions between their molecules are minimal [138]. Similar phase diagrams were published for ceramides with the sphingosine base and phospholipids [139].

In the case of the DMPC/Cer[AP] system, the situation is similar, however, the fact that the phase transition shifts to higher temperatures with the increasing ceramide concentration is unusual. This implies that a certain degree of miscibility exists between both lipids already in the gel phase. The higher amount of hydroxyl groups in the Cer[AP] molecule can be responsible for the more intensive formation of the intermolecular hydrogen bonds with DMPC than in the case of Cer[NP]. Due to this, the hydrocarbon chains of DMPC melt at higher temperatures than in the neat state.

According to the DSC results, three temperatures were chosen for the following experiments. At 13, 32, and 60 °C, all the systems are in a state before, in, and after the main phase transition, respectively.

The X-ray diffraction studies clearly show that the incorporation of both phytosphingosine-type ceramides into a DMPC matrix induces a longer lamellar repeat distance compared to that of the pure DMPC membrane. However, at every measured temperature, there is a different influence of the ceramide concentration.

At a temperature of 13 °C, both ceramide types increase the lamellar repeat distance in comparison to that of pure DMPC vesicles. However, especially in the system DMPC/Cer[NP], the intensity of the diffraction peaks is very weak. Such weakening of the diffraction intensity can be connected with the membrane undulation appearing in the ripple phase (P_{β}) [103]. Perhaps, similarly to the pure DMPC membrane, the DMPC/Cer

systems are in the ripple phase at 13 °C. This is supported by Holopainen, who described the P_{β} phase in the systems of DMPC/spingosine-type ceramide [139].

At 32 °C, there is a nearly linear increase in the lamellar repeat distance with increasing ceramide concentration, in particular in the system DMPC/Cer[AP]. On the other hand, at 60 °C, the addition of Cer[NP] increases the repeat distance compared to that of pure DMPC, but a dependence on the ceramide concentration is not so obvious. This is even more distinct in the DMPC/Cer[AP] system, where the repeat distance slightly increases up to a Cer[AP] content of $X_{\text{Cer[AP]}}=0.1$; further increase in the Cer[AP] concentration decreases the D-value again.

It seems that ceramides influence the repeat distance of the DMPC membrane by a complex of effects, which antagonize each other. The increasing repeat distance is a consequence of the longer hydrocarbon chains of ceramides in comparison to DMPC and of the increasing phase transition temperature resulting from the ceramide content, which is obvious in particular at 32 °C. On the other hand, the ceramide head group is small and its hydration is limited [79]. This could cause a decrease in the lamellar repeat distance. Hence, which effect predominates, depends on the sample composition and the momentary phase state of the membrane.

Remarkable is the peak at 0.166 \AA^{-1} , which arises in the DMPC/Cer[NP] system at all temperatures measured and grows with increasing Cer[NP] concentration. At first sight, one can anticipate that this peak signifies a hexagonal phase in the system. However, the exact determination of the peak positions does not confirm this assumption. Moreover, the peak at about 0.5 \AA^{-1} was detected in the sample with $X_{\text{Cer[NP]}}=0.25$. These facts hint that a new lamellar phase originates with a repeat distance of about 38 \AA . This value agrees with data presented by some authors [140,141], who described one of the polymorphs of Cer[NP] as a V-shaped form. This form can appear not only in neat Cer[NP] but also in mixtures with water [78] or with other lipids [142]. Comparing our results with the published data, we assume that in the DMPC/Cer[NP] mixtures, Cer[NP] in the V-shaped form separates from the membrane and causes a new ceramide enriched domain with a shorter periodicity. Such a phase separation was observed only at higher Cer[NP] content in the membrane ($X_{\text{Cer[NP]}} \geq 0.08$). Presumably, the DMPC membrane is able to incorporate a distinct amount of Cer[NP]. First when the DMPC membrane becomes saturated, Cer[NP] begins to create its own domain.

Unlike Cer[NP], Cer[AP] does not induce a new phase, which could be detected by SAXD. This finding indicates a higher miscibility of Cer[AP] with DMPC compared to Cer[NP] and is in accordance with the DSC results. As suggested above, the difference between the

Cer[NP] and Cer[AP] behaviour may be connected with the higher hydrophilicity of the polar head group of Cer[AP] compared to Cer[NP]. Probably, the Cer[AP] molecules are able to create more hydrogen bonds with the DMPC headgroups than Cer[NP] which seems to be a very important property for the miscibility of ceramides and phospholipids.

The analysis of the ceramide content after extrusion verified that whereas the concentration of Cer[AP] remains unchanged, the Cer[NP] content decreases during the extrusion. The phase separation detected by SAXD is likely to be related with this ceramide loss. Such a distinct domain with a predominating ceramide content is presumably very hydrophobic and rigid and of course difficult to extrude. This is also supported by the fact that no diffraction peak of the phase with a 38 Å periodicity was detectable in the SANS curves of the DMPC/Cer[NP] ULVs.

The Kratky-Porod analysis of the SANS curves confirms that both ceramide types increase the average membrane thickness by about 5 Å at 32 °C. No significant difference has been found between Cer[NP] and Cer[AP] in influencing the membrane thickness. The calculated membrane thickness of all systems in D₂O and D₂O with 20% sucrose is also not significantly different.

The SANS curves allow to calculate the vesicle radius from the position of q_{Rmin} . According to this method, ceramides increase the vesicle radius of the DMPC membrane. This effect is evident both in pure D₂O and in the 20% sucrose solution in D₂O and indicates an increasing rigidity of the DMPC membrane due to the ceramide incorporation. The R_v values in the sucrose solution are in all systems smaller than in pure D₂O. This result is consistent with the report of Kiselev [143]. As can be seen in Fig. 4.8a and c, the position of q_{Rmin} is more distinct in the pure DMPC samples than in the systems of DMPC/ceramides. This hints that ceramides increase not only the vesicle radius but also the polydispersity of the samples in comparison to pure DMPC.

While the vesicle radius determined by SANS describes the size of the pure vesicles, the hydrodynamic radius determined by DLS includes also a hydration layer on the vesicle surface. Consequently, the hydrodynamic radius derived from the DLS measurements gains generally higher values than the radius calculated from the SANS curves. As expected, the R_h value of the DMPC vesicles in the 20% sucrose solution is larger than that in pure water, because sucrose increases the hydration layer on the vesicle surface.

Interestingly, the DMPC/ceramide systems show an opposite behaviour. In the case of DMPC/Cer[NP] system, the hydrodynamic radii determined by DLS are higher than the vesicle radii determined by SANS. However, the R_h value of the ULVs in the sucrose solution is smaller than in water. This effect can be explained by the assumption that the

hydration layer of the vesicles decreases with the presence of Cer[NP] in the membrane. This is related to the decreased hydrophilicity of the DMPC membrane due to the ceramides. Another explanation is that sucrose can stabilize the ULVs.

The SANS and DLS results of the DMPC/Cer[AP] system in water are quite different. Based on DLS studies, the system shows two populations, one with an R_h value of about 422 Å and another one in the micrometer range. Because of the q -range used in our SANS measurements, only one q_{Rmin} position could be observed. The derived vesicle radius correlates with the population of the small particles detected by DLS. We suppose that this population constitutes of unilamellar vesicles. The other population in the micrometer range could not be detected by SANS. This population represents aggregates, which arise immediately after the extrusion. Note that the SANS curve does not show a diffraction peak attributed to a multilamellar structure. The aggregates do not show a multilamellar arrangement. With growing time after extrusion, the population of the large particles enhances to the detriment of the population of ULVs.

The DMPC/Cer[AP] system in the 20% sucrose solution shows only one population with an R_h value of 462 Å. This value is again larger than the vesicle radius determined by SANS, which is caused by the hydration layer located on the vesicle surface. Micrometer sized particles were not detected in this sample. Evidently, sucrose averts the aggregation of the DMPC/Cer[AP] vesicles.

The stability experiment has confirmed that an aggregation effect, can also be seen in the system of DMPC/Cer[NP] in water. A new population in the micrometer range arises on the 15th day of the stability experiment. For comparison, the pure DMPC samples and the DMPC/ceramide systems in sucrose solution show no aggregation during the time period of one month. A similar effect of ceramides has been found by a number of authors [123,144] and seems to be connected with the molecular shape organization of phospholipids and ceramides [145,146].

4.5 *Conclusions*

The present study proves that ceramides with phytosphingosine base cause similar effects on a phospholipid membrane like the sphingosine-type ceramides. Both ceramides used in this study, Cer[NP] and Cer[AP], increase the lamellar repeat distance of the DMPC membrane. This increase is linearly dependent on the ceramide concentration at 32 °C, however, at 13 and 60 °C, the concentration dependence has a quite different evolution. In contrast to Cer[AP], Cer[NP] induces a new phase that is detectable by SAXD. The incorporation of ceramide into the DMPC membrane causes an increase in both the membrane thickness and the vesicle radius of ULVs. Ceramides cause instability of the DMPC ULVs, which results in an aggregation into micrometer sized non-multilamellar structures. Sucrose avoids the aggregation of DMPC/ceramide ULVs.

5 Influence of cholesterol on the structure of stratum corneum lipid model membrane

Abstract

This study describes the influence of cholesterol on a model membrane consisting of four SC lipids: ceramide[AP], cholesterol, palmitic acid and cholesterol sulphate. Using small-angle X-ray diffraction (SAXD) on multilamellar vesicles (MLVs), the lamellar repeat distance, D , was determined. Small-angle neutron scattering (SANS) on unilamellar vesicles (ULVs) was used to obtain the membrane thickness and the average area of the membrane surface per molecule. Immediately after the sample preparation, the membranes show one lamellar phase. During next days, the systems separate into two lamellar phases and crystalline cholesterol. On heating the samples to 85 °C, the domains merge into one phase, the D -value of which increases slightly with increasing cholesterol concentration. On cooling the samples to 32 °C, only one phase is observable again. Unlike at high temperatures, D decreases with the increasing cholesterol content. No influence of pH on the D -value was found. The membrane thickness determined by SANS decreases and the area of the membrane surface per molecule increases with increasing cholesterol concentration in the membranes. Likely, cholesterol fluidises the SC lipid membranes in the phase with ordered hydrocarbon chains and condenses the membranes in the liquid crystalline phase.

5.1 *Introduction*

The skin barrier plays an essential role in the protection of body against xenobiotics from the environment and against water evaporation from the organism. Stratum corneum (SC), the outermost skin layer, is responsible for the permeability properties of mammalian skin. This membrane consists of keratin-rich corneocytes embedded in a lipid matrix with a lamellar organization. Ceramides of nine types, free fatty acids, cholesterol and its derivatives are the most abundant lipids in the SC [6,147].

The SC lipids show a complex behaviour, which is dependent on the particular lipid composition in the SC matrix. In diseased skin, a deviation in lipid composition has often been found. The recessive X-linked ichthyosis (RXLI) is associated with the steroid sulphatase deficiency; the enzyme which converts sulphated steroids to steroids [148,149]. Due to this, increased levels of cholesterol sulphate (CS) connected with decreased levels of cholesterol (CHOL) were found in the affected skin [10]. Although the CS accumulation seems to be the principal and primary mechanism contributing to the barrier abnormalities in RXLI, the reduced CHOL levels play also an important role especially in the altered membrane dynamics. Topically administrated CHOL reverses the pathologic effects of excess CS on SC membrane structure, barrier function, and desquamation [150]. Additionally, ichthyotic symptoms were induced by cholesterol-lowering drugs [151].

CHOL is an essential component not only in the mammalian skin but also in most biological membranes. For this reason the investigations of the phase behaviour of CHOL mixtures with phospholipids and/or sphingolipids are current research topics (for reviews see [152,153]). CHOL incorporation into lipid membranes induces a range of various effects, which depend not only on the CHOL concentration in the membrane but also on the type of the other concerned lipids; their headgroups and properties to participate on hydrogen bonding, their chain length and degree of saturation. It was described that CHOL is mostly non-uniform distributed in membranes [154], shows limits of saturation in membranes [155] and induces a phase separation into CHOL-rich and -poor domains [156,157]. CHOL has been found to broaden and shift the phase transitions and to affect the transitions into other than lamellar phases [158]. CHOL can influence the bilayer thickness of phospholipid membranes as well [159,160].

Although, there are several studies focusing on the role of CHOL in the SC, the exact influence of CHOL on the SC lipid membrane structure is not enough elucidated yet.

The role of CHOL in the epidermal barrier seems to be providing a degree of fluidity to what could otherwise be a rigid, possibly brittle membrane system [20]. It was described that CHOL disorders the lipid gel phase whereas it orders the liquid crystalline phase in SC lipid model membranes [161]. Ceramides were found to create eutectic mixtures with CHOL [61]. The miscibility of ceramides with CHOL depends on their chain length. The solubility of CHOL in SC lipid membranes is limited [36]. After the membrane saturation, CHOL separates from the SC lipid membranes to form CHOL monohydrate crystals. CHOL was described to mix well with ceramide 2 (ceramide [NS]) but not with free fatty acid, at physiological temperatures [162] and to increase the mixing properties between fatty acid and ceramide above 40 °C [41]. Additionally, CHOL can phase-separate ceramides that are normally miscible in the absence of CHOL [163].

The present study describes the effect of CHOL on a model membrane imitating the native SC lipid matrix. This model consists of ceramide [AP] (Cer[AP]), palmitic acid (PA), CHOL and CS. Two types of samples, multilamellar and unilamellar vesicles (MLVs and ULVs, respectively), were developed from the (semi)synthetic lipids. MLVs were measured by small-angle X-ray diffraction (SAXD) to determine the lamellar repeat distance (D). The small-angle neutron scattering (SANS) on ULVs enabled us to calculate the membrane thickness parameter, d , which is a value related to the real membrane thickness [100]. SANS is not an unusual method in the studies on various phospholipid systems [164,165]; however, in this paper, SANS was used to characterize SC lipid model membranes for the first time.

5.2 *Material and Methods*

5.2.1 *Material*

N- α -Hydroxyoctadecanoylphyto sphingosine (Cer [AP]) was a gift from Cosmoferm (Delft, The Netherlands). Cholesterol (CHOL), cholesterol sulphate (CS), and PA, as well as Trizma[®] (Tris), Bis-tris buffer, and sodium chloride were purchased from Sigma-Aldrich (Taufkirchen, Germany). D₂O (99.98% deuteration) was purchased from Chemotrade (Leipzig, Germany). Water, chloroform and methanol used were of HPLC grade.

5.2.2 Vesicle preparation

The composition of the lipid system used in this study was chosen regarding previous data [166,167]. A basic system that should mostly imitate the real SC lipid composition consists of 55% (in weight) Cer[AP], 25% CHOL, 15% PA and 5% CS (mixture IV). This system was also used to study the influence of pH. The other samples were prepared varying the proportion of CHOL (from 10 to 30%), the relative ratio of other lipids remaining constant. The samples used in the study are listed in Table 5.1.

MLVs were prepared by the ‘thin layer method’ [108]. The lipids were dissolved separately in chloroform/methanol mixture 2/1 (in volume). The required amounts of the solutions were mixed together and dried down using a rotary evaporator. To remove the rest of the solvent, the samples were kept under vacuum for one day. An appropriate amount of 10 mM Tris or Bis-tris buffer, pH=6.0-9.0 with 100 mM NaCl in water or in D₂O was added to the dry sample. The samples were then heated for one hour to 90 °C and mixed on a vortex every 30 min till a milky MLV suspension was formed.

The ULVs were prepared from the MLV suspension by extrusion through polycarbonate filters with a pore diameter of 500 Å at 75 °C using a LiposoFast Basic extruder from Avestin (Ottawa, Canada).

Table 5.1 Lipid composition of the model systems (in weight %). The concentration of cholesterol in ULVs (after extrusion) is given in brackets.

Lipid	I	II	III	IV	V
cholesterol	10 (8.6)	15 (14.2)	20 (-)*	25 (21.6)	30 (27)
ceramide[AP]	66	62.3	58.7	55	51.3
palmitic acid	18	17	16	15	14
cholesterol sulphate	6	5.7	5.3	5	4.7

* not measured.

5.2.3 Vesicle characterization

The concentration of lipids in the ULVs after extrusion was determined by high performance thin layer chromatography (HPTLC) using Automatic TLC Sampler 4, AMD 2 development chamber and TLC scanner 3 (Camag, Muttenz, Switzerland) according to

Farwanah et al. [136]. Integration and quantification based on peaks areas were performed using CATS software (Camag).

The size and stability of prepared ULVs (1% w/w of lipids in buffer) was checked by photon correlation spectroscopy using a particle size analyser (Malvern HPPS-ET, Malvern Instruments, UK). The measurements were carried out at 32 °C. The hydrodynamic radius and the polydispersity have been calculated from the correlation function by the CONTIN algorithm using the HPPS-Malvern program for dispersion technology and light scattering systems.

5.2.4 Small angle X-ray diffraction

Small angle X-ray diffraction (SAXD) data were collected on the Soft Condensed Matter beamline A2 of HASYLAB at the storage ring Doris III of the Deutsches Elektronen Synchrotron. A two-dimensional CCD detector was used for data acquisition. The MLVs with 20% (w/w) lipid concentration in Tris or Bis-tris buffer with 100 mM sodium chloride were measured ten days after preparation at 32, 85, and 32 °C again in specially designed copper cells with a polyimide-foil (Kapton[®], DuPont, Luxembourg) window (50 µl in volume). The sample-to-detector distance was 585 mm and the X-ray wavelength was 1.5 Å. The acquisition time of each sample was 3 minutes. Silver behenate and rat tendon tail collagen were used for calibration. Prior to each measurement, the sample was allowed to equilibrate for 5 minutes.

The data evaluation was carried out using the FIT2D software. The scattering intensity was measured as a function of scattering vector, q . The latter is defined as $q = (4\pi/\lambda) \sin \Theta$, where 2θ is the scattering angle and λ is the X-ray wavelength. The lamellar repeat distance, D , was calculated from the first order diffraction peak according to $D = 2\pi/q$. Using a Lorentzian function, the diffraction peaks were fitted to determine the exact positions. This function was chosen instead of the usual Gaussian one because of the higher fit accuracy.

A STOE STADI-IV diffractometer (Stoe and Cie, Darmstadt, Germany) equipped with CuK α radiation (wavelength 1.54 Å) and a linear position sensitive detector was used to measure the samples about 3 hours after the preparation. The samples were placed in a quartz capillary and measured in a transmission geometry at 20 °C with the 2Theta angle moving between 0 to 6 degrees for two hours.

5.2.5 Small angle neutron scattering

The ULVs with 1% (w/w) lipid concentration in Tris buffer in D₂O adjusted to the pH=9 of a water buffer were measured at the neutron wavelength of 8.1 Å at the SANS 1 spectrometer of the Geesthacht Neutron Facility, GKSS Research Centre, Germany. To receive scattering curves in a broad q-range, four sample-to-detector distances of 70.5, 180.5, 450.5, and 970.5 cm were used. The data were collected at 32 °C. The acquisition time at 70.5 cm was 1 hour, at other sample-to-detector distances 0.5 hour. For background subtraction, the scattering curve of the relevant buffer has been used, which was measured on the same way as the sample.

The analysis of the SANS curves has been achieved using two methods, namely the ‘model of separated form factors’ [96], and the Kratky-Porod analysis of the Guinier approximation [97,98,99].

The average excess scattering-length density per unit mass ($\Delta\rho_m$) of the lipid mixture in D₂O was determined from the known chemical composition [168]. The calculated values are listed in Table 5.2.

Table 5.2 The average excess scattering-length density ($\Delta\rho_m$) of the lipid mixtures in D₂O calculated per 1g of lipids.

Mixture	$\Delta\rho_m * 10^{10}$ [cm ³ *g ⁻¹]
I (10% CHOL)	-6.198
II (15% CHOL)	-6.189
IV (25% CHOL)	-6.170
V (30% CHOL)	-6.159

5.2.6 Molecular modelling

In order to determine the average excess scattering-length density per unit mass, the molecular volumes were calculated by Dr. Karel Palát (Faculty of Pharmacy, Charles University, Prague). Quantum-chemical calculations were run on a PC computer using software HyperChem for Windows v. 7.1, Hypercube Inc. The models of compounds were formed on RHF/AM1 level. The conformation of Cer[AP] with parallel aliphatic chains calculated as described previously [169] was used. Solvent accessible volumes, V_{SA} , of models of studied compounds were calculated via the grid method [170] using the atomic radii of Gavezzotti [171]. The solvent probe radius 0.4 Å and 20 points on the cube side were used.

The obtained V_{SA} -values of one molecule amount to 990.59 and 666.86 Å³ for Cer[AP] and CS, respectively. The volumes of CHOL and PA are 617.12 and 450.27 Å³, respectively.

The values are comparable with literature data obtained from volumetric measurements [172, 173].

5.3 Results

5.3.1 Small angle X-ray diffraction on MLVs

5.3.1.1 Influence of cholesterol on the SC lipid model system

Fig. 5.1 shows the diffraction patterns of the SC lipid model MLVs with 10 and 25% CHOL (mixtures I and IV, respectively) measured three hours after the preparation. The samples show only one diffraction peak at 0.137 \AA for 25% CHOL and 0.131 \AA for 10% CHOL, which indicates one phase with the lamellar repeat distance of 45.9 \AA and 48.0 \AA , respectively.

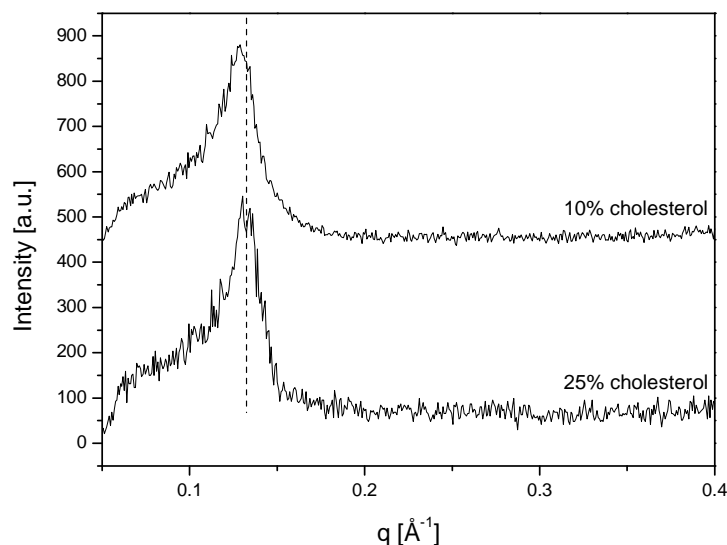


Fig. 5.1 X-ray diffraction patterns from the systems with 25 and 10% CHOL measured three hours after the sample preparation.

The diffraction patterns of the SC lipid model systems measured on the synchrotron ten days after the sample preparation with various CHOL concentrations are given in Fig. 5.2 a, b, and c. The obtained results are summarized in Table 5.3.

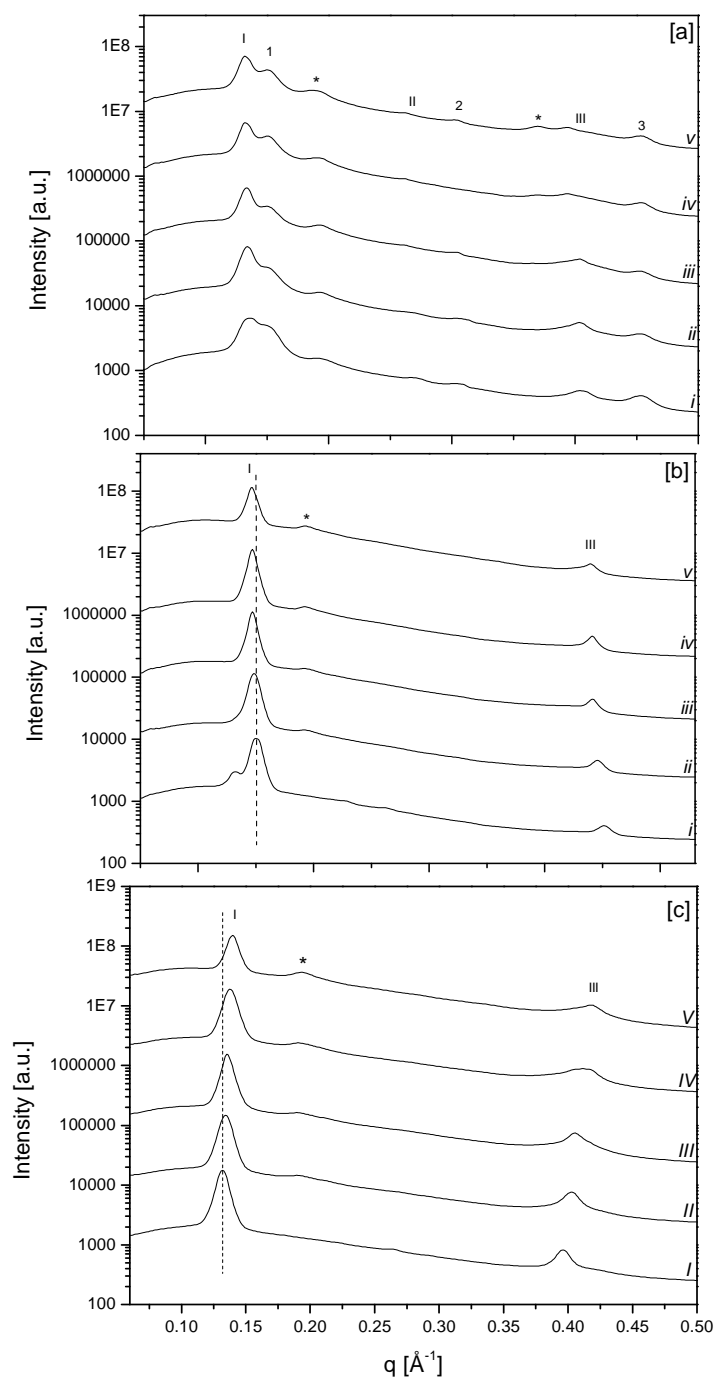


Fig. 5.2 X-rays diffraction patterns of the SC lipid model system with various CHOL concentrations; 20% of lipids in Tris buffer (pH=9) at [a] 32 °C before heating, [b] 85 °C, and [c] 32 °C after heating. From bottom to top: (i) 10% cholesterol, (ii) 15% cholesterol, (iii) 20% cholesterol, (iv) 25% cholesterol, and (v) 30% cholesterol. The Arabic numerals label the particular reflections of the S-phase; the Roman numerals label the particular reflections of the L-phase; the asterisks label the CHOL monohydrate reflections.

At 32 °C before heating, the diffractograms are quite complex (Fig. 5.2a). The positions of the diffraction peaks indicate that the systems are separated into two lamellar phases, namely a 'short' one (the S-phase) with the lamellar repeat distance of about 42 Å and a 'long' one (the L-phase) with the lamellar repeat distance of about 47 Å. Both phases induce three diffraction orders in the diffractograms. It is apparent in Fig. 5.3 that with increasing CHOL content from 10 to 30% the calculated periodicity of the L-phase increases slightly from 46.7 ± 0.2 Å to 47.5 ± 0.2 Å, whereas the periodicity of the S-phase remains almost unchanged.

Table 5.3 Lamellar repeat distances calculated from the X-ray diffraction patterns for the mixtures 1-5. The Roman numerals in brackets describe the particular reflections.

Sample (CHOL content)	Lamellar repeat distance [Å] (reflections [Å ⁻¹])		
	32 °C before heating	85 °C	32 °C after heating
Mixture I (10%)	33.6 (I: 0.187) 41.7 (I: 0.151; II: 0.306; III: 0.453) 46.7 Å (I: 0.135; II: 0.272; III: 0.405)	41.8 (I: 0.150; III: 0.451)	47.6 Å (I: 0.132; III: 0.397)
Mixture II (15%)	33.6 (I: 0.187) 41.8 (I: 0.150; II: 0.309; III: 0.454) 47.0 (I: 0.134; II: 0.267; III: 0.405)	33.6 (I: 0.187) 42.3 (I: 0.149; III: 0.446)	33.6 (I: 0.187) 46.9 (I: 0.134; III: 0.403)
Mixture III (20%)	33.6 (I: 0.187) 41.9 (I: 0.150; II: 0.304; III: 0.454) 47.2 (I: 0.133; II: 0.265; III: 0.404)	33.6 (I: 0.187) 42.7 (I: 0.147; III: 0.441)	33.6 (I: 0.187) 46.3 (I: 0.136; III: 0.408)
Mixture IV (25%)	33.6 (I: 0.187; II: 0.370) 41.9 (I: 0.150; III: 0.455) 47.3 (I: 0.133; III: 0.396)	33.6 (I: 0.187) 42.7 (I: 0.147; III: 0.441)	33.6 (I: 0.187) 45.5 (I: 0.138; III: 0.413)
Mixture V (30%)	33.6 (I: 0.187; II: 0.370) 41.9 (I: 0.150; II: 0.306; III: 0.455) 47.5 Å (I: 0.132; II: 0.263; III: 0.394)	33.6 (I: 0.187) 42.8 (I: 0.147; III: 0.439)	33.6 (I: 0.187) 44.9 (I: 0.140 Å; III: 0.419)

In all the samples, a small peak is detectable at 0.187 Å⁻¹. This peak position corresponds to a repeat distance of 33.6 ± 0.1 Å and was assigned to crystalline CHOL monohydrate [174]. The peak intensity increases with the increasing concentration of CHOL in the mixture,

while the position is stable. In the diffractograms of the samples with 25 and 30% CHOL even more diffraction orders of crystalline CHOL monohydrate are detectable.

When the systems are heated to 85 °C (Fig. 5.2b), the S- and L-phases merge into one phase, whose repeat distance increases with the CHOL content from 41.8 ± 0.2 Å for the sample with 10% CHOL to 42.8 ± 0.2 Å for the sample with 30% CHOL (Fig. 5.3). Regarding the peak at 0.187 \AA^{-1} , a small amount of crystalline CHOL is still present particularly in the samples with higher CHOL concentrations.

When the samples are cooled back to 32 °C, they show only one lamellar phase (Fig. 5.2c). This phase is strongly affected by the concentration of CHOL in the system. The periodicity decreases almost linearly with increasing CHOL concentration from 47.6 ± 0.2 Å for 10% CHOL to 44.9 ± 0.2 Å for 30% CHOL (Fig. 5.3). The peak belonging to crystalline CHOL is slightly observable especially in the samples with higher CHOL content.

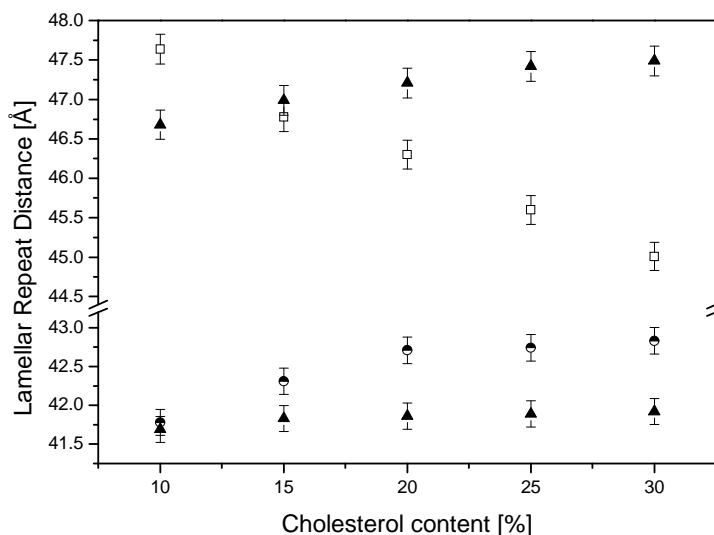


Fig. 5.3 Lamellar repeat distance of the SC lipid model system with various CHOL concentrations measured at 32 °C before heating (filled triangles), 85 °C (partly filled circles), and 32 °C after heating (open squares). The repeat distance was calculated using a Lorentzian function to fit the first order of diffraction.

The recovery of the system with 25% CHOL (mixture IV) into the initial state has been studied further. Fig. 5.4 shows the X-ray diffraction patterns of the sample measured 20 minutes, 1 day, and 10 days (the initial measurement) after the heating. 20 minutes after the heating, there is one diffraction peak at 0.138 \AA^{-1} , which indicates one phase with 45.5 Å.

One day later, the sample still shows only one peak at 0.136 \AA^{-1} which corresponds to the D-value of 46.2 \AA . The diffractogram measured 10 days after the heating shows two peaks indicating the phase separation into the S- and L- phase.

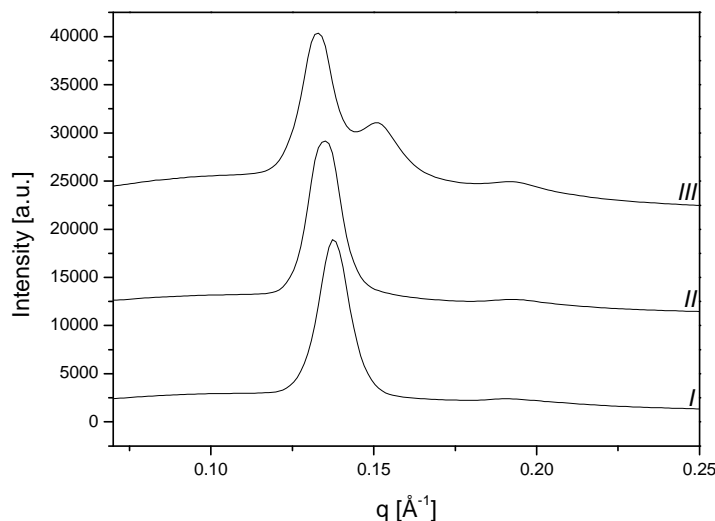


Fig. 5.4 The recovery of the system with 25% CHOL (mixture IV) into the phase-separated state. From bottom to top: system measured (i) 20 minutes after the heating, (ii) 1 day after the heating, (iii) 10 days after the heating.

5.3.1.2 SC lipid model system measured at various pH values

The diffraction patterns of the MLVs with 25% CHOL (mixture IV) in various pH-environments measured 10 days after the sample preparation are shown in Fig. 5.5a, b, and c. All the samples show the same phase separation effect, namely two phases and crystalline CHOL before the heating, the mixing effect at higher temperatures, and one phase after heating with a trace amount of crystalline CHOL. The peak positions at each temperature measured do not change with pH variation. Fig. 5.6 shows the calculated lamellar repeat distances of the samples. It has been found that the pH value of the environment influences neither the D-values nor the peak intensities.

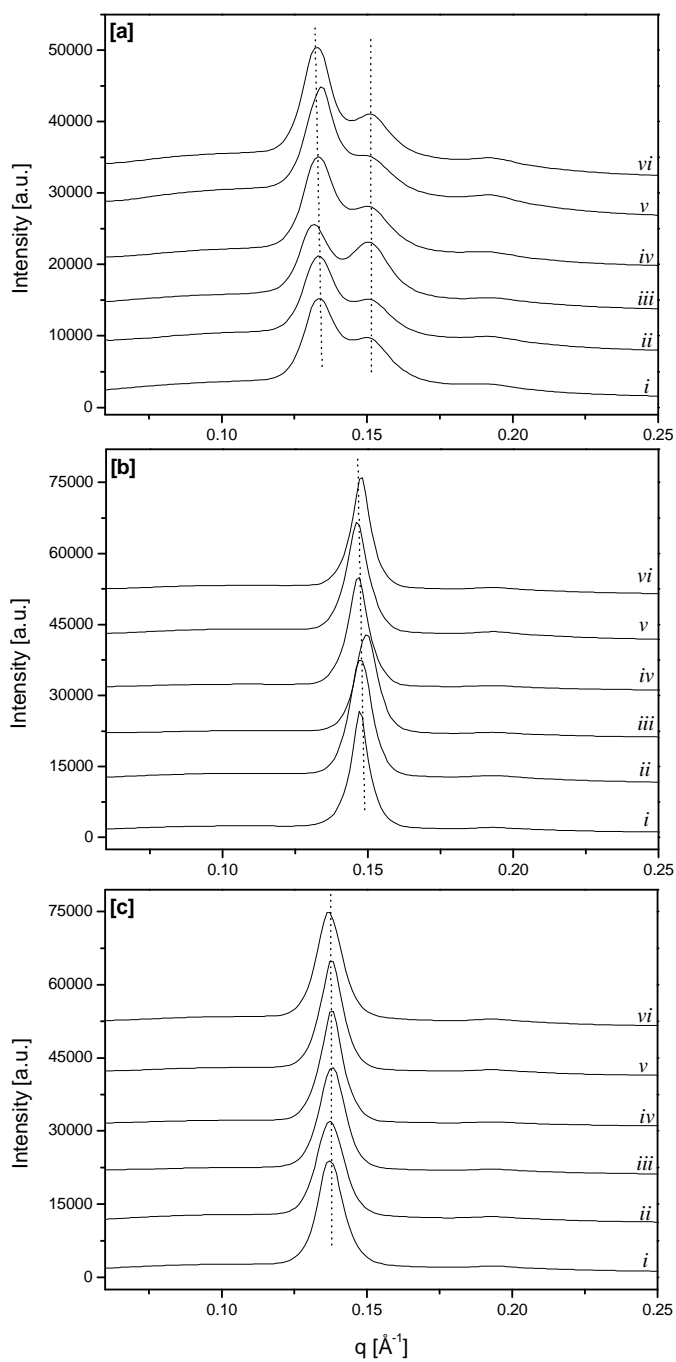


Fig. 5.5 X-rays diffraction patterns of the SC lipid model system in various pH environments measured 10 days after the sample preparation at [a] 32 °C before heating, [b] 85 °C, and [c] 32 °C after heating. From bottom to top: (i) pH = 6.0 (in Bis-tris buffer), (ii) pH = 6.6 (in Bis-tris buffer), (iii) pH = 7.2 (in Tris buffer), (iv) pH = 7.8 (in Tris buffer), (v) pH = 8.4 (in Tris buffer), and (vi) pH = 9.0 (in Tris buffer).

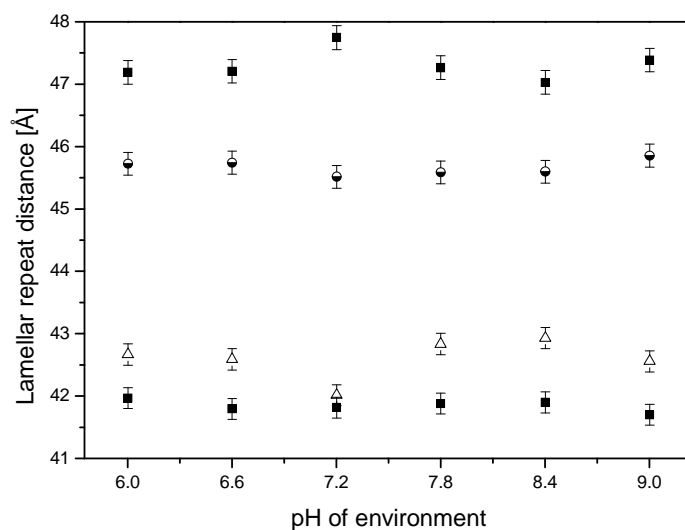


Fig. 5.6 Lamellar repeat distance of the SC lipid model system in various pH environments measured at 32 °C before heating (filled squares), 85 °C (open triangles), and 32 °C after heating (partly filled circles). The repeat distance was calculated using a Lorentzian function to fit the first order of diffraction.

5.3.2 Characterization of ULVs

The HPTLC analysis of the lipids in the ULV and MLV samples confirms that the substances are stable during the sample preparation and shows that the CHOL content was slightly reduced after the extrusion. The concentration of CHOL in the ULVs is given in brackets in Table 5.1. The difference in the proportions of the other lipids in MLVs and ULVs was negligible.

According to DLS studies, all the ULV samples showed a monomodal population

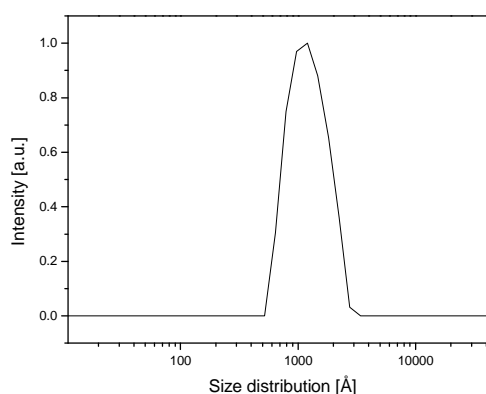


Fig. 5.7 The size distribution of the mixture IV (25% cholesterol); 1% (w/w) of lipids in D₂O buffer extruded through 500 Å filters.

with an average hydrodynamic radius between 550 - 650 Å and a polydispersity of about 30%. Fig. 5.7 shows the size distribution of the sample with 25% CHOL (mixture IV). No influence of CHOL concentration in the system on the hydrodynamic radius and the polydispersity was found. The ULVs were stable for at least 7 days at pH 9 and laboratory temperature.

5.3.3 Small angle neutron scattering from ULVs

Fig. 5.8a shows the neutron scattering curves of the ULVs with various CHOL concentrations. No diffraction peak of a multi- or oligolamellar arrangement or of a crystalline CHOL phase as in the case of MLVs is present.

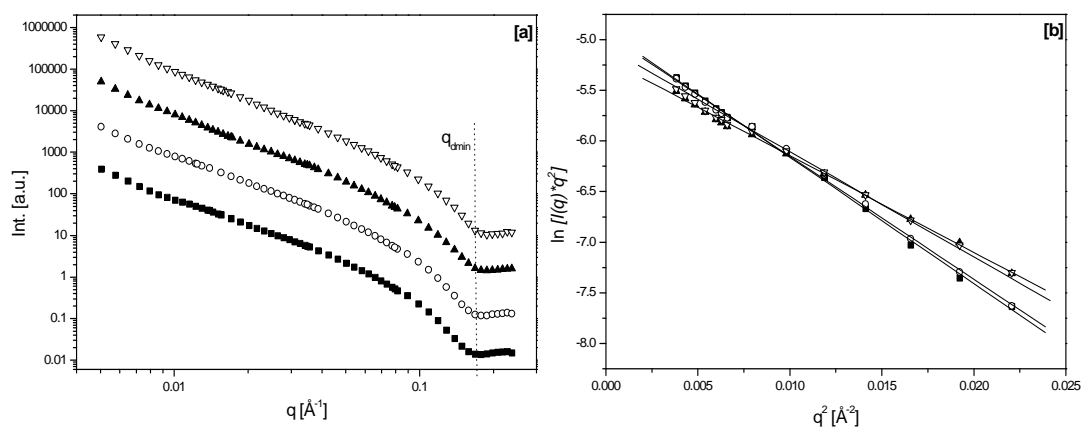


Fig. 5.8 [a] Neutron scattering curves of the SC lipid model system with various CHOL concentrations. The dashed line is a guide to the eye in order to emphasize the shift in the q_{dmin} position. From bottom to top: 10% CHOL (filled squares), 15% CHOL (open circles), 25% CHOL (filled triangles), and 30% CHOL (open triangles). [b] The corresponding Kratky-Porod plots of the SANS curves (Legend: as [a]).

The minimum of the membrane thickness, q_{dmin} , is distinct at about 0.18 Å⁻¹ and shifts its position to higher q -values with the increasing CHOL content. The membrane thickness parameters, d , calculated from the minimum q_{dmin} according to the model of separated form factors with an accuracy of 5% amount to 36.9 Å, 36.4 Å, 35.3 Å, and 34.6 Å for mixtures I (9% CHOL), II (14% CHOL), IV (20% CHOL), and V (27% CHOL), respectively (Fig. 5.9a).

The Kratky-Porod plots of the measured scattering curves (Fig. 5.8b) show a linear area in the q -range between 0.06 and 0.14 Å⁻¹. The slopes of the plots, which correspond to the square of the radius of gyration, decrease with increasing concentration of CHOL in the

samples. The membrane thickness parameters, d_g , calculated from the R_g values show the same tendency and amount to 38.7 ± 0.8 , 38.2 ± 0.8 , 35.3 ± 0.7 , and 33.9 ± 0.7 Å for mixtures I (9% CHOL), II (14% CHOL), IV (20% CHOL), and V (27% CHOL), respectively (Fig. 5.9a).

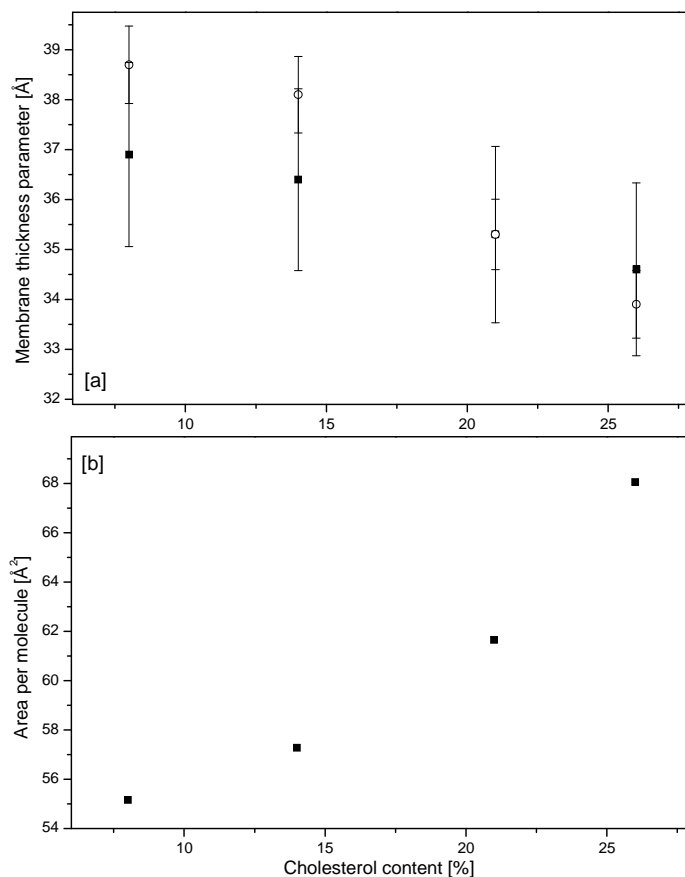


Fig. 5.9 [a] Membrane thickness parameter of the SC lipid model system in the dependence of CHOL concentration calculated from the scattering curves as d according to the ‘model of separated form factors’ (filled squares) and d_g according to the Guinier approximation (open circles). [b] Average area of membrane surface per molecule in the dependence of CHOL concentration.

The average area per molecule A of the membrane surface has been calculated from the $I(0)$ values. The determined A -values are 55.16, 57.27, 61.65, and 68.05 Å² for mixtures I (9% CHOL), II (14% CHOL), IV (20% CHOL), and V (27% CHOL), respectively. Because the molar volumes were determined by the molecular modelling and not by real measurements, a statistical error can affect the results partway; however, the tendency that the increasing CHOL concentration increases the area per molecule of the membrane surface is obvious (Fig. 5.9b).

The minimum, q_{Rmin} , related to the average vesicle radius, is not visible in the scattering curves in any of the samples measured.

The data obtained from the SANS measurements are summarized in Table 5.4.

Table 5.4 Membrane parameters of the SC lipid model systems in dependence of CHOL concentration calculated from the scattering curves according to the ‘model of separated form factors’ and the Guinier approximation.

Evaluation method	Model of separated form factors		Guinier approximation		
	System	$q_{dmin} [\text{\AA}^{-1}]$	$d [\text{\AA}]$	$R_g^2 [\text{\AA}^2]$	$d_g [\text{\AA}]$
I (10 / 8.6)*	0.170±0.009	36.9±1.9	124.7±2.5	38.7±0.8	55.16
II (15 / 14.2)*	0.172±0.009	36.4±1.8	121.3±2.4	38.2±0.8	57.27
IV (25 / 21.6)*	0.178±0.009	35.3±1.8	103.7±2.1	35.3±0.7	61.65
V (30 / 27)*	0.181±0.009	34.6±1.7	95.5±1.9	33.9±0.7	68.05

* % of cholesterol before and after extrusion.

5.4 Discussion

This study introduces SANS on ULVs into the methods for the characterization of the SC lipid membranes. In order to carry out those measurements successfully, it was important to prepare stable unilamellar vesicles of a SC lipid model system. The composition was chosen according to previous studies [166,167]. To create stable ULVs, high pH values of the environment are mandatory [166,175]. At pH = 9, the charged components (PA and CS in the present system) are fully ionized. Due to this, vesicles can be extruded without a loss of lipids. Contrary to ULVs prepared at pH = 6, vesicles prepared at pH = 9 have been found to be stable for 4-6 weeks [166]. A decrease in the pH to 6 activated vesicle fusion and lysis [176]. Because the SANS measurements take quite a long time (several days), stable ULVs are needed. For this reason, samples with high pH values of the environment were used for SANS.

The SAXD experiments were carried out at the same pH as the SANS to make an easy comparison possible. Because pH of the skin is much acid (about 5.5), an additional experiment of the pH influence on the lamellar repeat distance was carried out. These measurements should describe how extensive are the differences in the data obtained at various pH values.

The SAXD measurements demonstrate that the SC lipid model system shows a complex phase behaviour. Immediately after the preparation, the MLVs show one phase with the lamellar repeat distance of 45.9 Å and 48.0 Å for 25 and 10% CHOL, respectively.

The measurements carried out ten days after the sample preparation indicate that the systems separated into three phases with the repeat distances of about 33.6, 42, and 47 Å during this time.

The phase with a repeat distance of 33.6 Å has been assigned to CHOL separated into CHOL monohydrate crystals [174]. This separation of CHOL from membranes was often described previously in SC model systems of synthetic [177] or isolated lipids [178,179], even in the neat SC [31].

The S-phase with a periodicity of about 42 Å was difficult to interpret. A similar phase separation was observed in other studies [180], where, besides the phase-separated CHOL, two other phases with a periodicity of about 54 and 41 Å, respectively, were described, too. The L-phase detected in our system has a lamellar repeat distance of about 47 Å; the longer phase in the article mentioned above has a periodicity of 54 Å. The difference in the lamellar repeat distance between these phases can be attributed to the differences in the chain lengths of the ceramides used. The periodicity of the S-phase of about 41 Å is nearly the same as in our case. The phase separation into the L- and S- phase indicates very limited miscibility between the membrane components at low temperatures. Formation of separated free fatty acid- and ceramide-rich domains has been described in SC lipid model mixtures [41,43,161,181] and confirms the domain mosaic SC organization proposed by Forslind [45]. According to the published IR data [41,162], the hydrocarbon chains of both phases should exhibit a highly ordered arrangement.

We suppose that the S-phase in our system is composed mainly of PA, a free fatty acid with a relatively short chain. It was described that while fatty acids with C14-18 chains can induce such a phase separation in a system of isolated SC lipids, the longer fatty acids (C20-26) are fully miscible with the other membrane components [32]. This phenomenon has been interpreted by the mismatch in chain lengths of fatty acids and ceramides. Interestingly, a similar effect occurs in our study although the chain length of the ceramide used is comparable with the chain length of PA. Thus, the phase separation observed

seems not to be connected only with the differences in the chain lengths but also with some other effect. It is possible that the phases can separate e.g. due to the repulsion forces between the ionized and unionized components in the system.

It is difficult to define from the present data whether the S-phase includes only the neat PA or also other components of the mixture. Nevertheless, the content of CHOL incorporated in the S-phase is probably very limited, because only a minimum influence of the CHOL concentration on the lamellar repeat distance of the S-phase has been detected. Furthermore, a low degree of miscibility between free fatty acid and CHOL has been described [162].

Comparing our results with previous studies [32], a striking difference can be found. While the cited paper reports that all the observed changes are thermally fully reversible, our system shows a mixing effect during the heating, which persists when the sample is cooled down. The phase arising after the heating is stable at room temperature for at least one day.

The results of the SAXD measurements of the SC lipid model at various pH are somewhat unexpected. The pH value of the environment shows neither an influence on the lamellar repeat distance nor on the phase separation effect. This finding is very interesting, because other studies have shown a strong influence of pH on the repeat distance of SC lipid membranes [107]. However, these authors used ceramides isolated from native SC, which contained ceramide 1 [EOS], too. Ceramide [EOS] was found to be responsible for the formation of the so-called 'long periodicity phase' (LPP) with a periodicity of about 130 Å [36]. In our systems, only a phase comparable with the so-called 'short periodicity phase' (SPP) was present. It seems that the LPP can be strongly affected by the pH of the environment, but the SPP is not. This assumption is also in accordance with Bouwstra [178], who described a similar effect for systems with pH values between 5 and 7.4.

The influence of CHOL concentration on the membrane structure has been studied. The well-mixed system originating after heating shows a high sensitivity of the lamellar repeat distance on the CHOL content. In the concentration range used, the periodicity of the lamellar phase decreases with increasing content of CHOL in the system. This dependence seems to have a linear tendency. A similar effect has been described elsewhere [36]. Moreover, our results show that in the liquid-crystalline phase (L_{α}) (at 85 °C), CHOL contrarily increases the periodicity. This fact excludes the possibility that CHOL decreases the membrane thickness only because its molecule is smaller than that of the long-chain components.

The effect of CHOL on the hydration of the polar head groups of the membrane is improbable, too. If the change of water layer between the membranes would be

responsible for the decreasing periodicity with increasing CHOL content, the real membrane thickness would not change as it has been detected by SANS. Furthermore, the water layer between the membranes was described to be extremely thin (about 0.8 Å under full hydration) in comparison to other biological membranes [182].

The most probable explanation of the CHOL effect on the membrane properties is that at 32 °C, CHOL decreases the order of the well ordered hydrocarbon chains which causes a higher fluidity in the membrane. This is accompanied by the decrease in the membrane thickness. Also the finding that the area per molecule of the membrane surface increases with the increasing CHOL concentration in the system supports our hypothesis. The increasing area/molecule of the membrane surface can indicate that the intermolecular interactions between the particular lipids (H-bonds in the head group region) weaken which is again connected with the increase in the membrane fluidity. This is in accordance with other authors [183]. It is also possible, that CHOL plays a role in the interdigitation and/or tilting of the hydrocarbon chains to the base plane of the membrane.

On the contrary, in the L_{α} -phase, CHOL increases the periodicity, which is a consequence of the increasing chain order. A similar hypothesis was proposed in a previous study [161].

The question is why CHOL does not show this effect in the phase-separated state with well-ordered chains before heating. The S-phase is almost not affected and the periodicity of the L-phase increases slightly with increasing CHOL content. It can be connected with the fact that in this state, a considerable portion of CHOL is separated into CHOL monohydrate crystals and the CHOL amount incorporated in the other phases is limited. Because of the phase-separation, different interactions between the incorporated CHOL and the other components seem to arise as in the mixed state. Due to this, the function of CHOL in this state can be different.

As mentioned above, the SANS measurements enabled us to determine the membrane thickness and to confirm that it decreases with increasing CHOL concentration in the membrane. The minimum at q_{Rmin} related to the average vesicle radius which is normally observable in SANS curves of phospholipid vesicles [101,184], did not occur in the scattering curves in any of the samples measured. This indicates that the vesicle radii of the SC lipid ULVs are larger than the detection limit of the SANS measurements (about 600 Å). This fact implies that the SC lipid model membrane is more rigid than that of phospholipid systems, because the membrane properties do not allow to create a higher curvature. Interestingly, the hydrodynamic vesicle radius according to DLS data was also found to be about 600 Å. For comparison, DMPC vesicles show a much larger hydrodynamic radius revealed by DLS as the radius measured by SANS [143,184]. The

difference is due to the hydration layer on the vesicle surface. The fact that the SC lipid model vesicles do not show a difference between both radii suggests that the hydration layer on the vesicle surface is minimal.

5.5 Conclusions

The present study describes the phase behaviour of SC lipid model membranes in MLVs and ULVs. The influence of CHOL and pH on the lamellar repeat distance has been studied. Immediately after the sample preparation, the membranes show one lamellar phase. During next days, the systems separate into three phases, one with a lamellar spacing of 33.6 Å consists predominantly of crystalline CHOL. The other two phases with a periodicity of 41.5 Å and 46.5 Å, respectively, are barely affected by variation of the CHOL content in the membrane. Due to heating the systems over the main phase transition temperature, the different phases merge into one with a periodicity of about 42.5 Å. This value increases slightly with increasing CHOL concentration. After heating, the lipids remain in one phase with a periodicity of about 45.5 Å in the membrane. The lamellar spacing of this phase decreases with increasing CHOL concentration. Surprisingly, there is no influence of the pH value on the periodicity at each temperature measured.

SANS on ULVs seems to be a powerful method for the SC lipid research, which allows one to determine the membrane thickness parameter and the area of the membrane surface per molecule. An increase in CHOL concentration in the membrane causes a reduction of the membrane thickness as well as in the membrane density.

The present data support the hypothesis that CHOL decreases the order of the well ordered hydrocarbon chains in the state below the main phase transition and increases the order of chains in the liquid crystalline phase.

6 Thermotropic phase behaviour of a SC lipid model system in the variation of cholesterol concentration

6.1 *Introduction*

This study follows the experiments presented in Chapter 5 and is aimed at describing the thermotropic phase behaviour of the SC lipid system. The presented results should contribute to elucidate the role of CHOL in the lipid miscibility and in the phase separation effect in more detail.

Two methods, DSC and SAXD on MLVs are used.

6.2 *Methods*

6.2.1 **Material and sample preparation**

Cer[AP] was a gift from Cosmoferm (Delft, The Netherlands). Cholesterol (CHOL), cholesterol sulphate (CS), and palmitic acid (PA) were purchased from Sigma-Aldrich (Taufkirchen, Germany). Water, chloroform and methanol used were of HPLC grade. The MLVs were prepared as described in Chapter 5.2.2. The compositions of the prepared samples are listed in Table 5.1.

6.2.2 **Differential scanning calorimetry**

The MLVs with 20% lipids in water (w/w) were measured in the temperature range from 10 °C to 85 °C with a differential scanning calorimeter DSC 200 (Netzsch Gerätebau, Selb,

Germany) with an empty cell as reference. The scan rate was 5 K min⁻¹. Transition temperatures were inferred from peak onset temperatures using the Netsch software. The samples were prepared one week before the measurement and stored at 5 °C.

6.2.3 Small angle X-ray diffraction

The time-resolved X-ray diffraction patterns from the MLVs (10% of lipids w/w in water) in the small-angle region were collected on the D22 line at DCI synchrotron source (LURE, Orsay, France) at the wavelength of 1.39 Å. The samples were placed in a quartz capillary. The linear position sensitive detector was arranged in the sample-to-detector distance of 1813 mm. The heating rate was 1 K min⁻¹. The diffraction patterns were acquired every 60 s. Known samples of DMPC and DPPC were used as standards for calibration.

The obtained diffraction peaks were fitted with Gaussian functions in order to minimize the statistical error. The lamellar repeat distance was calculated from the position of the first diffraction peak according to: $D = 2\pi/q$.

6.3 Results

6.3.1 Differential scanning calorimetry

The thermograms of the SC lipid MLVs with various CHOL content acquired during the first and second heating are shown in Fig. 6.1. The mixture with 15% CHOL exhibits a relatively sharp endothermic peak with an onset at 68.5 °C during the first heating. Presumably, the peak represents the main phase transition from gel to liquid crystalline phase that is connected with the decrease in the hydrocarbon chains order. With the increasing CHOL concentration in the system, the onset temperature of the main phase transition decreases and the peak broadens, the offset temperature remaining constant. In the systems with 25 and 30% CHOL, at least two peaks with the onset temperatures at about 44 and 60 °C, respectively, are detectable.

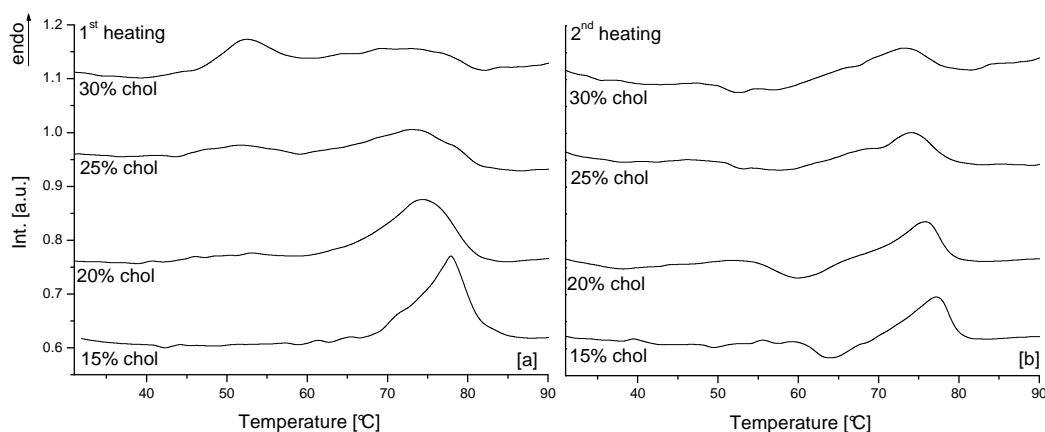


Fig. 6.1 The DSC-curves of the SC lipid MLVs with various CHOL concentrations acquired during the [a] first and [b] second heating.

During the second heating (Fig. 6.1b), the phase behaviour has a considerably different progress. In all the samples, the main phase transition is observable; however, almost no shift in the onset value of the main phase transition can be detected. On the other hand, an exothermic transition foregoing the main phase transition is detectable in all the DSC curves. This transition has its onset at about 60 °C for the mixture with 15% CHOL and 49.5 °C for the mixture with 30% CHOL.

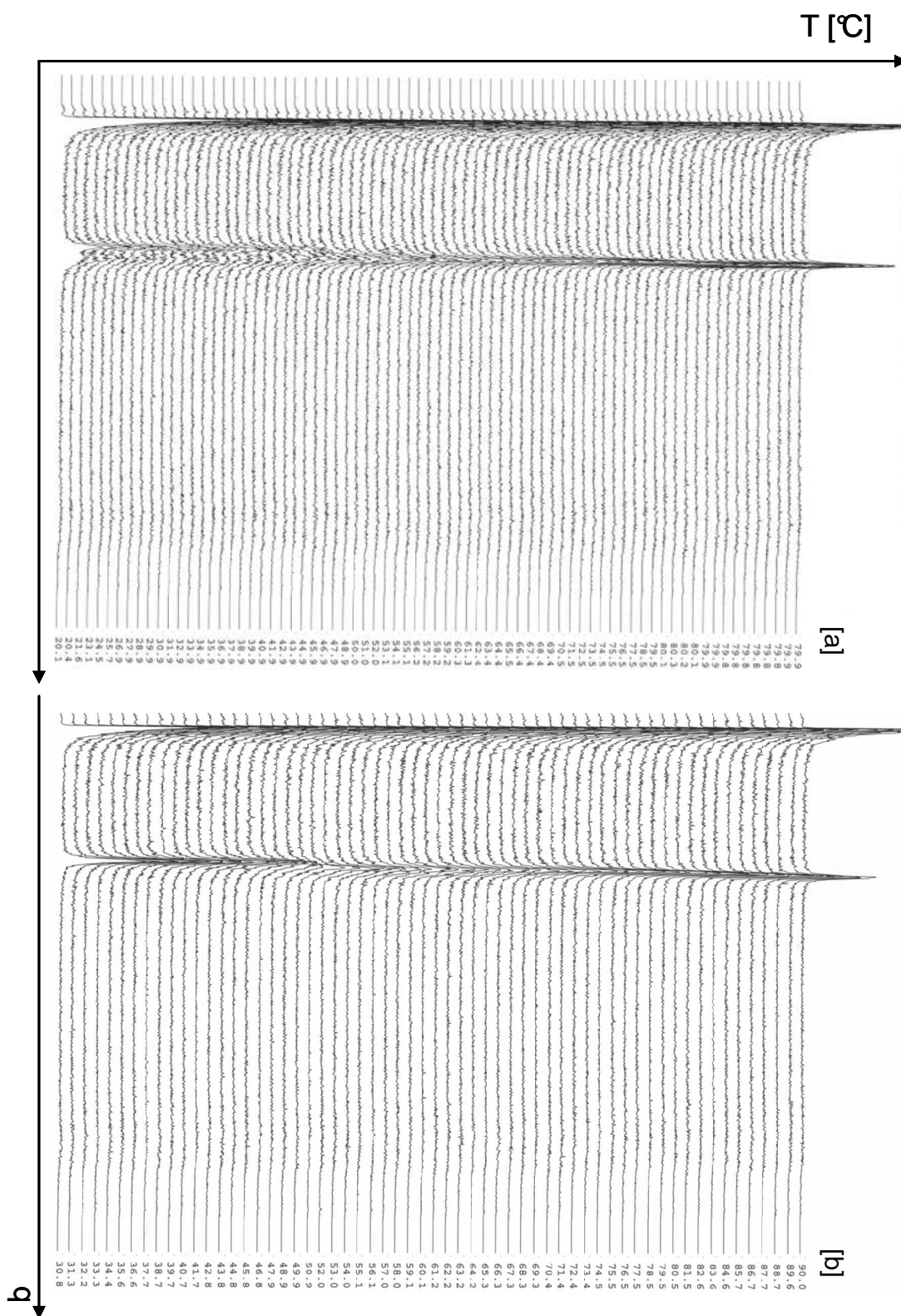


Fig. 6.2 The X-ray diffraction patterns from the SC lipid MLVs with 25% CHOL acquired during the [a] first and [b] second heating.

6.3.2 Small angle X-ray diffraction

6.3.2.1 The basic sample with 25% CHOL

Fig. 6.2 shows the X-ray diffraction patterns from the system containing 25% CHOL measured during the first and second heating. The lamellar repeat distance has been calculated from the position of the diffraction peaks according to $D = 2\pi/q$ and is plotted as a function of temperature in Fig. 6.3. Similarly to the previous SAXD measurements, the MLV membrane shows a separation into two phases with the D-values of 46.5 (the L-phase) and 42.8 Å (the S-phase) at 32 °C before heating. With the increasing temperature, the periodicity of the L-phase continuously decreases while that of the S-phase slightly increases. A dramatic change is distinct at about 46 °C when the phases merge suddenly into another one with a periodicity of 43.4 Å. This phase seems to be stable till approximately 70 °C when the periodicity starts to decrease continuously, which indicates the main phase transition to the liquid-crystalline phase.

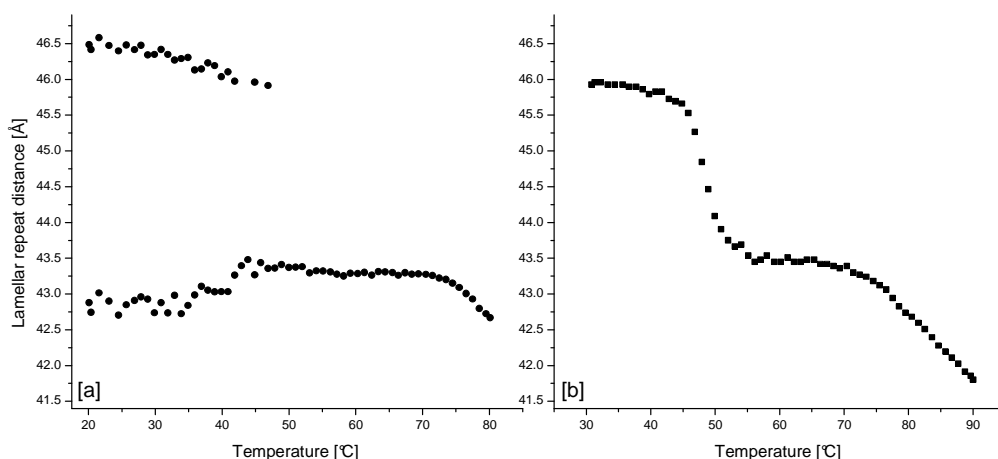


Fig. 6.3 Evolution of the lamellar repeat distance of the MLVs with 25% CHOL during the [a] first and [b] second heating.

After cooling the system back to 30 °C, one phase is distinct with a periodicity of 45.9 Å. During the second heating, the phase shows a very slight decrease in its periodicity till 45 °C. Between 45 and 53 °C, the D-value decreases abruptly to about 43.6 Å. This new phase is then stable till 70 °C. Above this temperature, the hydrocarbon chains start to melt, which causes a decrease in the periodicity.

6.3.2.2 The influence of CHOL on the thermotropic phase behaviour

Fig. 6.4 shows the evolution of the lamellar repeat distance during the first heating for the samples containing 30 and 25% CHOL. At 32 °C, the sample with 30% CHOL is separated into two phases with similar D-values as in the sample with 25% CHOL. At about 40 °C, a phase transition can be observed. However, no mixing of the phases as in the sample with 25% CHOL occurs during this transition. While the S-phase increases in the periodicity to about 43 Å, the periodicity of the L-phase increases to 48.3 Å. Both phases mix together first only at 70 °C when the melting of the hydrocarbon chains starts.

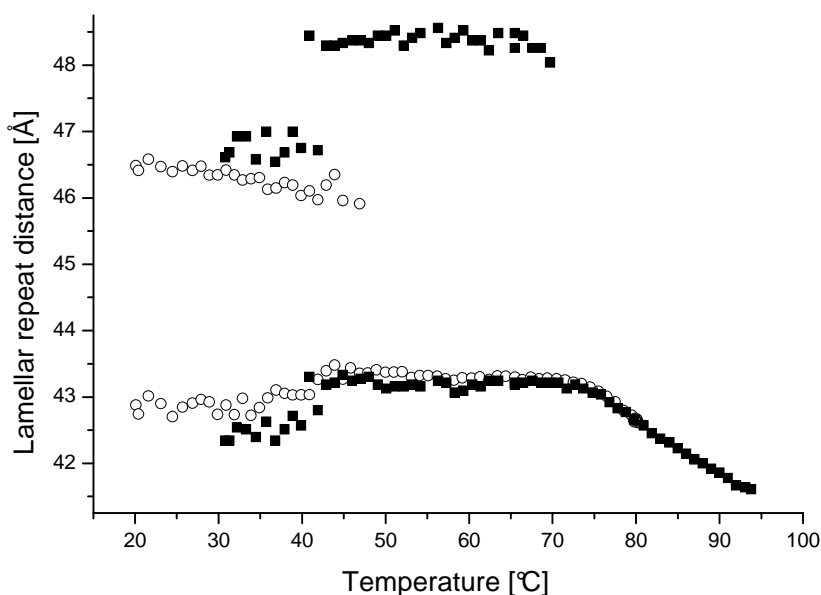


Fig. 6.4 Evolution of the lamellar repeat distance of the MLVs with 25% (open circles) and 30% (filled squares) CHOL during the first heating.

The evolution of the lamellar repeat distance during the second heating of the samples with various CHOL concentrations is presented in Fig. 6.5. At 32 °C, only one phase is detectable in all the samples. In the samples containing 25 and 30% CHOL, the evolution of the lamellar repeat distance shows a similar behaviour with increasing temperature. In both cases, the first phase transition arises at about 45 °C when the periodicity decreases from approx. 46 to 43.5 Å. The resulting phase is stable till 70 °C when the hydrocarbon chains start to melt and the main phase transition occurs.

The thermotropic phase behaviour of the samples with 15 and 20% CHOL is significantly different in comparison with the other samples. In both cases, only one broad transition is detectable. At about 57 °C, the lamellar repeat distance starts to decrease continuously till the end of the measurement (94 °C).

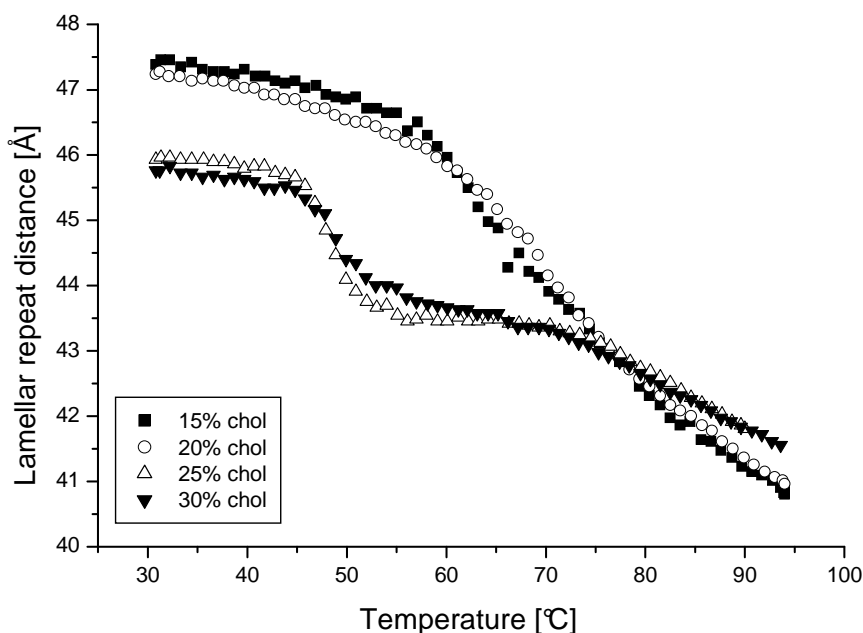


Fig. 6.5 Development of the lamellar repeat distance of the SC lipid MLVs with 15% (filled squares), 20% (open circles), 25% (open triangles), and 30% (filled triangles) CHOL during the second heating.

6.4 Discussion

Though the particular DSC technique used for the measurements is not the best for such diluted samples, there is reasonable correlation between the DSC and the SAXD results. It is obvious from the DSC curves that CHOL broadens the main phase transition of the systems similarly as it was shown for two-component systems of CHOL and ceramides [61] and for a three-component system of a ceramide analogue, stearic acid and CHOL [183]. Interestingly, in our case, the second-heating curve shows a preceding exothermic transition, which fades into an endothermic one.

As it was shown in Chapter 5, the samples show a phase separation before the heating at 32 °C. This effect could be explained as follows: the shorter chains of the PA separate from the lipid matrix and create their own domain. This is in concurrence with the domain-mosaic model [45]. The present DSC and SAXD results can elucidate the phase-separation phenomenon in more detail.

In the sample with 25% CHOL, the phase-separated state persists till 45 °C. The immiscibility of the lipid components in this state is obvious. At 45 °C, the phases suddenly merge into a new one with a D value of 43 Å. Evidently, a mixing process occurs at this temperature. Assuming that the S-phase is mostly composed of PA, it is very probable that the S-phase melts at this temperature and becomes more miscible with the other lipids.

However, because a shift in the D-value of both separated phases occurs, both the PA and ceramide hydrocarbon chains should participate on the first phase transition. A similar effect has been observed elsewhere [41,43,44,185]. According to the published results, it is presumable that at the temperatures below 45 °C, the lipid chains are in a crystalline phase separated into two crystalline domains. Above 45 °C, the membrane is supposed to transform into a gel phase where the membrane fluidity and the miscibility of the lipids increase [41].

The gel phase in our system is stable with further heating up to 70 °C when the periodicity starts to decrease continuously. This can be explained by the melting of the mixed system.

When the CHOL concentration in the system is by 5% higher (the sample with 30% CHOL) the thermotropic phase behaviour changes dramatically. Two separated phases, similar to both phases in the system with 25% CHOL, are recognizable till 45 °C. At this temperature, two new phases with D-values of 43 and 48.5 Å arise. This indicates that the lipids partly mix together in a gel phase with 43 Å similarly as in the system with 25% CHOL. However, the arising phase with 48.5 Å signifies that a part of the lipids remains phase-separated in a more rigid state. Therefore, the increasing amount of CHOL in the membrane supports the phase-separation effect and hinders the lipid chains to mix together. At 75 °C, both phases start to melt together in a eutectic mixture and the lipid components become more miscible.

After the first heating, the systems are in a mixed state. In all the measured samples only one lamellar phase is observable. The phase behaviour of the systems with 25 and 30% CHOL during the second heating shows many similarities. A mixed phase with a repeat distance of 45.9 Å is stable till 45 °C, at which temperature the D-value decreases to 43.6 Å. The down-shift in the periodicity can again be connected with the melting of a part of the lipids. Afterwards, the systems are stable in the gel phase till the main phase transition at 70 °C, when the rest of the hydrocarbon chains melt.

The systems with lower CHOL concentrations (15 and 20% CHOL) show different thermotropic phase behaviour in comparison to that with higher CHOL levels. During the second heating, only one broad phase transition can be recognized. In both samples (15 and 20% CHOL), the repeat distance starts to decrease continuously at about 60 °C. This indicates a slow melting process. From the present data, it cannot be deducted whether all the lipids melt together or, more probably, the transition consists of stepwise melting processes of the particular components.

According to the results, CHOL promotes the formation of the gel-phase during the second heating which is also in concurrence with other authors [41]. This effect indicates a separated melting of the particular lipid components and related lower miscibility than in the system with lower CHOL levels. Our results moreover show that a too high level of

CHOL can cause a new phase separation at temperatures above 45 °C, as can be observed during the first heating.

Thus, the concentration of CHOL in a SC lipid mixture is crucial for its phase behaviour and the miscibility between the particular components.

During the second heating, the first phase transition has been found to be exothermic. This signifies that the mixtures at 32 °C after the first heating are in a metastable state that is not energetically favourable. As this state is not stable, the systems release some energy when they transfer during the first phase transition. This effect explains also why the mixtures are not stable in time and transfer into the phase-separated state at room temperature during approximately one week.

6.5 Conclusion

During the first heating, the SC lipid model system with the basic composition shows two phase transitions. Below the first transition, the system is separated into two crystalline phases which indicates immiscibility of the lipid components. The first transition at about 45 °C is connected with an increase in miscibility when both phases merge into a gel phase. On further heating, the gel phase remains till about 70 °C, when, due to the melting of the hydrocarbon chains, the second phase transition from the gel to the liquid crystalline phase occurs.

After cooling the system back to 32 °C, only one mixed phase is detectable. In the course of the second heating, the mixed phase persists till 45 °C, when it again transforms into the gel phase. This first phase transition exhibits an exothermic character which indicates an energetic instability of the phase arising after the heating. Similar to the first heating, the chains start to melt at about 70 °C.

CHOL promotes formation of the gel phase. However, a too high CHOL levels cause new phase separation in the system above 45 °C.

7 Neutron diffraction on the SC lipid model system

Published in: Kiselev MA, Ryabova NY, Balagurov AM, Dante S, Hauss T, Zbytovská J, Wartewig S, Neubert RHH, 2005. *New insights into the structure and hydration of a stratum corneum lipid model membrane by neutron diffraction. Eur. Biophys. J.* 34, 1030-1040.

7.1 Introduction

This Chapter introduces neutron diffraction on multilamellar lipid films into the investigation methods of the skin research. Neutron diffraction offers the great opportunity to characterize the internal structure of a membrane and herewith brings a new way to describe the mode of action of skin permeation enhancers.

Unlike vesicles, which are mainly prepared in excess of water, hydration of the multilamellar films deposited on a quartz substrate can be varied during the measurements.

7.2 Methods

7.2.1 Material

Cer[AP] was a gift from Cosmoferm (Delft, The Netherlands). Cholesterol (CHOL), cholesterol sulphate (CS), and palmitic acid (PA) as well as sodium bromide (NaBr) and potassium sulphate (K_2SO_4) were purchased from Sigma-Aldrich (Taufkirchen, Germany). Water, chloroform and methanol used were of HPLC grade.

7.2.2 Sample preparation

The composition of the lipid system used in this study was chosen according to previous X-ray and neutron scattering experiments. A basic system which should mostly imitate the real SC lipid composition consists of 55% (in weight) Cer[AP], 25% CHOL, 15% PA and

5% CS. The other samples were prepared varying the proportion of CHOL (from 10 to 40%), the relative ratio of the other lipids remaining constant.

The multilayer films on the quartz substrate were prepared according to Seul and Sammon [186]. The particular lipids were dissolved separately in chloroform/methanol (2/1 in volume) and the appropriate volumes were then mixed together in order to prepare a solution with the total lipid concentration of 10 mg/ml. 600 μ l of the solution were applied on a 3.25 x 2.50 cm quartz plate (Spectrosil 2000, Saint-Gobain, Wiesbaden, Germany) and dried at room temperature. The rest of the solvents were removed under vacuum. After drying, the samples were heated in a horizontal position above the temperature of the main phase transition (up to 90 °C).

7.2.3 Neutron diffraction measurements

The neutron diffraction patterns were acquired at the V1 neutron diffractometer at Hahn-Meitner Institute (HMI), Berlin, Germany, equipped with two-dimensional position sensitive ^3He detector. The wavelength of the cold neutron radiation was 4.517 Å and the sample-to-detector distance 101.8 cm. The diffractograms were recorded as particular rocking curves of each diffraction order at correspondent fixed scattering angles.

The samples were measured at 32 and 82 °C, in a state below and above the main phase transition, respectively. Three humidity levels 60, 99% as well as water excess were chosen for the experiment. The exact value of humidity was achieved by adding supersaturated solution of various salts into the measuring cell [187] (Table 7.1).

In order to determine the phases, the samples were measured at three ratios of $\text{H}_2\text{O}/\text{D}_2\text{O}$ in the vapour environment. The concentration of D_2O in H_2O was adjusted to 8, 20, and 50% (v/v), respectively. Before each measurement, the samples were equilibrated for 12 hours under the defined humidity and at the defined temperature.

Table 7.1 Supersaturated solutions used to achieve relative humidity in the sample environment.

Humidity	Salts
60%	NaBr
99%	K_2SO_4

The mathematical determination of the neutron scattering length density profiles has been carried out by Dr. Kiselev from JINR, Dubna.

7.3 Results

7.3.1 Neutron diffraction measurements from the mixtures with various CHOL concentrations

The neutron diffraction pattern of the sample with the basic composition (25% CHOL) measured at 32 °C, 60% humidity and 8% (v/v) H₂O is shown in Fig. 7.1. This concentration of D₂O in H₂O corresponds to the zero scattering length density of water. In the pattern, five diffraction orders are detectable. The lamellar repeat distance was calculated according to: $D = n2\pi/q_n$ for each diffraction order and amounts to 45.63 ± 0.04 Å after averaging over all three measurements at different D₂O/H₂O ratios. The high number of reflections obtained enabled us to calculate the neutron length density profile using the Fourier analysis (see later).

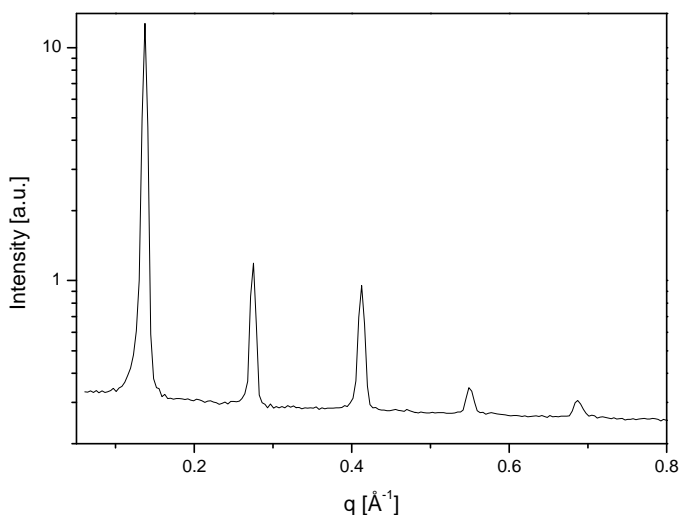


Fig. 7.1 The neutron diffraction pattern from the oriented multilamellar sample consisting of 55% Cer[AP], 25% CHOL, 15% PA, and 5% CS. Measured at 32 °C, 60% humidity, and 8% D₂O.

The influence of the relative humidity on the lamellar repeat distance has been studied. As expected, the position of the diffraction peak shifts to the lower q -values with the increasing relative humidity in the environment (Fig. 7.2a). Therefore, the relevant D -values increase with increasing humidity (Table 7.2).

With increasing hydration, the intensity of the diffraction signal becomes weaker. At full hydration, only three diffraction orders were detectable which does not allow calculating the neutron length density profile.

Table 7.2 Influence of relative humidity in the environment on the lamellar repeat distance of the sample with 25% CHOL at 32°C.

Relative humidity [%]	D [Å]
60	45.63±0.04
99	46.13±0.1
100	46.45±0.03

The effect of CHOL concentration in the sample on the membrane parameters has been investigated. Fig. 7.2b presents the neutron diffraction patterns from the samples with 40 and 10% CHOL. As can be seen from the shift in the position of the diffraction peaks the lamellar repeat distance decreases with increasing CHOL concentration (Table 7.3).

Table 7.3 Influence of CHOL concentration on the lamellar repeat distance of the SC lipid model membranes organized as oriented multilamellar systems at 32°C and 60% humidity.

Sample	D [Å]
10% CHOL	46.1±0.1
25% CHOL	45.63±0.04
40% CHOL	43.9±0.3

Similarly to the sample with 25% CHOL, the sample with 10% CHOL shows five diffraction orders. Unfortunately, the signal from the sample with 40% CHOL is weaker and only three reflections are detectable. This number is not enough to calculate the neutron scattering length density profile.

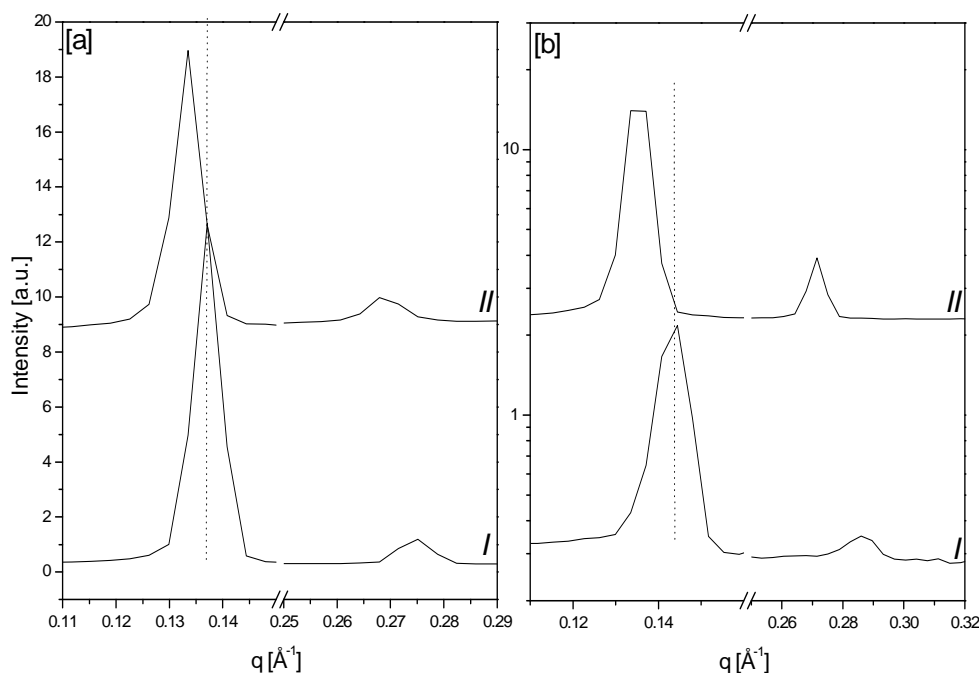


Fig. 7.2 The neutron diffraction patterns from the oriented multilamellar membranes consisting of Cer[AP]/CHOL/PA/CS measured at 32 °C. [a] Influence of relative humidity on the system with 25% CHOL: (i) 60% relative humidity, (ii) water excess. [b] Influence of CHOL concentration on the system measured at 60% relative humidity: (i) 40% CHOL and (ii) 10% CHOL; the ratio of the other components remains constant.

7.3.2 Neutron scattering length density profiles of the SC lipid model membrane

(Calculated by Dr. M. Kiselev [182])

The membrane profile of neutron scattering length density of the sample with 25% CHOL has been calculated. The structure factor for each diffraction order was determined according to $|F_h| = \sqrt{C_h I_h}$ and corrected to the Lorentz factor of the oriented membrane [103]. Because only an absolute value of the structure factor could be calculated, the phases had to be determined. This determination has been performed using the isotopic substitution of H₂O by D₂O [104,105,106].

The obtained $|F_h|$ values were set linearly as described in Chapter 3.3.4 [188] (Fig. 7.3). The phases were determined from the plots as: -, +, -, +, and - for the diffraction order $h = 1, 2, 3, 4,$ and $5,$ respectively.

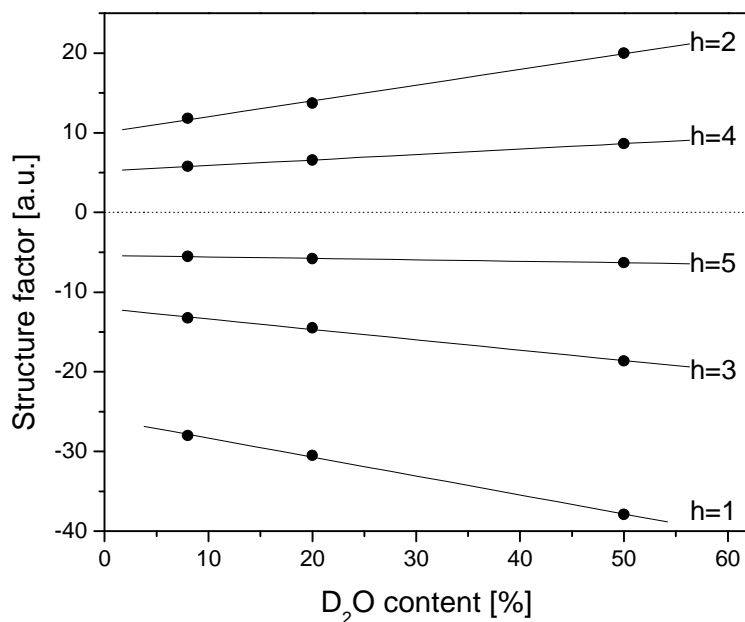


Fig. 7.3 The dependence of the membrane structure factor, F_h , on the D_2O content for oriented bilayers calculated for diffraction orders 1-5. Measured at 32 °C and 60% relative humidity.

The profile of neutron scattering length density of the bilayer, $\rho_s(x)$, was calculated using simplified equation 3.16:

$$\rho_s(x) = \frac{2}{D} \sum_{h=1}^{h_{\max}} F_h \cos\left(\frac{2\pi hx}{D}\right) \quad (7.1)$$

Fig. 7.4 shows the neutron scattering length density profiles for 8, 20, and 50% D_2O in arbitrary units. This function describes the internal membrane structure in a real space. Both maxima in the profiles are related to the hydrophilic head groups on the lateral sides of the membrane. The intensity of the contrast increases here, because the D_2O molecules are able partly to penetrate between the hydrophilic groups and participate on the hydrogen-bonds with them. The distance between the two maxima, which amounts to 45.6 Å, can be interpreted as the real membrane thickness, d_m . The part of the profile with the lower contrast values describes the interior part of the membrane consisting of the hydrocarbon chains with the hydrophobic methylen and methyl groups.

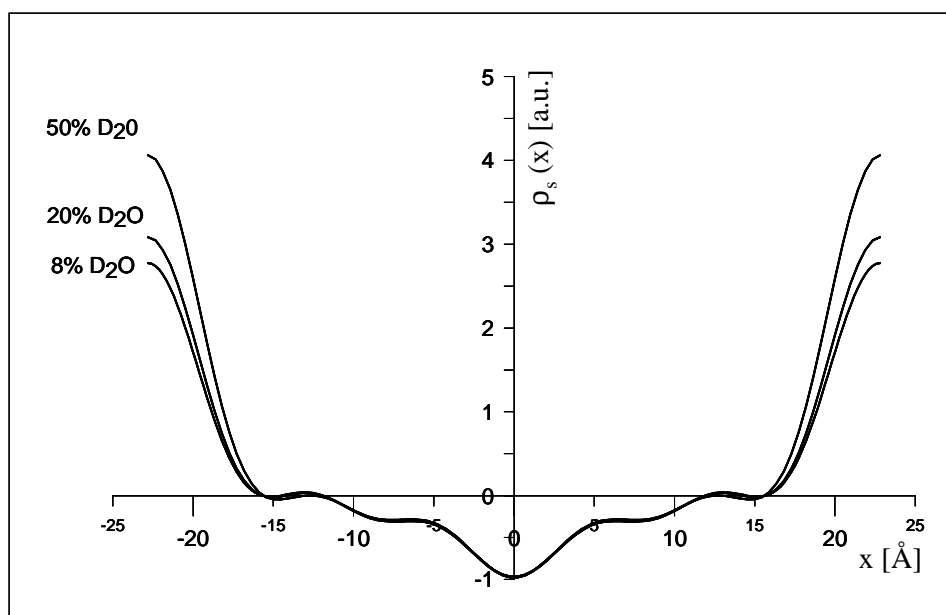


Fig. 7.4 The profiles of the neutron scattering length density of the membrane consisting of 55% (in weight) Cer[AP], 25% CHOL, 15% PA, and 5% CS. Measured at 32 °C and 60% humidity in 8, 20, and 50% D₂O.

By subtracting the profile measured at the lower D₂O content from that one measured at the higher D₂O content, one obtains the water distribution function across the membrane (Fig. 7.5):

$$\rho_w = \rho_{50\% D_2O} - \rho_{8\% D_2O} \quad (7.2)$$

The dashed lines in Fig. 7.5 show the hydrophobic-hydrophilic (HH) boundary where the water distribution function ρ_w is near to zero. Therefore, the HH-boundary is characteristic of the water penetration region in the membrane. The position of the HH boundary has been found to be at 15.6 ± 0.1 Å. The thickness of the hydrophilic region is given by the difference between the half of the membrane thickness d_m and the HH boundary and amounts to 7.22 ± 0.24 Å for the sample at 60% humidity. The thickness of the hydrophobic part of the membrane is 31.2 ± 0.2 Å.

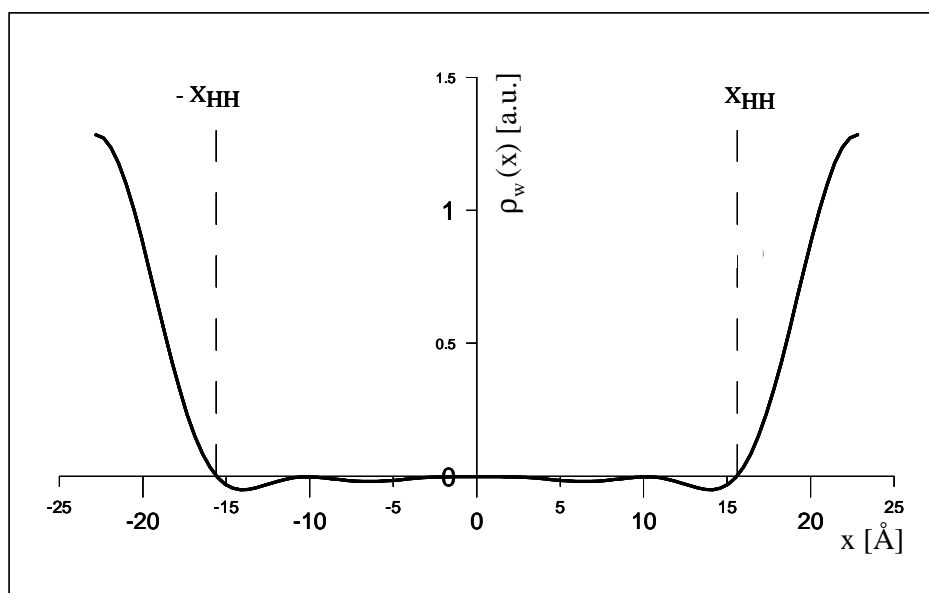


Fig. 7.5 Water distribution function across the bilayer for the sample composition of 55% Cer[AP], 25% CHOL, 15% PA and 5% CS measured at 60% humidity and 32 °C.

To characterize numerically the internal membrane structure, the neutron length density profile has been fitted. Four Gaussian functions belonging to the CH₃ and CH₂ groups as well as to the cholesterol molecule and the polar head group region were used to fit the profile. The fit-curve of the Fourier profile is shown in Fig. 7.6. The fitting results are summarized in Table 7.4. Besides the membrane thickness, two important parameters, namely the position of the Gaussian function attributed the individual molecular group and the area under the curve, are presented.

The thickness of the water layer, d_w , between the membranes has been determined as the difference between the lamellar repeat distance and the membrane thickness:

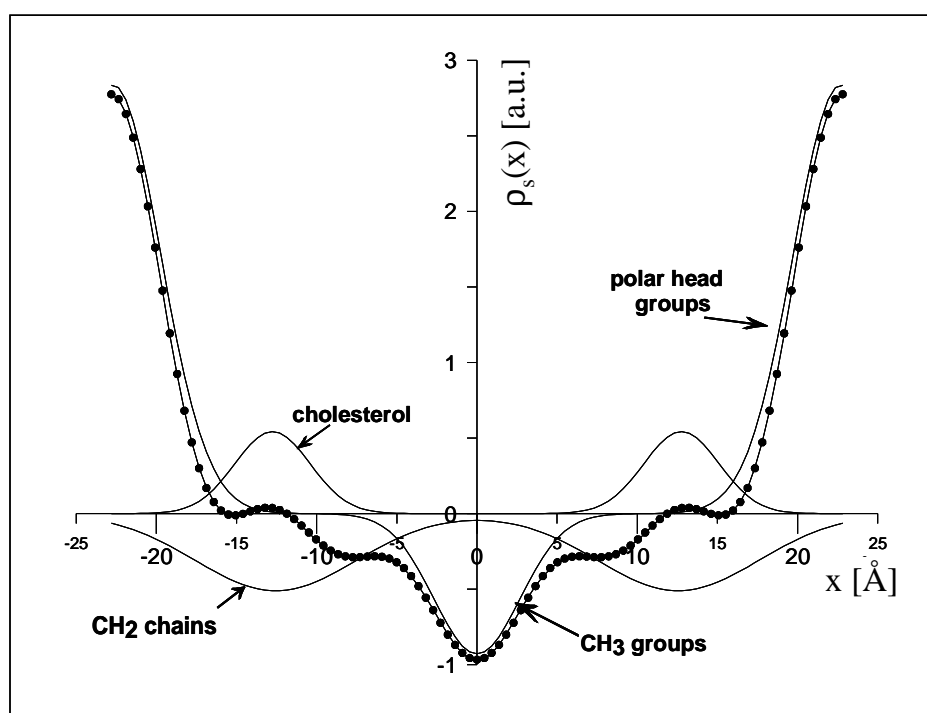
$$d_w = D - d_m \quad (7.3)$$

By comparing the membranes with 25% CHOL at 60% relative humidity and water excess, d_w increases with the increasing humidity in the environment. At 60% relative humidity, there is no significant difference between the membrane thickness and the repeat distance; therefore, the water layer is near to zero. Under the full hydration, the d_w value amounts to 0.82 ± 0.07 Å.

Table 7.4 Parameters of the calculated neutron length density profiles of the samples with 10 and 25% cholesterol at 32°C and 60% humidity.

	10% cholesterol	25% cholesterol
Lamellar repeat distance [Å]	46.1	45.6
Membrane thickness [Å]	46.1	45.64
Thickness of the water layer [Å]	0	0
Polar head group position [Å]	23.05	22.82
Polar head group area [a.u.]	23.4	20.9
CH ₂ position [Å]	13.83	12.55
CH ₂ area [a.u.]	-7.56	-6.437
Cholesterol position [Å]	12.93	12.76
Cholesterol area [a.u.]	3.36	3.197
CH ₃ position [Å]	0	0
CH ₃ area [a.u.]	-7.17	-6.256

Similarly to the sample with 25% CHOL at 60% humidity, the water layer of the sample with 10% CHOL is also near to zero. No influence of the CHOL concentration in the membrane on the thickness of the water layer has been found.

**Fig. 7.6** The profile of the neutron scattering length density of the membrane consisting of 55% Cer[AP], 25% CHOL, 15% PA, and 5% CS. Measured at 32 °C and 60% humidity in 8% D₂O.

7.4 Discussion

As it was shown in Chapter 5, SC lipid model membranes under full hydration organized in MLVs undergo a phase separation into the ‘longer’ (L-) and ‘shorter’ (S-) phase with a periodicity of 47.2 and 41.9 Å, respectively. On the contrary, at 32 °C, organized multilamellar samples show only one phase with the repeat distance of 45.6 and 46.5 Å at 60 and 100% humidity, respectively. These values correspond with that one, which originates in the MLV-samples after heating. However, in MLVs, this phase is not stable and separates back during several days. In comparison to this effect, the membranes organized in a multilamellar planar system stored at the air-humidity (30-40%) were found to be stable for at least six months (data not shown).

Interestingly, a phase separation analogous to that in MLVs occurred in organized multilayers when it was hydrated at 97% relative humidity and 80 °C. This confirms that the phase separation monitored in our system is conditioned by a high humidity level in the sample environment. Probably, water facilitates the lateral diffusion of lipids across the membrane.

Though the role of water in the phase separation of the membranes has been postulated, the water layer between the membranes has been found to be extremely thin (about 1 Å) and the time needed to reach the full hydration of the membranes very long in comparison to that of phospholipids [182]. On the other hand, according to the HH-boundary values, water penetrates relatively deeply into the membranes and occurs even partly in the region of the hydrocarbon chains.

In the sample with 25% CHOL, the membrane thickness is about 45.6 Å. The thickness of the polar headgroups amounts to about 3.5 Å and of the hydrocarbon chain part about 38.6 Å. According to Small [189], it is possible to calculate the theoretical hydrocarbon chain length in the all-*trans* (most rigid) conformation. Calculating the length of the longest chain in the present mixture (the stearyl- chain in Cer[AP]) one obtains a value of 22.9 Å per chain. Taking two of these values together, the thickness of the hydrocarbon chain part of the membrane should be 45.8 Å. There are several opportunities why the 7 Å difference between the measured and calculated values occurs.

The first assumption that the membrane is not in the rigid state can be simply excluded by the Raman spectroscopy measurements (Appendix B). The positions of the symmetric stretching CH₂ vibration at 2846 cm⁻¹, of the CH₃ rocking mode at 889 cm⁻¹, antisymmetric and symmetric CC stretching vibration at 1062 and 1130 cm⁻¹, respectively, indicate a highly ordered structure with high number of *trans*-conformations.

The other possibility, which cannot be excluded is that the hydrocarbon chains are tilted with respect to the base plane of the membrane at an angle θ , where $\theta \neq 90^\circ$. Moreover, the interdigitation of the stearyl chains in the membrane centre is very probable, because

there are chains with various chain lengths. It is also possible, that both the tilted hydrocarbon chains and the interdigitation occur.

The effect of CHOL concentration on the internal membrane structure has been studied. CHOL affects the lamellar repeat distance of the membranes organized in planar multilayer system under 60% hydration similarly as in the MLVs under full hydration. In both cases, the membrane periodicity decreases with increasing CHOL concentration in the sample. This result supports the assumption that CHOL does not participate on the external membrane hydration and does not affect the thickness of the water layer between the membranes (Chapter 5).

As can be seen in Table 7.4, a decrease of CHOL concentration in the membrane from 25 to 10% increases the membrane thickness from 45.64 to 46.1 Å. The position of the CHOL molecule has been determined at 12.76 Å deep in the membrane. In this area of the neutron length density profile, an increased level of the scattering contrast has been detected. This can be connected with the fact that the steroid core contains less hydrogen atoms, which decrease the contrast in comparison to the hydrocarbon chains [182]. However, the exact CHOL position in the membrane has to be confirmed by further experiments.

Nevertheless, the variation in the CHOL concentration in the membrane induces distinct changes in the internal membrane structure. There is a shift in the position of the fitting curve belonging to the hydrocarbon chains from 12.55 Å at 25% CHOL to 13.83 Å at 10% CHOL. The area under the curve increases with the decreasing CHOL content. This can be interpreted as the hydrocarbon chains became more extended with decreasing CHOL concentration. This fact confirms the assumption that CHOL decreases the rigidity of the hydrocarbon chains of the SC lipid system in the state below the main phase transition. It can be possible as well, that CHOL plays a role in the tilting and/or interdigitation of the hydrocarbon chains.

7.5 Conclusions

This study introduces the neutron diffraction into the research of the SC lipid structures. A model SC lipid membrane was prepared as an oriented multilayer system whose low mosaicity allowed to calculate the neutron scattering length density profiles. The membrane thickness, the thickness of the membrane hydration layer, the thickness of the polar head groups as well as the hydrocarbon chain regions have been determined. The thickness of the water layer between the membranes under full hydration has been found to be extremely thin. Nevertheless, water seems to play an important role in the phase separation of the model membrane. Increased amount of CHOL decreases the membrane thickness.

It is most probable that the hydrocarbon chains are partly interdigitated in the membrane centre and/or tilted with respect to the base plane of the membrane.

8 Influence of permeation modulators on the behaviour of a SC lipid model mixture

8.1 *Introduction*

In the foregoing parts of this thesis, a model membrane system of SC lipids has been developed and characterized. The methods used allowed to elucidate the role of CHOL, as one constituent of the original membrane, in the SC lipid model and herewith in the native SC.

The final part of the thesis attends to the question whether the developed membrane model can be used to describe interactions with other substances, which are not components of the original model membrane, and whether the mode of action of permeation modulators can be studied using the SC lipid model system. For the present study, three different substances, namely urea, oleic acid (OA), and *N*-lauroylglycine lauryl ester (12G12) were chosen. Urea is believed to be a permeation enhancer which affects the hydrophilic parts of the SC membranes [8,9], while OA and 12G12 should enhance the transport of substances due to influencing the hydrocarbon tails.

Urea is a hydrophilic and well water-soluble compound, which is supposed to be concentrated in the water phase of the system. It is a physiological substance occurring in mammalian tissues. In the human SC, urea plays an important role as a component of natural moisturizing factor [190]. The effect of urea can be summarized as proteo- and keratolytic, water-binding, and itching alleviative. The decreased urea levels in SC were found in the dry skin syndrome [191]. Urea is used in the treatment of many skin diseases as psoriasis, ichthyosis, dry skin, dystrophic nails, etc. (for a review see [53,192]). Urea and especially its derivatives were described to enhance transdermal permeation of several drugs by facilitating hydration of the SC and by the formation of hydrophilic diffusion channels within the barrier [193]. For these reasons it is sometimes classified as enhancer for the hydrophilic pathway [8]. The keratolysis induced by urea plays also a role in its transdermal penetration enhancement mode of action.

Unlike urea, OA and 12G12 are of lipid type and probably incorporate into the membrane. The physiological presence of OA in human SC is controversially discussed. While some earlier studies have detected OA in its free fatty acid form as an important constituent of the SC lipid matrix [194]; more recently, this assumption has not been confirmed [20,195]. Indeed, some OA is generated in the stratum granulosum as a product of phospholipid degradation; it is, however, esterified by CHOL before it reaches SC [196]. Thus only very small trace amounts of free OA are detected in SC.

Nevertheless, OA is known as an efficient transdermal permeation enhancer which interacts with and modifies the lipid domains of the SC due to the *cis* double bond at C9. The presence of the double bond causes a kink in the hydrocarbon chain of OA, which is likely to disrupt the ordered array of the predominantly saturated highly ordered skin lipid chains and increase the fluidity of the SC lipid membranes [57]. In SC lipid mixtures, OA lowers the main phase transition temperature and forms a separate domain with disordered chains within the SC lipid membranes [197]. Ceramides and OA are immiscible in the solid state and their mixtures show a monotectic behaviour [62]. It has been suggested that such a domain formation of OA and some SC lipids is responsible for the decreased capacity of skin barrier function [198].

In essential fatty acid deficiency, acylceramides are produced, where linoleate is replaced by oleate. It has been suggested that the modified acylceramide acts as an endogenous permeation enhancer [21].

Ceramide analogue 12G12 has been synthesized and evaluated as a potential permeation enhancer. According to recent studies, the substance shows a pronounced enhancing effect on human skin [199,200]. The thermotropic phase behaviour of 12G12 in the bulk phase has been studied within the framework of the present thesis and the main results are summarized in Appendix C. The mode of action of 12G12 is proposed to be the interaction with SC lipid matrix. The present study should bring more information about the mode of action of this novel enhancer.

8.2 Methods

8.2.1 Material

Cer[AP] was a gift from Cosmoferm (Delft, The Netherlands). Cholesterol (CHOL), cholesterol sulphate (CS), and palmitic acid (PA) as well oleic acid (OA) and urea were purchased from Sigma-Aldrich (Taufkirchen, Germany). *N*-lauroylglycine lauryl ester (12G12) was synthesised and purified by Dr. Vávrová, Dept. of Inorganic and Organic Chemistry, Faculty of Pharmacy, Charles University, Prague. Water, chloroform and methanol used were of HPLC grade.

8.2.2 Sample preparation

The MLVs (10% of lipids in water) were prepared by the 'thin layer method' as described previously (Chapter 5.2.2). The basic composition of all the samples is 55% ceramide[AP], 25% CHOL, 15% PA, and 5% CS. To the samples, OA or 12G12 in various molar concentrations were added. A part of the samples with the basic composition was prepared in buffers with various urea concentrations.

8.2.3 SAXD measurements

The time-resolved X-ray diffraction patterns from the MLVs (10% w/w of lipid in water) in the small-angle region were collected on the D22 line at DCI synchrotron source (LURE, Orsay, France) at the wavelength of 1.39 Å. The samples were placed in a quartz capillary. In order to eliminate the phase separation, the samples were heated for 15 min at 90 °C before the measurement.

The acquisition time was 10 min for the static measurements at 32 °C and 1 min for the continuous measurements during the heating. The heating rate was 1 °C min⁻¹. The linear position sensitive detector was arranged in the sample-to-detector distance of 1813 mm. X-ray diffraction from DMPC or DPPC MLVs was used as known calibration standards.

The obtained diffraction peaks were fitted with Gaussian functions in order to minimize the statistical error. The lamellar repeat distance was calculated from the position of the first diffraction peak according to: $D = 2\pi/q$.

8.3 Results and discussion

8.3.1 Influence of urea on the SC lipid system

Fig. 8.1 shows the X-ray diffraction patterns from the MLVs with the basic composition prepared in buffers with various urea concentrations at 32 °C after the heating. As can be seen, the position of the diffraction peak is not affected by the presence of urea in the environment. The determined repeat distance is very similar in all the samples and amounts to about 46.3 Å.

The obtained information is striking, because the effect of urea on the hydration of SC is well known and the influence on the water layer between the SC lipid membranes can be assumed. The present results, however, bring the evidence that the thickness of the water layer between the membranes is not affected by urea.

During the heating of the samples, the membrane repeat distance changes. As it has been described previously (Chapter 6), the thermotropic behaviour of the system with the basic

composition without the presence of urea in the environment shows two phase transitions. During the first transition at about 45 °C, the lamellar repeat distance decreases abruptly from 46.3 to 43.6 Å. The first transition seems to be connected with the melting of a part of the SC lipids. The other phase transition starts at 70 °C, when a further decrease in the periodicity occurs indicating the melting of all hydrocarbon chains.

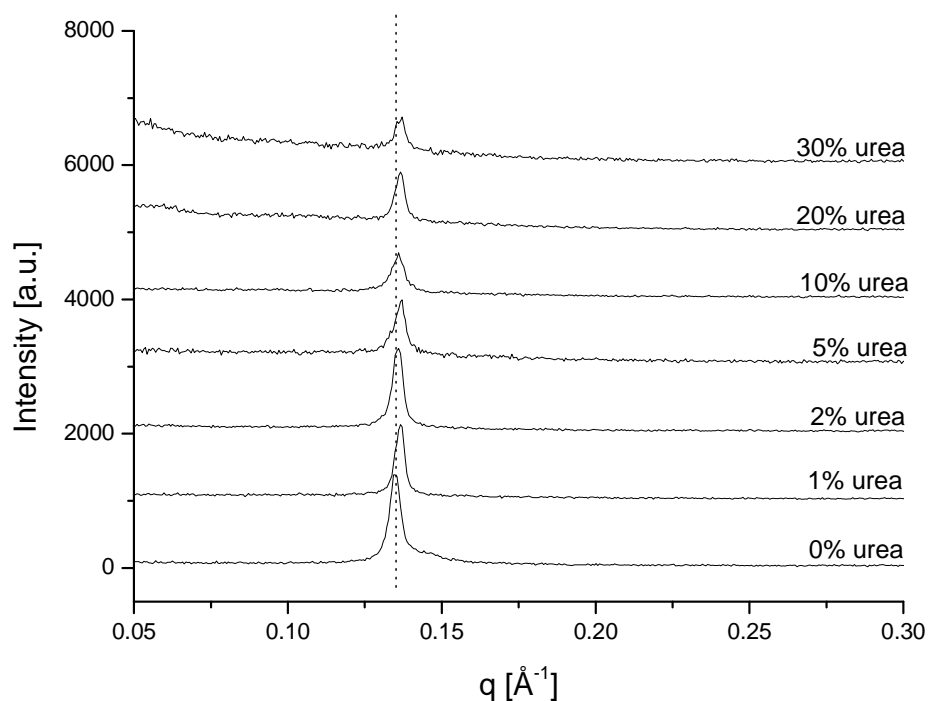


Fig. 8.1 X-ray diffraction patterns from the SC lipid MLVs in buffers with various urea concentrations at 32 °C.

As can be seen in Fig. 8.2, the presence of urea in the water environment influences the thermotropic phase behaviour of the SC lipid system. When 2-5% of urea in the buffer is present, the first phase transition shifts to higher temperatures and becomes less distinct.

Further increase in the urea concentration to 10% causes that both phase transitions merge into a broad one. The system starts to melt continuously at about 42 °C and no gel phase can be observable. There is an apparent influence of urea on the phase behaviour of the SC lipid membranes. The smoothing of the first phase transition and the merging of both transitions into the broad one indicates that in the state below the first phase transition, the particular lipid components became more miscible in the presence of urea and do not melt separately. This effect could be explained by displacement of some water molecules bound by the hydrogen bonds to the polar headgroups of the SC lipids by urea. Herewith, the miscibility of the system can increase.

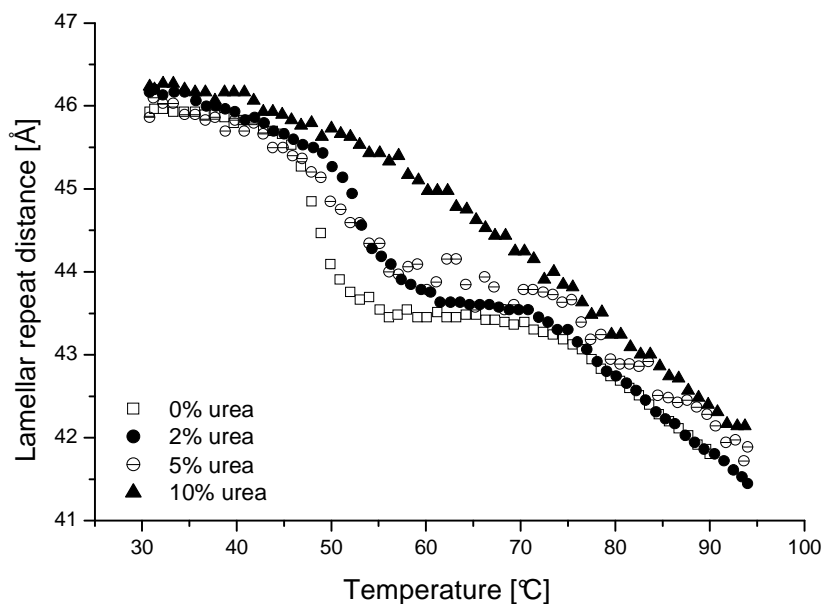


Fig. 8.2 Lamellar repeat distance of the membranes with various urea concentrations vs. temperature. Urea induces an up-shift in the first phase transition temperature and merging of both phase transitions together.

8.3.2 Influence of oleic acid on the SC lipid system

The X-ray diffractograms from the SC lipid system with various OA concentrations measured at 32 °C are shown in Fig. 8.3a. When only 2-5 molar % of OA is incorporated in the membrane, the systems show one diffraction peak at nearly the same position. The calculated repeat distance (Fig. 8.3b) decreases by about 0.5 Å in comparison to that of the neat SC lipid system. A different situation arises when higher concentrations of OA (10-15 molar %) are present in the mixture. In that case, the membrane separates into two phases: the longer one (the L-phase) with the periodicity of about 46.6 Å and the shorter one (the S-phase) with the repeat distance of 43.5 Å. As described previously (Chapter 5), a similar phase separation occurs also in the pure SC lipid model system, but the process requires much longer time (several days). Evidently, OA enhances the formation of a new domain (the S-phase) in the SC lipid system at 32 °C.

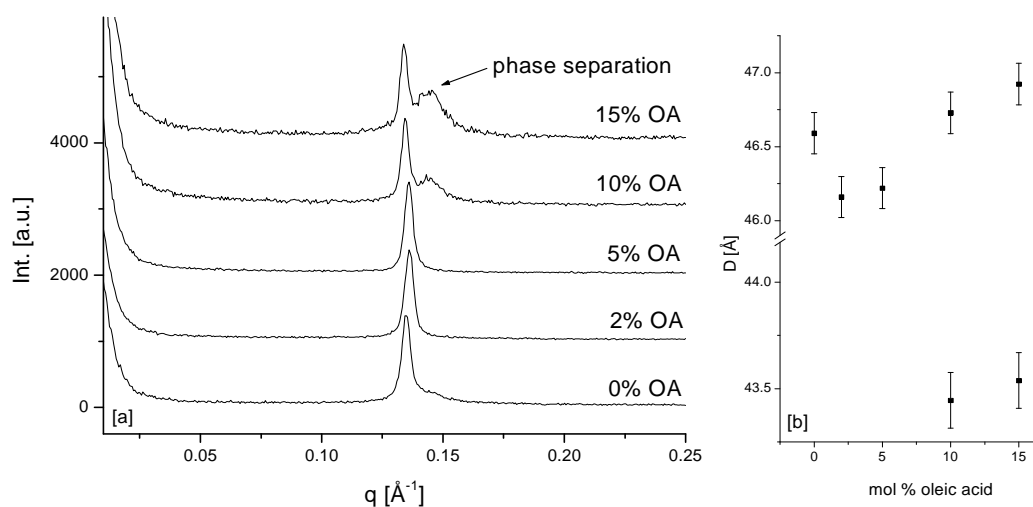


Fig. 8.3 [a] X-ray diffraction patterns from the SC lipid MLVs with various oleic acid molar concentrations at 32 °C. [b] The determined lamellar repeat distance of the membranes.

The thermotropic response of the lamellar repeat distance of the systems with various OA concentrations is shown in Fig. 8.4. All the systems show two phase transitions during the heating; the first one at about 45 °C, the other one starting at about 70 °C.

The phase behaviour of the system with 2% OA is very similar to that one without OA. In the course of the first phase transition, the periodicity of the membrane decreases suddenly to about 43.3 Å.

In the membrane with 5% OA, a new phase with a D-value of 43.3 Å can be detected besides the L-phase at 40 °C. During the first phase transition, the phases merge together into a resulting phase with 43.8 Å. Increasing the OA concentration in the membrane to 10%, the phase separation occurs already at 30 °C. During the first phase transition at about 50 °C, the phases mix together into another one with a repeat distance of about 44 Å.

In all the samples, the second phase transition at about 70 °C is connected with melting of the remaining hydrocarbon chains.

From the present data, it is apparent that the miscibility of OA with the SC lipids is very limited in the state below the main phase transition. Only a small amount of OA (up to 2%) can be fully incorporated into the membrane. Higher amounts of OA in the system start to create a new domain that predominantly consists of OA presumably in the fluid phase. This phase, however, does not consist only of OA, but most probably also of the other lipid components as PA. This assumption is supported by the fact that the periodicity

of the L-phase in the separated state increases compared to the SC lipid system without OA.

Unexpectedly, OA decreases the temperature of neither the first nor the second phase transition. This again hints to the strong immiscibility of the SC lipid system with OA.

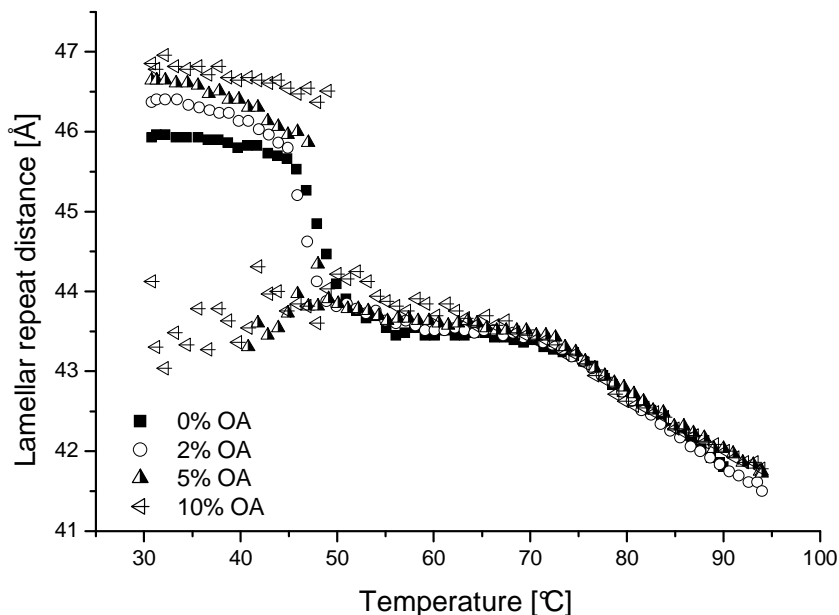


Fig. 8.4 Lamellar repeat distance of the membranes with various molar concentrations of oleic acid vs. temperature. The phase separation is distinct in the samples with 10% and 5% OA at 32 and 40 °C, respectively.

The phase separation of OA from SC lipids has also been described earlier [197]. The mode of action of OA as the permeation enhancer is most probably connected with the phase separation effect. The new fluid domain will be more permeable for a drug as the more rigid regions.

8.3.3 Influence of 12G12 on the SC lipid system

The diffractograms from the SC lipid systems including various concentrations of 12G12 measured at 32 °C are shown in Fig. 8.5a. As can be seen, there is a shift in the peak position to higher q -values with increasing amount of 12G12 in the system. The corresponding repeat distances are plotted in Fig. 8.5b. The values decrease with the increasing 12G12 concentration. In the concentration range used, the dependence has an exponential character. This decay in the periodicity can be connected with the fact that the hydrocarbon chains of 12G12 are shorter than the other chains in the system.

Interestingly, one diffraction peak only is detectable in all the patterns. This indicates that 12G12 incorporates into the SC lipid membrane and does not create its own domain, as it

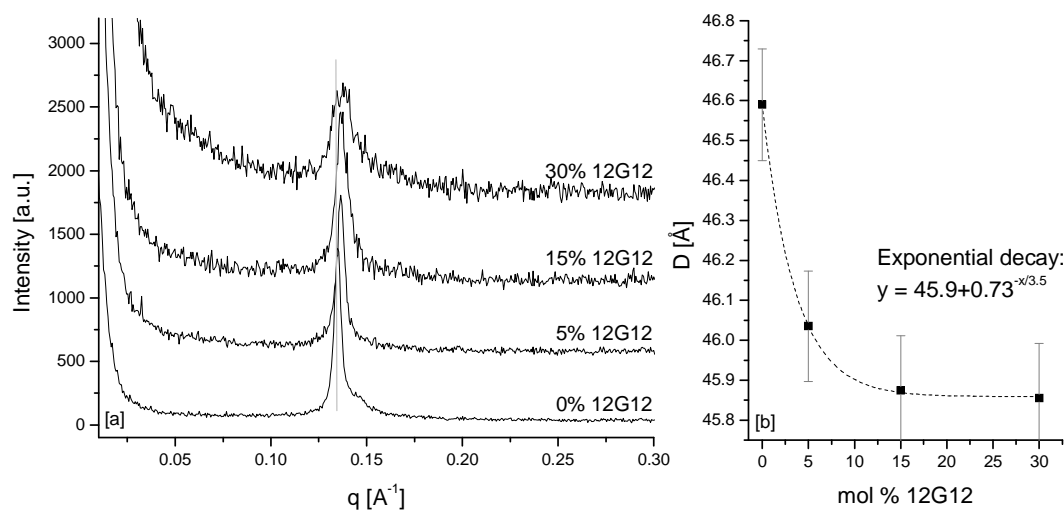


Fig. 8.5 [a] X-ray diffraction patterns from the SC lipid MLVs with various 12G12 molar concentrations at 32°C. [b] The determined lamellar repeat distance of the SC lipid membrane decreases with the increasing 12G12 concentration.

can be presumable for the lipid mixtures with mismatch in the hydrocarbon chain lengths.

Simultaneously with the increasing concentration of 12G12 in the system, the intensity of the diffraction signal becomes weaker. As it has been suggested earlier [103,184], such weakening in the diffraction intensity can be related to the increasing membrane undulations due to higher concentrations of 12G12 in the membrane.

The dependence of the repeat distance on the temperature for the systems with various 12G12 concentrations is presented in Fig. 8.6. As mentioned above, the SC lipid system without the permeation enhancer shows two phase transitions at about 45 and 70 °C.

When 5% of 12G12 is incorporated into the membrane, the first phase transition shifts to higher temperatures. The repeat distance of the membrane starts to decrease continuously at about 50 °C. Between 57 and 61 °C, the downshift of the repeat distance is not so rapid as before. Presumably, the gel phase can be detectable in this temperature range. Above 61 °C, the periodicity decreases more abruptly again.

The sample with 15% 12G12 shows quite different behaviour. The lamellar repeat distance starts to decrease continuously at about 40 °C in one broad phase transition. The process does not show a separation into two phase transitions.

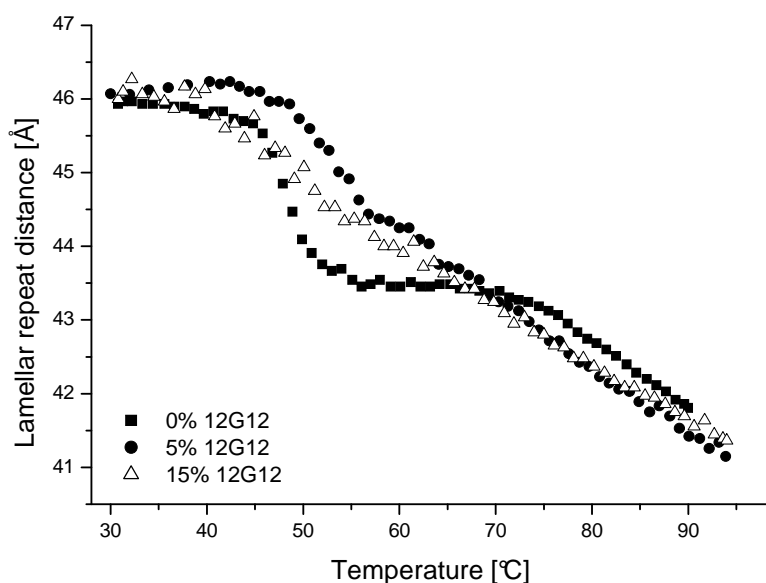


Fig. 8.6 Lamellar repeat distance of the membranes with various molar concentrations of 12G12 vs. temperature. 12G12 shifts the first phase transition to higher temperatures.

The shift of the first phase transition to higher temperatures in the sample with 5% 12G12 indicates that the SC lipids become more miscible after the addition of enhancer. Assuming that the first transition is due to separated melting of a domain including predominantly PA (Chapters 5, 6), this domain is affected by 12G12. Probably, the enhancer interacts with PA and causes an increase in the melting temperature compared to neat PA. The fact that 12G12 affects the miscibility of the SC lipids can be important for the mode of action of the enhancing effect.

8.4 Conclusions

In the present study, the effect of three permeation modulators and/or skin moisturizers as urea, oleic acid and 12G12 has been studied. Urea is a very hydrophilic and well water-soluble compound with moisturizing and enhancing effect, which is supposed to be concentrated in the water phase of the system. The permeation enhancers, oleic acid (OA) and 12G12 are of lipid type and probably incorporate into the lipid bilayers.

Urea does not affect the lamellar repeat distance of the SC lipid system at 32 °C; however, its influence on the thermotropic phase behaviour of the SC lipids is confirmed. Probably, displacement of some water molecules bound to the SC lipid headgroups by the hydrogen bonds causes a higher miscibility between the lipids.

Oleic acid shows a very limited miscibility with the SC lipid system. Higher concentrations of OA induce a phase separation. A new domain with a repeat distance of about 43.3 Å consists predominantly of OA. The phase transitions temperatures are not affected by OA. This behaviour seems to be connected with the enhancing effect of OA.

12G12 incorporates into the SC lipid matrix and does not induce a phase separation of the membrane. The increasing concentration of 12G12 in the system decreases the lamellar repeat distance. 12G12 affects the miscibility properties of the SC lipids.

The presented study confirms that the SC lipid model system developed and characterized in the framework of this thesis is convenient to describe the mode of action of permeation enhancers and other agents influencing the SC lipid organization.

9 Summary and Perspectives

This thesis is aimed at describing the development and physicochemical characterization of membrane models containing ceramides. The major purpose is to prepare a membrane model of stratum corneum lipids, which will be appropriate for further studies on the skin permeation enhancers' mode of action.

In the first part of the thesis (Chapter 4), two phytosphingosine-type ceramides, Cer[AP] and Cer[NP] were incorporated into the DMPC membrane. The prepared two-component systems should contribute to the elucidation of ceramides behaviour in biological membranes and of the role of ceramides in cell apoptosis.

The following part of the thesis (Chapters 5-7) describes a four-component stratum corneum lipid model system analogous to the composition of the native stratum corneum lipid matrix. The phase behaviour of the system and the influence of cholesterol on the stratum corneum lipid membrane have been described.

Finally, the application of the system and methods used for studying the effects of exogenous substances, e.g. permeation enhancers, has been evaluated (Chapter 8).

The detailed results of the experiments are summarized in sections 'Conclusion' at the end of every Chapter mentioned above.

Within the thesis, three types of membrane models have been prepared, namely the *multilamellar* and *unilamellar vesicles* as well as *oriented multilamellar lipid films*. The prepared samples have been tested by several conventional techniques as differential scanning calorimetry, X-ray diffraction and dynamic light scattering. Additionally, small angle neutron scattering on unilamellar vesicles and neutron diffraction on oriented lipid films have been applied. Both these methods are relatively well-known in the phospholipid research; nevertheless, they have been used to study stratum corneum lipid models for the first time within this dissertation.

The experience with the methods applied can be resumed as follows:

X-ray diffraction on multilamellar vesicles is an appropriate technique for the initial characterization of the prepared systems. The main advantage is the relatively easy sample preparation and the fact that X-ray diffraction measurements are not so time demanding. Therefore, it is possible to acquire a considerable number of results in a short time. A drawback is the relatively limited information obtained from the diffraction measurements. Although the lamellar repeat distance is a crucial membrane parameter, it does not provide information about the internal structure of the membrane.

From this point of view, *small angle neutron scattering* on unilamellar vesicles brings deeper insight into the membrane structure. The technique allows determining the average vesicle radius, the membrane thickness and the average area of membrane surface per molecule, which are important characteristics of the given membrane. Even more detailed information can be obtained by fitting the scattering curve using a mathematical model, yet it requires an advanced level of mathematical knowledge. A disadvantage of small angle neutron scattering is a need for stable unilamellar vesicles from stratum corneum lipids, which are difficult to prepare, however. Additionally, the fact that the stratum corneum lipid vesicles can be prepared only at high pH values must be taken into consideration while interpreting the SANS results, because the pH of the native stratum corneum is approximately 5.5.

A real insight into the internal membrane structures is achieved by *neutron diffraction* on oriented multilamellar lipid films. The profile of neutron scattering length density determined by Fourier transformation provides detailed information about the membrane structure, e.g. the thickness of the membrane, of the polar head group and of the hydrocarbon chain region, the position of a molecule in the membrane or the water distribution profile of the membrane. A negative side of neutron diffraction is again somewhat difficult sample preparation, because only very well organised lipid films with a low mosaicity provide a strong diffraction signal with a sufficient number of Bragg's reflections for neutron length density profile calculation. Neutron diffraction measurements are also time demanding.

In summary, all the applied techniques show some positives and negatives. It is just the conjunction of the methods, what seems to be suitable for the detailed stratum corneum lipid membrane characterization.

The experiments described in this thesis are useful for a range of the subsequent studies. As mentioned above, the prepared stratum corneum lipid model system and the methods used can be applied in studying the mode of action of skin permeation enhancers at the molecular level. However, also the effect of the particular components of the membrane model (e.g. cholesterol sulphate) should be described more deeply. This can contribute to elucidate the molecular backgrounds of skin diseases with symptoms of damaged skin barrier (e.g. ichthyosis or psoriasis). Herewith, the treatment could be improved.

10 Zusammenfassung und Ausblick

Diese Arbeit beschreibt die Entwicklung und physikochemische Charakterisierung von Membranmodellen, welche Ceramide enthalten. Das Hauptvorhaben ist, ein Membranmodell aus Stratum corneum-Lipiden bereitzustellen, welches in weiteren Studien für die Untersuchung der Wirkungsmechanismen von Hautpenetrationsmodulatoren einsetzbar wäre.

Im ersten Teil der Arbeit (Kapitel 4) werden zwei Ceramide des Phytosphingosin-Typus, Cer[AP] und Cer[NP], in eine DMPC-Membran eingefügt. Diese binären Systeme sollten zur Erklärung der Rolle der Ceramiden bei der Apoptose beitragen.

Die folgenden Teile der Arbeit (Kapitel 5-7) befassen sich mit dem quaternären Lipidmodellsystem, welches die Struktur der nativen Stratum corneum-Lipidmatrix imitiert. Das Phasenverhalten der hergestellten Systeme und der Einfluss von Cholesterol auf die Stratum corneum-Lipidmembran werden hier beschrieben.

Schließlich werden die Anwendung des entwickelten Stratum corneum-Lipidmodells sowie die Methoden, die beim Studium der Effekte ausgewählter exogener Substanzen (z.B. der Penetrationenhancer) verwendet wurden, bewertet (Kapitel 8).

Die ausführlichen Ergebnisse der einzelnen Studien werden im Teil ‚Conclusions‘ am Schluss der jeweiligen Kapitel zusammengefasst.

Im Rahmen dieser Arbeit wurden drei Typen von Membranmodellen hergestellt. Es handelt sich dabei um *multi-* und *unilamellare Vesikel* sowie um *organisierte multilamellare Lipidfilme*. Die vorbereiteten Proben wurden mit einigen konventionellen Methoden wie differential scanning calorimetry, Röntgendiffraktion und dynamischer Lichtstreuung charakterisiert. Zusätzlich wurden hier ebenfalls die Neutronenkleinwinkelstreuung an den unilamellaren Vesikeln und die Neutronendiffraktion an den organisierten multilamellaren Filmen angewendet. Beide Methoden werden in der Phospholipidforschung verwendet. Davon abgesehen werden diese Techniken innerhalb dieser Dissertation zum ersten Mal bei der Erforschung der Stratum corneum-Lipidsysteme angewendet.

Die Erfahrung mit den verwendeten Methoden kann folgendermaßen zusammengefasst werden:

Die *Röntgendiffraktion* an multilamellaren Vesikeln ist eine einsetzbare Technik für die Primärcharakterisierung der vorbereiteten Systeme. Die Hauptvorteile dieser Methoden sind die relativ einfache Probenvorbereitung und die kurzen Messzeiten. Dadurch kann eine relativ große Menge von Ergebnissen innerhalb kurzer Zeit gewonnen werden. Auf der anderen Seite sind die Informationen, welche von den Röntgenmessungen zu erhalten werden, weniger ergiebig. Der lamellare Wiederholabstand ist zwar ein entscheidender Membranparameter, jedoch liefert er keine Aussage über die innere Membranstruktur.

Von diesem Gesichtspunkt aus bringt die Neutronenkleinwinkelstreuung an unilamellaren Vesikeln einen neuen Einblick in die Membranstruktur. Diese Technik ermöglicht es, den durchschnittlichen Vesikelradius, die Membrandicke und die durchschnittliche Fläche der Membranoberfläche per Molekül zu bestimmen. Das Fitten der Streukurven durch ein mathematisches Modell, welches allerdings sehr gute mathematische Kenntnisse vorausgesetzt, bietet sogar noch viel ausführlichere Informationen. Ein Nachteil der Neutronenkleinwinkelstreuung ist die Notwendigkeit stabiler unilamellarer Vesikel, welche jedoch schwierig herzustellen sind. Da der pH-Wert des nativen Stratum corneum nur 5.5 beträgt und die Vesikel der Stratum corneum-Lipide nur bei hohen pH-Werten hergestellt werden können, sind auch die Ergebnisse kritisch zu diskutieren.

Einen differenzierten Einblick in die innere Membranstruktur ermöglicht die Neutronendiffraktion an organisierten multilamellaren Lipidfilmen. Das mittels der Fourier Transformation gewonnene Neutronenstredichteprofil macht es möglich, detaillierte Informationen über den Aufbau der Membranstruktur zu gewinnen. Unter anderem können die Membrandicke, die Dicke der Region der polaren Kopfgruppen und der Kohlenwasserstoffketten, die Lage der einzelnen Moleküle sowie die Wasserverteilung in der Membran bestimmt werden. Das Problem bei der Neutronendiffraktion ist wiederum eine etwas komplizierte Probenvorbereitung. Nur sehr gut organisiertes Probenmaterial mit niedriger Mosaizität liefert ein starkes Diffraktionsignal mit einer genügenden Anzahl von Bragg'schen Reflexionen, welche für die Berechnung des Neutronenstredichteprofiles benötigt wird. Die Neutronendiffraktionsmessungen sind auch relativ zeitaufwendig.

Insgesamt weisen alle benutzten Messmethoden einige Vor- und Nachteile auf. Gerade die Kombination der Techniken scheint aber höchst günstig für eine detaillierte Charakterisierung der Stratum corneum-Lipidmembranen zu sein.

Die in dieser Arbeit beschriebenen Experimente sind nutzbringend für eine Vielzahl von künftigen Studien. Wie schon oben erwähnt wurde, sind das entwickelte Stratum corneum-Lipidmodellsystem und die eingesetzten Methoden anwendbar in der Erforschung der Wirkungsmechanismen von Penetrationsmodulatoren auf molekularer Ebene. Gleichzeitig

sollten Effekte der einzelnen Komponenten des Membranmodells (z.B. Cholesterolsulfates) ausführlicher beschrieben werden, was zur Erklärung des molekularen Hintergrundes von Erkrankungen mit pathologischen Symptomen in der Hautbarriere (z.B. Ichthyosis oder Psoriasis) beitragen und die Optimierung der Therapie fördern könnte.

References

- [1] Chuong, C.M., Nickloff, B.J., Elias, P.M., Goldsmith, L.A., Macher, E, Maderson, P.F.A., Sunberg, J.P., Tagami, H., Plonka, P.M., Thestrup-Pedersen, K., Bernard, B.A., Schroder, J.M., Dotto, P., Chang, M.H.C., Williams, M.L., Feingold, K.R., King, L.E., Klingman, A.M., Rees, J.L., Christophers, E., 2002. What is the 'true' function of skin? *Exp. Dermatol.* 11, 159-187.
- [2] Menon, G.K., 2002. New insights into skin structure: scratching the surface. *Adv. Drug Del. Rev.* 54, Suppl. 1, S3-S17.
- [3] Elias, P. M., Feingold, K.R., Fluhr, J. Skin as organ of protection. In: *Fitzpatrick's Dermatology in general medicine*. Edited by Freedberg, I. et al. McGraw – Hill Comp., 2003.
- [4] Elias, P. M., 2005. Stratum corneum defensive functions: An integrated view. *J. Invest. Dermatol.* 125, 183-200.
- [5] Windsor, T. and Burch, G.E. 1944. Differential roles of layers of human epigastric skin on diffusion rate of water. *Arch. Intern. Med.* 74, 428-436.
- [6] Wertz, P. W., and van den Bergh, B., 1998. The physical, chemical and functional properties of lipids in the skin and other biological barriers. *Chem. Phys. Lipids* 91, 85-96.
- [7] Asbill, C.S. and Michniak, B.B., 2000. Percutaneous penetration enhancers: local versus transdermal activity. *PSTT*, 3, 36-40.
- [8] Neubert, R. H. H., Wohlrab, W. A., Marsch, W. Ch. *Dermatopharmazie*, Wissenschaftliche Verlagsgesellschaft mbH, Stuttgart, 2001, p. 3-25, 105-134.
- [9] Neubert, R., Schmalfuß, U., Wohlrab, W., Huschka, Ch., 1996. Wirkstoffpenetration in die Haut und deren Modulation. *Pharmazeutische Zeitung* 141 (17), 1483-1493.
- [10] Williams, M. L. and Elias, P. M., 1981. Stratum corneum lipids in disorders of cornification. *J. Clin. Invest.* 68, 1404-1410.
- [11] Motta, S., Monti, M., Sesana, S., Mellese, L., Ghidoni, R., Caputo, R., 1994. Abnormality in water barrier function in psoriasis: Role of ceramide fractions. *Arch. Dermatol.* 130, 452-456.
- [12] Motta, S., Sesana, S., Monti, M., Giuliani, A., Caputo, R., 1994. Interlamellar lipid differences between normal and psoriatic stratum corneum. *Acta derm. venerol., Supp.* 186, 131-132.

- [13] Hara, J., Higuchi, K., Okamoto, R., Kawashima, M., Imokawa, G., 2000. High-expression of sphingomyelin deacylase is an important determinant of ceramide deficiency leading to barrier disruption in atopic dermatitis. *J. Invest. Dermatol.* 115, 406-413.
- [14] Choi, M.J., Maibach, H.I., 2005. Role of ceramides in barrier function of healthy and diseased skin. *Am. J. Clin. Dermatol.* 6, 215-223.
- [15] Michaels, A.S., Chandrasekaran, S.K., Shaw, J.E., 1975. Drug permeation through human skin. Theory and in vitro experimental measurements. *AIChE J.* 21, 985-996.
- [16] Coderch, L., López, O., de la Maza, A., and Parra, J., 2003. Ceramides and skin function. *Am. J. Clin. Dermatol.* 4, 107-129.
- [17] Madison, K.C., 2003. Barrier function of the skin: 'La raison d'être' of the epidermis. *J. Invest. Dermatol.* 121., 231-241
- [18] Landmann, L., 1986. Epidermal permeability barrier: transformation of lamellar granule-disks into intercellular sheets by a membrane fusion process, a freeze-fracture study. *J. Invest. Dermatol.* 87, 202-209.
- [19] Norlén, L., 2001. Skin barrier formation: The membrane folding model. *J. Invest. Dermatol.* 117, 823-829.
- [20] Wertz, P. W., 2000. Lipids and barrier function of the skin. *Acta Derm. Venerol.; Supp.* 208, 7-11.
- [21] Wertz, P., 1996. The nature of the epidermal barrier: biochemical aspects. *Adv. Drug Del. Rev.* 18, 283-294.
- [22] Ponc, M., Weerheim, A., Lankhorst, P., and Wertz, P., 2003. New acylceramide in native and reconstructed epidermis. *J. Invest. Dermatol.* 120, 581-588.
- [23] Wertz, P.W. and Downing, D.T., 1983. Ceramides of pig epidermis: structure determination. *J. Lipid. Res.* 24, 759-765.
- [24] Motta, K., Monti, M., Sesana, S. Caputo, R, Carelli, S., and Ghidoni, R., 1993. Ceramide composition of the psoriatic scale. *Biochim. Biophys. Acta.* 1182, 145-151.
- [25] Breathnach, A.S., Goodnam, T., Stolinsky, C., Gross, M., 1973. Freeze fracture replication of cells of stratum corneum human epidermis. *J. Anat.* 114, 65-81.
- [26] Bouwstra, J.A., Honeywell-Nguyen, P.L., 2002. Skin structure and mode of action of vesicles. *adv. Drug Del. Rev.* 54, Suppl. 1., S41-S55.
- [27] Madison, K.C., Schwartzendruber, D.C., Wertz, P.W., and Downing, D.T., 1987. Presence of intact intercellular lipid lamellae in the upper layers of the stratum corneum. *J. Invest. Dermatol.* 88, 714-718.
- [28] White, S.H., Mirejovsky, D., King, G.I. 1988. Structure of lamellar lipid domains and corneocyte envelopes of murine stratum corneum. An x-ray diffraction study. *Biochemistry* 27, 3725-3732.
- [29] Bouwstra, J.A., Gooris, G.S., Van der Speck, J.A., Braas, W., 1991. Structural investigations of human stratum corneum by small-angle X-ray scattering. *J. Invest. Dermatol.* 97, 1005-1012.

- [30] Bouwstra, J.A., Gooris, G.S., Salomons-de Vries, M.A., Van der Spek, J.A., Bras, W., 1992. Structure of human stratum corneum as a function of temperature and hydration: A wide-angle X-ray diffraction study. *Int. J. Pharm.*, 84, 205-216.
- [31] Bouwstra, J. A., Gooris, G. S., Bras, W., and Downing, D. T., 1995. Lipid organization in pig stratum corneum. *J. Lipid. Res.* 36, 685-695.
- [32] Bouwstra, J.A., Gooris, G.S., Cheng, K., Weerheim, A., Bras, W., Ponec, M., 1996. Phase behaviour of isolated skin lipids. *J. Lipid. Res.* 37, 999-1011.
- [33] McIntosh, T.J., Stewart, M.E., Downing, D.T. 1996. X-ray diffraction analysis of isolated skin lipids: reconstitution of intercellular lipid domains. *Biochemistry* 35, 3649-3653.
- [34] de Jager, M.W., Gooris, G.S., Dolbnya, I.P., Bras, W., Ponec, M., Bouwstra, J.A., 2003. The phase behaviour of skin lipid mixtures based on synthetic ceramides *Chem. Phys. Lipids* 124, 123-134.
- [35] Hill, J. R. and Wertz, P.W., 2003. Molecular models of the intercellular lipid lamellae from epidermal stratum corneum. *Biochim. Biophys. Acta* 1616, 121-126.
- [36] Bouwstra, J.A., Gooris, G.S., Dubbelaar, F.E.R., Weerheim, A.M., Ijzerman, A.P., Ponec, M., 1998. Role of ceramide 1 in the molecular organization of the stratum corneum lipids. *J. Lipid. Res.* 39, 186-196.
- [37] Bouwstra, J.A., Pilgram, G., Gooris, G., Koerten, H., and Ponec, M., 2001. New aspects of the skin barrier organization. *Skin Pharmacol. Appl. Skin Physiol.* 14, Suppl. 1, 52-62.
- [38] Vávrová, K., 2003. Modification of the skin barrier properties; permeation enhancers and the stratum corneum repair. Dissertation, Faculty of Pharmacy Hradec Králové, Charles University in Prague.
- [39] Wegener, M., Neubert, R., Rettig, W., Wartewig, S., 1996. Structure of stratum corneum lipids characterized by FT-Raman spectroscopy and DSC. I. ceramides. *Int. J. Pharm.* 128, 203-213.
- [40] Garidel, P., 2002. Calorimetric and spectroscopic investigations of phytosphingosine ceramide membrane organisation. *Phys. Chem. Chem. Phys.*, 4, 1934-1942.
- [41] Velkova, V., Lafleur, M., 2002. Influence of the lipid composition on the organization of skin lipid model mixtures: an infrared spectroscopy investigation. *Chem. Phys. Lipids* 117, 63-74.
- [42] Bouwstra, J.A., Gooris, G.S., Dubbelaar, F.E.R., Ponec, M., 2001. Phase behaviour of lipid mixtures based on human ceramides: coexistence of crystalline and liquid phases. *J. Lipid. Res.* 42, 1759-1770.
- [43] Kitson, N., Thewalt, J., Lafleur, M., and Bloom, M., 1994. A model membrane approach to the epidermal permeability barrier. *Biochemistry* 33, 6707-6715.
- [44] Fenske, D.B., Thewalt, J.L., Bloom, M., and Kitson, N., 1994. Model stratum corneum intercellular membranes: ^2H NMR of macroscopically oriented multilayers. *Biophys. J.* 67, 1562-1573.
- [45] Forslind, B., 1994. A domain mosaic model of the skin barrier. *Acta Derm. Venerol.* 74, 1-6.

- [46] Schwarzendruber, D.C., Wertz, P.W., Kitko, D.J., Madison, K.C., and Downing, D.T., 1989. Molecular models of the intercellular lamellae in mammalian stratum corneum. *J. Invest. Dermatol.* 92, 251-257.
- [47] Kuempel, D., Schwarzendruber, D.C., Squier, C.A., Wertz, P.W., 1998. In vitro reconstitution of stratum corneum lipid lamellae. *Biochim. Biophys. Acta* 1372, 135-140.
- [48] Bouwstra, J.A., Honeywell-Nguyen, P.L., Gooris, G.S., and Ponec, M., 2003. Structure of the skin barrier and its modulation by vesicular formulations. *Prog. Lipid Res.* 42, 1-36.
- [49] Norlén, L., 2001. Skin barrier structure and function: The single gel phase model. *J. Invest. Dermatol.* 117, 830-836.
- [50] Corcery, R.W., 2002. The anti-parallel, extended or splayed-chain conformation of amphiphilic lipids. *Coll. Surf. B* 26, 3-20.
- [51] Bouwstra, J.A., Pilgram, S.K., Ponec, M., 2002. Does the single gel phase exist in stratum corneum? *J. Invest. Dermatol.* 118, Letters to the editor, 897-898.
- [52] Norlén, L., 2002. Reply-letters to the editor. *J. Invest. Dermatol.* 118, 889-901.
- [53] Purdon, C. H., Azzi, C.G., Zhang, J., Smith, E.W., Maibach, H.I., 2004. Penetration enhancement of transdermal delivery – current permutations and limitations. *Crit. Rev. Ther. Drug Carr. Syst.* 21, 97-132.
- [54] Potts, R.O. and Guy, R.H., 1992. Predicting skin permeability. *Pharm. Res.* 9, 663-669.
- [55] Marrink, S.J., Berendsen, J.C., 1996. Permeation process of small molecules across lipid membranes studied by molecular dynamics simulations. *J. Phys. Chem.* 100, 16729-16738.
- [56] Prausnitz, M.R., Mitragotri, S., Langer, R., 2004. Current status and future potential of transdermal drug delivery. *Nature Reviews, Drug Disc.* 3, 115-124.
- [57] Williams, A.C. and Barry, B.W., 2004. Penetration enhancers. *Adv. Drug Del. Rev.* 56, 603-618.
- [58] López-Cervantes, M., Márquez-Mejía, E, Cázares-Delgadillo, J., Quintanar-Guerrero, D., Ganem-Quintanar, A., 2006. Chemical enhancers for the absorption of substance through the skin: Laurocapram and its derivatives. *Drug Develop. Indust. Pharm.* 32, 267-286.
- [59] Vávrová, K., Zbytovská, J., and Hrabálek, A., 2005. Amphiphilic transdermal permeation enhancers: structure-activity relationships. *Curr. Med. Chem.* 12, 2273-2291.
- [60] Clas, S.-D., Dalton, C.R., Hancock, B.C., 1999. Differential scanning calorimetry: applications in drug development. *P. S. T. T.* 2, 311-320.
- [61] Wegener, M., Neubert, R., Rettig, W., Wartewig, S., 1997. Structure of stratum corneum lipids characterized by FT-Raman spectroscopy and DSC. III. Mixtures of ceramides and cholesterol, *Chem. Phys. Lipids* 88, 73-82.
- [62] Wartewig, S., Neubert, R., Rettig, W., Hesse, K., 1998. Structure of stratum corneum lipids characterized by FT-Raman spectroscopy and DSC. IV. Mixtures of ceramides and oleic acid. *Chem. Phys. Lipids* 91, 145-152.

- [63] Raudenkolb, S., Hübner, W., Rettig, W., Wartewig, S., Neubert, R., 2003. Polymorphism of ceramide 3. Part 1: an investigation focused on the head group of N-octadecanoylphytosphingosine. *Chem. Phys. Lipids* 123, 9-17.
- [64] Zbytovská, J., Raudenkolb, S., Wartewig, S., Hübner, W., Rettig, W., Pissis, P., Hrabálek, A., Doležal, P., Neubert, R., 2004. Phase behaviour of transkarbam 12. *Chem. Phys. Lipids* 129, 97-109.
- [65] Wartewig, S. and Neubert, R.H.H., 2005. Pharmaceutical applications of Mid-IR and Raman spectroscopy. *Adv. Drug Del. Rev.* 57, 1144-1170.
- [66] Colthup, N.B.; Daly, L.H.; Wiberley, S.E.: *Introduction to Infrared and Raman spectroscopy*, Academic Press, Inc., 1990.
- [67] Mendelsohn, R., Moore, D.J., 1998. Vibrational spectroscopic studies of lipid domains in biomembranes and model systems. *Chem. Phys. Lipids* 96, 141-157.
- [68] Snyder, R.G., Schachtschneider, J.H. 1963 *Spectrochim. Acta* , Vibrational analysis of the n-paraffins I : Assignments of infrared bands in the spectra of C_3H_8 through $n-C_{19}H_{40}$, 85-116.
- [69] Brown, K., Bicknell-Brown, E., Ladjadj, M., 1987. Raman-active bands sensitive to motion and conformation at the chain termini and backbones of alkanes and lipids. *J. Phys. Chem.* 91, 3436-3442.
- [70] Moore, D.J., Rerek, M.E., Mendelsohn, R., 1997. FTIR Spectroscopy Studies of the Conformational Order and Phase Behavior of Ceramides. *J. Phys. Chem. B* 101, 8933-8940.
- [71] Snyder, R.G., Hsu, S.L., Krimm, S., 1978, Vibrational spectra in the carbon-hydrogen stretching region and the structure of the polymethylene chain *Spectrochim. Acta* 34A, 395-406.
- [72] Minoni, G., Zerbi, G., 1982. End effects on longitudinal accordion modes: fatty acids and layered systems. *J. Phys. Chem.* 86, 4791-4798.
- [73] Pasher, I., Lundmark, M., Nyholm, P.-G., Sundell, S., 1992. Crystal structures of membrane lipids. *Biochim. Biophys. Acta* 1113, 339-373.
- [74] Kobayashi, M., Kaneko, F., Sato, K., Suzuki, M., 1986. Vibrational spectroscopic study on polymorphism and order-disorder phase transition in oleic acid *J. Phys. Chem.* 90, 6371-6378.
- [75] Tandon, P., Foerster, G., Neubert, R., Wartewig, S., 2000. Phase transitions in oleic acid as studied by X-ray diffraction and FT-Raman spectroscopy *J. Mol. Struct.* 524, 201-215.
- [76] Anigbogu, A., Williams, A.C., Barry, B.W., Edwards, H.M.G., 1995. Fourier transform Raman spectroscopy of interactions between the penetration enhancer dimethyl sulfoxide and human stratum corneum. *Int. J. Pharm.* 125, 265-282.
- [77] Percot, A., Lafleur, M., 2001. Direct observation of domains in model stratum corneum lipid mixtures by Raman microspectroscopy. *Biophys. J.* 81, 2144-2153.
- [78] Raudenkolb, S., Wartewig, S., Neubert, R., 2003. Polymorphism of ceramide 3. Part 2: a vibrational spectroscopic and X-ray powder diffraction investigation of N-octadecanoyl phytosphingosine and the analogous specifically deuterated d35 derivative. *Chem. Phys. Lipids* 124, 89-101.

- [79] Chen, H.-C., Mendelsohn, R., Rerek, M.E., Moore, D.J., 2000. Fourier transform infrared spectroscopy and differential scanning calorimetry studies of fatty acid homogeneous ceramide 2 *Biochim. Biophys. Acta* 1468, 293-303.
- [80] Rerek, M.E., Chen, H.-C., Markovic, B., Van Wyck, D., Garidel, P., Mendelsohn, R., Moore, D.J. *J. Phys. Chem. B* 2001, 105, 9355.
- [81] Prince, E, 2001. Diffraction: X-ray, neutron and electron. In: *Encyclopedia of Chemical Physics and Physical chemistry*. Edited by Moore, J.H., Specer, N.D, Volume 2, Chapter B1.8. Inst. of physics Publ., Bristol, ISBN 0750303131.
- [82] King, S.M. Small angle neutron scattering. Downloaded 09/21/2005 at www.isis.rl.ac.uk/largescale/log/documents/sans.htm.
- [83] Loewenhaupt, M., 1987. Vergleich von Neutronen- und Röntgen- Streuung. In: *Synchrotronstrahlung in der Festkörperphysik. Vorlesungsmanuskripte des 18. IFF-Ferienkurses. Kernforschungsanlage Jülich*, pp. 36.3-36.12.
- [84] Grossmann, J.G. Shape determination of biomolecules in solution from synchrotron X-ray scattering. In: *Scattering and inverse scattering in pure and applied science*. Edited by Pike, R. and Sabatier, P. Academic Press, San Diego, San Francisco, New York, Boston, London, Sydney, Tokio, 2002. pp. 1123-1139.
- [85] Shukla, A., 2003. Characterization of microemulsions by using small angle scattering techniques. Dissertation, mathematisch-Naturwissenschaftlich-Technische Fakultät, Martin-Luther-University Halle-Wittenberg.
- [86] Jenkins, R., Snyder, R.L. *Introduction to X-ray powder diffractometry*, Willey, New York, 1996, pp. 1-94.
- [87] Michette, A.G., 2002. Fundamentals of X-ray scattering. In: *Scattering – Scattering and inverse scattering in pure and applied science*. Edited by Pike, R. and Sabatier, P. Academic Press, London , San Diego, 2002. pp.: 1099-1107.
- [88] Kučerka, N., Nagle, J.F., Feller, S. E., Balgavý, P., 2004. models to analyze small-angle neutron scattering from unilamellar lipid vesicles. *Phys. Rev. E* 69, 051903: 1-9.
- [89] Hou, S.Y.E., Rehfeld, S.J., Plachy, W.Z., 1991. X-ray diffraction and electron paramagnetic resonance spectroscopy of mammalian stratum corneum lipid domains. *Adv. Lipid Res.* 24, 141-171.
- [90] Laggner, P. X-ray diffraction of lipids. In: *Spectral properties of lipids*. Edited by Hamilton, R.J., Cast, J., Sheffield Academic Press, 1999; pp. 327-367.
- [91] Luzatti, V. X-ray diffraction of lipid-water systems. In. *Biological membranes*. Edited by Chapman, D., Academic Press London and New York, 1968; pp. 71-123.
- [92] Seddon, J.M., 1990. Structure of the inverted hexagonal (HII) phase, and non-lamellar phase transitions of lipids. *Biochim. Biophys. Acta* 1031, 1-69.
- [93] Dahlén, B., Pasher, I., 1972. Molecular arrangements in sphingolipids. Crystal structure of N-tetracosanoylphosphatidylcholine. *Acta Crystallogr. B* 28, 2396-2404.

- [94] Pasher, I., Sundell, S., 1992. Molecular arrangements in sphingolipids: crystal structure of the ceramide N-(2D,3D-dihydroxyoctadecanoyl)phytyosphingosine. *Chem. Phys. Lipids* 1992, 61, 79-86.
- [95] Wignall, G. D. and Melnichenko, Y.B., 2005. Recent applications of small-angle neutron scattering in strongly interacting soft condensed matter. *Rep. Prog. Phys.* 68, 1761-1810.
- [96] Kiselev, M.A., Lesieur, P., Kisselev, A.M., Lombardo, D., and Aksenov, V.L., 2002. Model of separated form factors for unilamellar vesicles. *Appl. Phys. A* 74, S1654-S1656.
- [97] Knoll, W., Haas, J., Stuhrmann, H.B., Fuldner, H.-H., Vogel, H., and Sackmann, E. 1981. Small-angle neutron scattering of aqueous dispersions of lipids and lipid mixtures. A contrast variation study. *J. Appl. Cryst.* 14, 191-202.
- [98] Feigin, L.A. and Svergun, D.I., 1987. Structure analysis by small-angle X-ray and neutron scattering. Plenum Publishing Corporation, New York.
- [99] Balgavý, P., Dubničková, M., Kučerka, N., Kiselev, M. A., Yaradaikin, S. P., and Uhríková, D., 2001. Bilayer thickness and lipid interface area in unilamellar extruded 1,2-diacylphosphatidylcholine liposomes: a small-angle neutron scattering study. *Biochim. Biophys. Acta* 1512, 40-52.
- [100] Kiselev, M.A., Zemlyanaya, E.V., Aswal, V.K., and Neubert, R., 2006. What can we learn about the lipid vesicle structure from the small-angle neutron scattering experiment? *Eur. Biophys. J. Biophys. Lett.* 35, 477-493.
- [101] Kiselev, M. A., Zbytovská, J., Matveev, D., Wartewig, S., Gapienko, I. V., Perez, J., Lesieur, P., Hoell, A., and Neubert, R. 2005. Influence of trehalose on the structure of unilamellar DMPC vesicles. *Colloid. Surface. A* 256, 1-7.
- [102] Garamus, V.M., Pedersen, J.S., Kawasaki, H., Maeda, H., 2000. Scattering from polymer like micelles of TDAO in salt/water solutions at semidilute concentrations. *Langmuir* 16, 6431-6437.
- [103] Nagle, J.F. and Tristram-Nagle, S. 2000. Structure of lipid bilayers. *Biochim. Biophys. Acta* 1469, 159-195.
- [104] Zaccai, G., Blasie, J.K., and Schoenborn, B.P., 1975. Neutron diffraction studies on the location of water in lecithin bilayer model membranes. *Proc. Nat. Acad. Sci. USA* 72, 376-380.
- [105] Schoenborn, B.P., 1976. Neutron scattering for the analysis of membranes. *Biochim. Biophys. Acta* 457, 41-55.
- [106] Franks N. P., Lieb, W. R., 1979. The structure of lipid bilayers and the effects of general anesthetics. *J. Mol. Biol.* 133, 469-500.
- [107] McIntosh, T., 2003. Organization of skin stratum corneum extracellular lamellae: diffraction evidence for asymmetric distribution of cholesterol. *Biophys. J.* 85, 1675-1681.
- [108] New, R.R.C., 1990. Liposomes – a practical approach. IRL Press at Oxford University Press, Oxford, New York, Tokyo.

- [109] Janich, M. 1998. Licht- und Neutronenstreuexperimente an Gallensalzmizellen. Dissertation, mathematisch-Naturwissenschaftlich-Technische Fakultät, Martin-Luther-University Halle-Wittenberg.
- [110] Finsy, R., 1994. Particle sizing by quasi-elastic light scattering. *Adv. Colloid. Interface Sci.* 52, 79-143.
- [111] Rama, J., Pino, R. Size characterization via photon correlation spectroscopy. Downloaded 09/20/2005 at www.meliorum.com.
- [112] Rheinboldt, W.C., Burkardt J. V., 1983. A locally parameterized continuation process. *ACM Trans. Math. Software* 9, 215-235.
- [113] Obeid, L. M. and Hannun, Y., A., 1995. Ceramide: a stress signal and mediator of growth suppression and apoptosis. *J. Cell. Biochem.* 58, 191-198.
- [114] Reynolds, C. P., Maurer, B. J., Kolesnick, R. N., 2004. Ceramide synthesis and metabolisms as a target for cancer therapy. *Cancer Lett.*, 206 169-180.
- [115] Radin, N. S., 2003. Designing anticancer drugs via the Achilles heel: ceramide, allylic ketones, and mitochondria. *Bioorg. Med. Chem.* 11, 2123-2142.
- [116] Holopainen, J. M., Angelova, M. I., Kinnunen, P. K. J., 2000. Vectorial budding of vesicles by asymmetrical enzymatic formation of ceramide in giant liposomes. *Biophys. J.* 78, 830-838.
- [117] Kolesnick, R. N., Goñi, F. M., Alonso, A., 2000. Compartmentalization of ceramide signaling: physical foundations and biological effects. *J. Cell. Physiol.* 184, 285-300.
- [118] Huang, H.-W., Goldberg, E. M., Zidovetzki, R., 1996. Ceramide induces structural defects into phosphatidylcholine bilayers and activates phospholipase A₂. *Biochem. Biophys. Res. Commun.* 220, 834-838.
- [119] Holopainen, J. M., Lehtonen, J. Y. A., and Kinnunen, P. K. J., 1997. Lipid microdomains in dimyristoylphosphatidylcholine-ceramide liposomes. *Chem. Phys. Lipids* 88, 1-13.
- [120] Veiga M. P., Arrondo J. L. R., Goñi, F. M., and Alonso, A., 1999. Ceramides in phospholipid membranes: Effect on bilayer stability and transition to nonlamellar phases. *Biophys. J.* 76, 342-350
- [121] Contreras, F. X., Villar, A. V., Alonso, A., Kolesnick, R., and Goñi, F. M., 2003. Sphingomyelinase activity causes transbilayer lipid translocation in model and cell membranes. *J. Biol. Chem.* 278, 37169-37174.
- [122] Contreras, F.X., Basáñez, G., Alonso, A., Herrmann, A., and Goñi, F. M., 2005. Asymmetric addition of ceramides but not dihydroceramides promotes transbilayer (Flip-Flop) lipid motion. *Biophys. J.* 77, 348-359.
- [123] Ruiz-Argüello, M. B., Basáñez, G., Goñi, F. M., and Alonso, A., 1996. Different effects of enzyme generated ceramides and diacylglycerols in phospholipid membrane fusion and leakage. *J. Biol. Chem.* 271, 43, 26616-26621.
- [124] Siskind, L. J. and Colombini, M., 2000. The lipids C₂- and C₁₆-ceramide form large stable channels. *J. Biol. Chem.* 275, 49, 38640-38644.

- [125] Kõiv, A., Mustonen, P., and Kinnunen, P. K. J., 1993. Influence of sphingosine on the thermal behavior of neutral and acidic phospholipid liposomes. *Chem. Phys. Lipids* 66, 123-134.
- [126] Mueller, E. and Blume, A., 1993. FTIR spectroscopic analysis of the amide and acid bands of ganglioside G_{M1}, in pure form and in mixtures with DMPC. *Biochim. Biophys. Acta* 1146, 45-51.
- [127] Pejewski, R., Djedovič, N., Harder, E., Ferdani, R., Schlesinger, P. H., and Gokel, G. W., 2005. Pore formation in and enlargement of phospholipid liposomes by synthetic models of ceramides and sphingomyelin. *Bioorg. Med. Chem.* 13, 29-37.
- [128] Maggio, B., Carrer, D. C., Fanani, M. L., Oliviera, R. G., and Rosetti, C. M., 2004. Interfacial behaviour of glycosphingolipids and chemically related sphingolipids. *Curr. Op. Coll. Int. Sci.* 8, 448-458.
- [129] Bielawska, A., Crane, H. M., Liotta, D., Obeid, L. M., and Hannun, Y. A., 1993. Selectivity of ceramide-mediated biology. Lack of activity of erythro-dihydroceramide. *J. Biol. Chem.* 168, 26226-26232.
- [130] Dickson, R. C., Nagiec, E. E., Skrzypek, M., Tillman, P., Wells, G. B., and Lester, R. L., 1997. Sphingolipids are potential heat stress signals in *Saccharomyces*. *J. Biol. Chem.* 272, 30196-30200.
- [131] Jenkins, G. M., Richards, A., Wahl, T., Mao, C., Obeid, L., and Hannun, Y., 1997. Involvement of yeast sphingolipids in the heat stress response of *Saccharomyces cerevisiae*. *J. Biol. Chem.* 272, 32566-32572.
- [132] Lee, J. S., Min, D. S., Park, C., Park, C. S., Cho, N. J., 2001. Phytosphingosine and C2-phytoceramides induce cell death and inhibit carbachol-stimulated phospholipase D activation in Chinese hamster ovary cells expressing the *Caenorhabditis elegans* muscarinic acetylcholine receptor. *FEBS Lett.* 499, 82-86.
- [133] Kim, T., Pak, J. H., Tchah, H., Lee, S., and Kook, M. S., 2005. Ceramide induced apoptosis in rabbit corneal fibroblasts. *Cornea* 24, 72-79.
- [134] Hwang, O., Kim, G., Jang, Y. J., Kim, S. W., Choi, G., Choi, H. J., Jeon, S. Y. J., Lee, D. G., and Lee, J. D., 2001. Synthetic phytoceramides induce apoptosis with higher potency than ceramides. *Mol. Pharmacol.* 59, 1249-1255.
- [135] Crowe, J. H., Crowe, L. M., Carpenter, J. F., Rudolph, A. S., Wistrom, A. A., Spargo, B. J., and Anchordogly, T. J., 1988. Interactions of sugars with membranes. *Biochim. Biophys. Acta* 947, 367-384.
- [136] Farwanah, H., Neubert, R., Zellmer, S., and Raith, K., 2002. Improved procedure for the separation of major stratum corneum lipids by means of automated multiple development thin-layer chromatography. *J. Chromatogr. B* 780, 443-450.
- [137] Kiselev, M.A., Lesieur, P., Kisselev, A.M., Lombardo, D., Killany, M., Lesieur, S., and Ollivon, M., 2001. A sucrose solutions application to the study of model biological membranes. *Nucl. Instr. Meth. Phys. Res. A* 470, 409-416.

- [138] Small, D. M., 1984. Lateral chain packing in lipids and membranes. *J. Lipid. Res.* 25., 1490-1500.
- [139] Holopainen, J. M., Lemmich, J., Richter, F., Mouritsen, O. G., Rapp, G., and Kinnunen, P. K. J., 2000. Dimyristoylphosphatidylcholine/C16:0-ceramide binary liposomes studied by differential scanning calorimetry and wide- and small- angle X-ray scattering. *Biophys. J.* 78, 2459-2469.
- [140] Dahlen, B. and Pasher, I., 1979. Molecular arrangements in sphingolipids. Thermotropic phase behavior of tetracosanoylphytosphingosine. *Chem. Phys. Lipids* 24, 119-133.
- [141] Raudenkolb, S., Hübner, W., Rettig, W., Wartewig, S., and Neubert, R., 2003. Polymorphism of ceramide 3. Part 1: an investigation focused on the head group of N-octadecanoylphytoshingosine. *Chem. Phys. Lipids* 123, 9-17.
- [142] de Jager, M. W., Gooris, G. S., Dolbnya, I. P., Bras, W., Ponec, M., and Bouwstra, J. A., 2004. Novel lipid mixtures based on synthetic ceramides reproduce the unique stratum corneum lipid organization. *J. Lipid Res.* 45, 923-932.
- [143] Kiselev, M. A., Wartewig S., Janich M., Lesieur., P., Kiselev, A. M., Ollivon, M., and Neubert, R., 2003. Does sucrose influence the properties of DMPC vesicles? *Chem. Phys. Lipids* 123, 31-44.
- [144] Carrer, D. C., Härtel, S., Mónaco, H. L., and Maggio, B., 2003. Ceramide modulates the lipid membrane organization at molecular and supramolecular levels. *Chem. Phys. Lipids* 122, 147-152.
- [145] Kinnunen, P. K. J., 1992. Fusion of lipid bilayers: a model involving mechanistic connection to HII phase forming lipids. *Chem. Phys. Lipids* 63, 251-258.
- [146] Holopainen, J. M., Lehtonen, J. Y. A., and Kinnunen, P. K. J., 1999. Evidence for the extended phospholipid conformation in membrane fusion and hemifusion. *Biophys. J.* 76, 2111-2120.
- [147] Stewart, M. E. and Downing, D. T., 1999. A new 6-hydroxy-4-sphingenine-containing ceramide in human skin. *J. Lipid. Res.* 40, 1434-1439.
- [148] Shapiro, L. J., Weiss, R., Buxman, M. M., Vidgoff, J., Dimond, R. L., Roller, J. A., and Wells, R. S., 1978. Enzymatic basis of typical X-linked ichthyosis. *Lancet* 2 (8093), 756-757.
- [149] Webster, D., France, J. T., Shapiro, L. J., and Weiss, R., 1978. X-linked ichthyosis due to steroid-sulphatase deficiency. *Lancet* 1 (8055), 70-72.
- [150] Zetttersen, E., Man, M.-Q., Sato, J., Denda, M., Farrell, A., Ghadially, R., Williams, M. L., Feingold, K. R., and Elias, P. M., 1998. Recessive X-linked ichthyosis: Role of cholesterol-sulfate accumulation in the barrier abnormality. *J. Invest. Dermatol.* 111, 784-790.
- [151] Williams, M. L., Feingold, K. R., Grubauer, G., and Elias, P. M., 1987. Ichthyosis induced by cholesterol-lowering drugs. Implications for epidermal cholesterol homeostasis. *Arch. Derm.* 123, 1535-1538.
- [152] Slotte, J. P., 1999. Sphingomyelin-cholesterol interactions in biological and model membranes. *Chem. Phys. Lipids* 102, 13-27.

-
- [153] McMullen, T. P. W. and McElhaney, 1996. Physical studies of cholesterol-phospholipid interactions. *Curr. Opin. Colloid Interface Sci.* 1, 83-90.
- [154] McMullen, T. P. W. and McElhaney, 1995. New aspects of the interaction of cholesterol with dipalmitoylphosphatidylcholine bilayers as revealed by high-sensitivity differential scanning calorimetry. *Biochim. Biophys. Acta* 1234, 90-98.
- [155] Huang, J. Y. and Feigenson, G. W., 1999. A microscopic interaction model of maximum solubility of cholesterol in lipid bilayers. *Biophys. J.* 76, 2142-2157.
- [156] Patta, V. and Dan, N., 2005. Effect of membrane characteristics on phase separation and domain formation in cholesterol-lipid mixtures. *Biophys. J.* 88, 916-924.
- [157] Téroová, B., Heczko, R., and Slotte, J. P., 2005. On the importance of the phosphocholine methyl groups for sphingomyelin/cholesterol interactions in membranes. *Biophys. J.* 88, 2661-2669.
- [158] Wang, X. and Quinn, P.J., 2002. Cubic phase is induced by cholesterol in the dispersion of 1-palmitoyl-2-oleoyl-phosphatidylethanolamine. *Biochim. Biophys. Acta* 1564, 66-72.
- [159] Gallová, J., Uhríková, D., Islamov, A., Kuklin, A., and Balgavý, P., 2004. Effect of cholesterol on the bilayer thickness in unilamellar extruded DLPC and DOPC liposomes. *Gen. Physiol. Biophys.* 23, 113-128.
- [160] Gallová, J., Uhríková, D., Hanulová, M., Teixeira, J., and Balgavý, P., 2004. Bilayer thickness in unilamellar extruded 1,2-dimyristoleoyl and 1,2-dierythrocoyl phosphatidylcholine vesicles: SANS contrast variation study of cholesterol effect. *Coll. Surfaces B* 38, 11-14.
- [161] Lafleur, M., 1998. Phase behaviour of model stratum corneum lipid mixtures: an infrared spectroscopy investigation. *Can. J. Chem.* 76, 1501-1511.
- [162] Chen, H.-C., Mendelsohn, R., Rerek, M.E., and Moore, D.J., 2001. Effect of cholesterol on miscibility and phase behavior in binary mixtures with synthetic ceramide 2 and octadecanoic acid. *Infrared studies. Biochim. Biophys. Acta* 1512, 345-356.
- [163] Sparr, E., Eriksson, L., Bouwstra, J. A., and Ekelund, K., 2001. AFM study of lipid monolayers: III. Phase behavior of ceramides, cholesterol and fatty acids. *Langmuir* 2001, 17, 164-172.
- [164] Kiselev, M. A., Lesieur, P., Kisselev, A. M., Grabielle-Madmond, C., and Ollivon, M., 1999. DMSO-induced dehydration of DPPC membranes studied by X-ray diffraction, small-angle neutron scattering, and calorimetry. *J. Alloys. Comp.* 286, 195-202.
- [165] Kučerka, N., Kiselev, M. A., and Balgavý, P., 2004. Determination of bilayer thickness and lipid surface area in unilamellar dimyristoylphosphatidylcholine vesicles from small-angle neutron scattering curves: a comparison of evaluation methods. *Eur. Biophys. J.* 33, 328-334.
- [166] Hatfield, R. M. and Fung, L. W. M., 1995. Molecular properties of a stratum corneum model lipid system: large unilamellar vesicles. *Biophys. J.* 68, 196-207.
- [167] Abraham, W. and Downing, D. T., 1989. Preparation of model membranes for skin permeability studies using stratum corneum lipids. *J. Invest. Dermatol.* 93, 809-813.

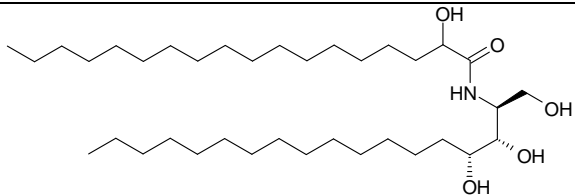
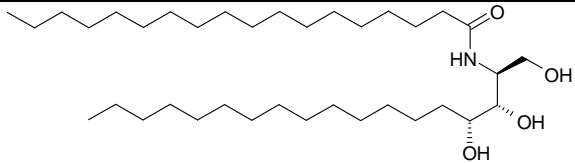
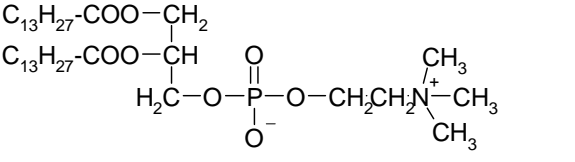
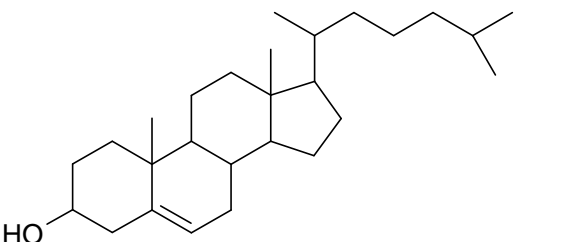
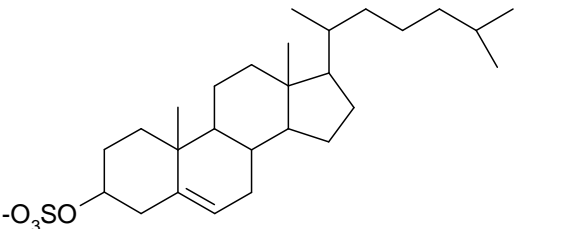
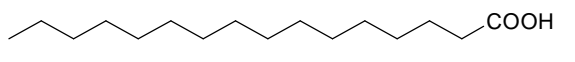
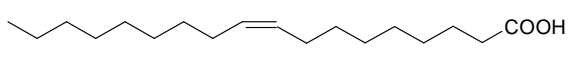
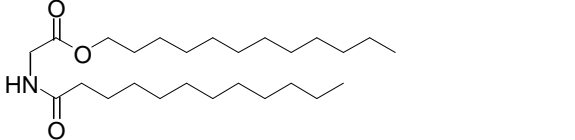
- [168] Chevalier, Y., Zemb, Y., 1990. The structure of micelles and microemulsions. *Rep. Prog. Phys.* 53, 279-371.
- [169] Vávrová, K., Zbytovská, J., Palát, K., Holas, T., Klimentová, J., Hrabálek, A., Doležal, P., 2004. Ceramide analogue 14S24 ((S)-2-tetracosanoylamino-3-hydroxypropionic acid tetradecyl ester is effective in skin barrier repair in vitro. *Eur. J. Pharm. Sci.* 21, 581-587.
- [170] Bodor, N., Gabanyi, Z., Wong, C., 1989. A new method for the estimation of partition coefficients. *J. Am. Chem. Soc.* 111, 3783-3786.
- [171] Gavezzotti, A., 1983. The calculation of molecular volumes and the use of volume analysis in the investigation of structured media and of solid state organic reactivity. *J. Am. Chem. Soc.* 105, 5220-5225.
- [172] Ayranci, E. and Akgul, G., 2003. Apparent Molar Volumes and Viscosities of Lauric, Palmitic, and Stearic Acids in 2-Butanol at (20, 30, 40, and 60) °C. *J. Chem. Eng. Data* 48, 56-60.
- [173] Góralski, P. and Wasiak, M., 2003. Influence of van der Waals interactions on volumetric properties of cholesterol in solvents of linear structure. *J. Chem. Thermodynamics* 35, 1623-1634.
- [174] Craven, B.M., 1976. Crystal structure of cholesterol monohydrate. *Nature* 260, 727-729.
- [175] Downing, D. T., Abraham, W., Wegner, B., Willman, K. W., Marshall, J. E., 1993. Partition of sodium dodecyl sulfate into stratum corneum lipid liposomes. *Arch. Dermatol. Res.* 285, 151-157.
- [176] Hatfield, R. M. and Fung, L. W. M., 1999. A new model system for lipid interaction in stratum corneum vesicles: effects of lipid composition, calcium, and pH. *Biochemistry* 38, 784-791.
- [177] de Jager, M., Gooris, G., Ponec, M., and Bouwstra, J., 2004. Acylceramide head group architecture affects lipid organization in synthetic ceramide mixtures. *J. Invest. Dermatol.* 123, 911-916.
- [178] Bouwstra, J. A., Gooris, G. S., Dubbelaar, F. E. R., and Ponec, M., 1999. Cholesterol sulfate and calcium affect stratum corneum lipid organization over a wide temperature range. *J. Lipid Res.* 40, 2303-2312.
- [179] Bouwstra, J. A., Dubbelaar, F. E. R., Gooris, G. S., Weerheim, A. M., and Ponec, M., 1999. The role of ceramide composition in the lipid organization of the skin barrier. *Biochim. Biophys. Acta* 1419, 127-136.
- [180] Bouwstra, J. A., Thewalt, J., Gooris, G. S., and Kitson, N., 1997. A model membrane approach to the epidermal permeability barrier: an X-ray diffraction study. *Biochemistry* 36, 7717-7725.
- [181] Moore, D.J. and Rerek, M.E., 2000. Insights into the molecular organization of lipids in the skin barrier from infrared spectroscopy studies of stratum corneum lipid models. *Acta Derm. Venerol.; Supp.* 208, 16-22.
- [182] Kiselev, M. A., Ryabova, N. Y., Balagurov, A. M., Dante, S., Hauss, T., Zbytovská, J., Wartewig, S., and Neubert, R., 2005. New insights into the structure and hydration of a stratum corneum lipid model membrane by neutron diffraction. *Eur. Biophys. J.*, in press.

- [183] Mizushima, H., Fukasawa, J.-I., and Suzuki, T., 1996. Phase behaviour of artificial stratum corneum lipids containing a synthetic pseudo-ceramide: a study of the function of cholesterol. *J. Lipid. Res.* 37, 361-367.
- [184] Zbytovská, J., Kiselev, M. A., Funari, S. S., Garamus, V., Wartewig, S., and Neubert, R., 2005. Influence of phytosphingosine-type ceramides on the structure of DMPC membrane, *Chem. Phys. Lipids* 138, 69-80.
- [185] Moore, D.J., Rerek, M.E., Mendelsohn, R., 1997. Lipid domains and orthorhombic phases in model stratum corneum: evidence from Fourier transform infrared spectroscopy studies. *Biochem. Biophys. Res. Commun.* 231, 797-801.
- [186] Seul, M., and Sammon, M.J., 1990. Preparation of surfactant multilayer films on solid substrates by deposition from organic solution. *Thin Solid Films* 185, 287-305.
- [187] O'Brien, F.E.M., 1948. The control of humidity by saturated salt solutions. *J. Sci. Inst.* 25, 73-76.
- [188] Worcester, D. L. Franks, N.P., 1976. Structural analysis of hydrated egg lecithin and cholesterol bilayers. II. Neutron diffraction. *J. Mol. Biol.* 100, 359-378.
- [189] Small, D.M. *The physical chemistry of lipids.* Plenum Press New York and London, 1986. pp. 21-25
- [190] Jacobi, O.K., 1959. Moisture regulation in the skin. *Drug. Cosmet. Ind.* 84, 732-812.
- [191] Niedner, R., Ziegenmeyer, J. *Dermatika: therapeutischer Einsatz, Pharmakologie und Pharmazie.* Wissenschaftliche Verlagsgesellschaft mgH Stuttgart, 1992, pp. 132-133.
- [192] Lodén, M., 2003. Role of topical emollients and moisturizers in the treatment of dry skin barrier disorders. *Am. J. Clin. Dermatol.* 4, 771-788.
- [193] Kim, C.K., Kim, J.J., Chi, S.C., Shim, C.K., 1993. Effect of fatty acids and urea on the penetration of ketoprofen through rat skin. *Int. J. Pharm.* 99, 109-118.
- [194] Lampe, M.A., Burlingame, A.L., Whitney, J.A., Williams, M.L., Brown, B.E., Roitman, E., Elias, P.M., 1983. Human stratum corneum lipids: characterization and regional variations. *J. Lipid Res.* 24, 120-130.
- [195] Norlén, L., Nicander, I., Lundsjö, A., Cronholm, T., Forslind, B., 1998. A new HPLC based method for the quantitative analysis of inner stratum corneum lipids with special reference to the free fatty acid fraction. *Arch. Dermatol. Res.* 290, 508-516.
- [196] Wertz, P., Schwarzendruber, D.C., Madison, K.C., Downing, D.T., 1987. Composition and morphology of epidermal cyst lipids. *J. Invest. Dermatol.* 89, 419-425.
- [197] Ongpipattanakul, B., Burnette, R.R., Potts, R.O., Francoeur, M.L., 1991. Evidence that oleic acid exists in a separate phase within stratum corneum lipids. *Pharm. Res.* 8, 350-354.
- [198] Tanojo, H., Bos-van Geest, A., Bouwstra, J.A., Junginger, H.E., Boddé, H., 1997. In vitro human skin barrier perturbation by oleic acid: Thermal analysis and freeze fracture electron microscopy studies. *Thermochim. Acta* 293, 77-85.

- [199] Vávrová, K., Hrabálek, A., Doležal, P., Holas, T., Zbytovská, J., 2003. L-serine and glycine based ceramide analogues as transdermal permeation enhancers: Polar head size and hydrogen bonding. *Bioorg. Med. Chem. Lett.* 13, 2351-2353.
- [200] Vávrová, K., Hrabálek, A., Doležal, P., Šámalová, L., Palát, K., Zbytovská, J., Holas, T., Klimentová, J., 2003. Synthetic ceramides analogues as skin permeation enhancers: structure-activity relationships. *Bioorg. Med. Chem.* 11, 5381-5390.

Appendix A

Table A 1 Structures of the chemical substances used in the sample preparation

Chemical structure	Substance	Abbreviation
	Ceramide [AP] α -hydroxy-N-octadecanoylphytosphingosine	Cer[AP]
	Ceramide [NP] N-stearoylphytosphingosine	Cer[NP]
	Dimystoylphosphocholine	DMPC
	Cholesterol	CHOL
	Cholesterol sulphate	CS
	Palmitic acid	PA
	Oleic acid	OA
	N-lauroylglycine lauryl ester	12G12
$\text{NH}_2\text{-CO-NH}_2$	Urea	

Appendix B

Raman spectroscopy of the stratum corneum lipid model system

Method

Bruker FT-Raman spectrometer RFS 100/S (Bruker Optik, Ettlingen, Germany)

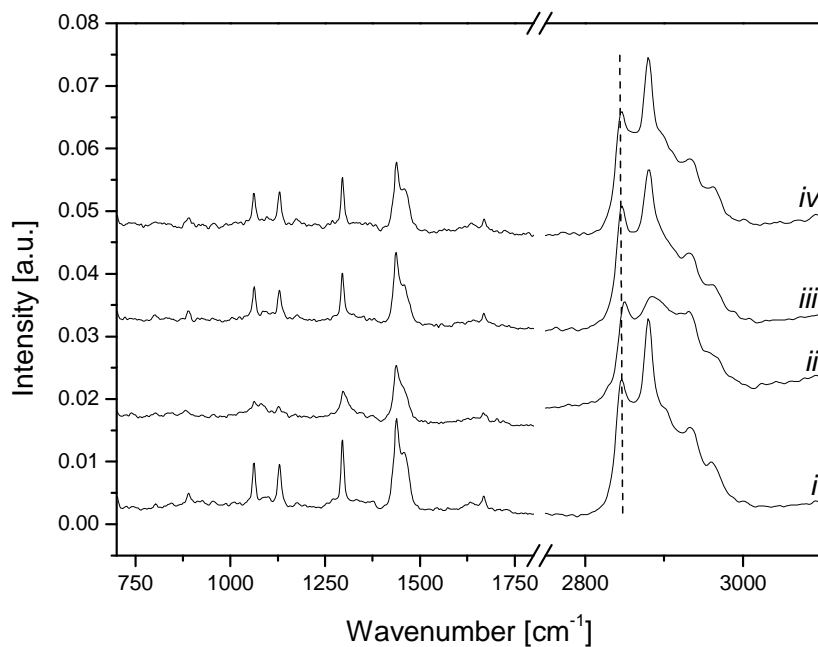


Fig. B1 Raman spectra of the stratum corneum lipid MLVs (20% of lipids in Tris buffer pH = 9) consisting of 55% (in weight) Cer[AP], 25% cholesterol, 15% palmitic acid and 5% cholesterol sulphate measured at [*i*] 32 °C before heating; [*ii*] 85 °C; [*iii*] 32 °C after heating; [*iv*] 32 °C 2 weeks after heating.

Table B1 Band assignment of the stratum corneum lipid MLVs (20% of lipids in Tris buffer pH = 9) consisting of 55% (in weight) Cer[AP], 25% cholesterol, 15% palmitic acid and 5% cholesterol sulphate.

Band position [cm ⁻¹]			Band assignment
32 °C before heating	85 °C	32 °C after heating	
889 (middle weak)		889 (weak)	$\delta(\text{CH}_3)$ rocking, tt-chain end conformation
1062	1063 (weak)	1063	$\nu_{\text{as}}(\text{C-C})$, 3 or more trans conformations in sequence
	1080		$\nu(\text{C-C})$, disordered structure
1130	1127(weak)	1129	$\nu_{\text{s}}(\text{C-C})$, 3 or more trans conformation in sequence
1295	1297	1295	$\delta(\text{CH}_2)$ twisting
1439	1438	1437	$\delta(\text{CH}_2)$ scissoring
1458	1455	1459	(split into a doublet)
1668	1668	1668	$\nu(\text{C=O})$ (head group)
2846	2850	2847	$\nu_{\text{s}}(\text{CH}_2)$
2880	2884	2881	$\nu_{\text{as}}(\text{CH}_2)$

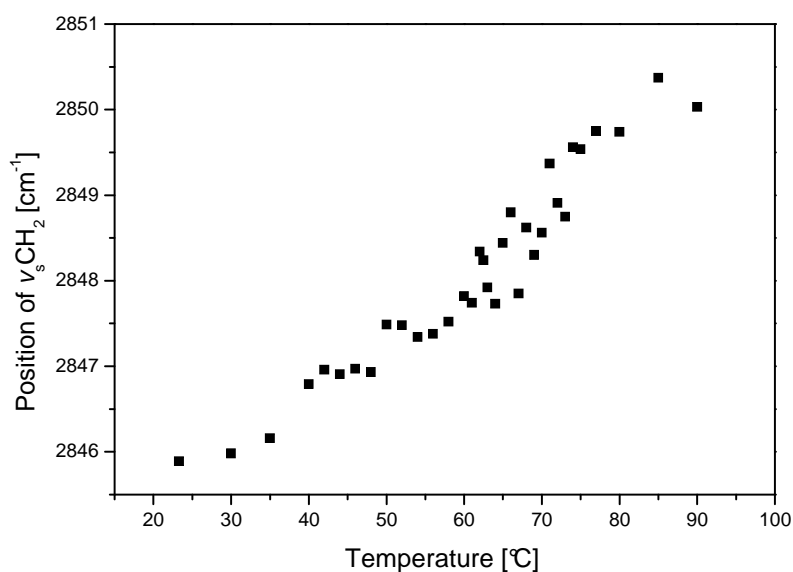


Fig. B2 Temperature dependence of the symmetrical stretching CH_2 mode of the stratum corneum lipid MLVs during the heating (20% of lipids in Tris buffer $\text{pH} = 9$; sample composition: 55% (in weight) Cer[AP], 25% cholesterol, 15% palmitic acid and 5% cholesterol sulphate).

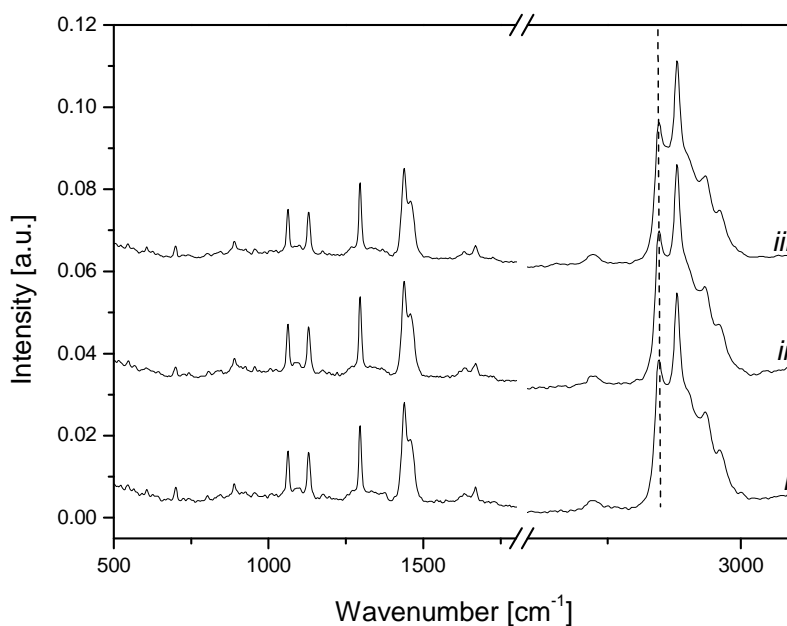


Fig. B3 Raman spectra of the stratum corneum lipid MLVs (20% of lipids in Tris or Bis/Tris buffers) consisting of 55% (in weight) Cer[AP], 25% cholesterol, 15% palmitic acid and 5% cholesterol sulphate measured at 32 °C and various pH levels: [i] $\text{pH} = 9$; [ii] $\text{pH} = 7.2$; [iii] $\text{pH} = 9$. The spectra are almost identical.

Appendix C

Thermotropic phase behaviour of 12G12

DIFFERENTIAL SCANNING CALORIMETRY

Method

DSC 7 differential scanning calorimeter (Perkin Elmer, Norwalk, USA)
Heating rate: 5 K min⁻¹

Values

1 endothermic peak – onset at 79.9°C

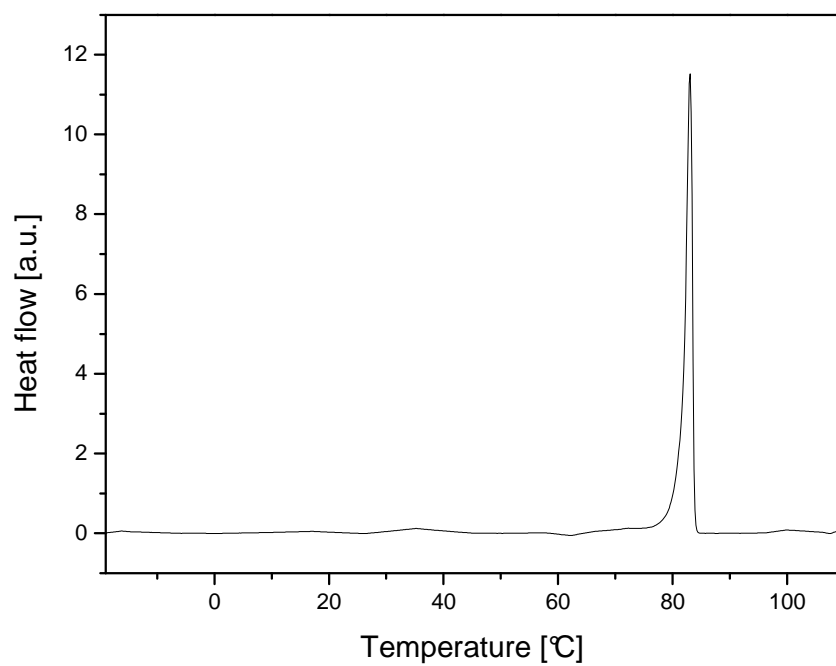


Fig. C1 The DSC curve of 12G12.

Thermotropic phase behaviour of 12G12

RAMAN SPECTROSCOPY

Method

Bruker FT-Raman spectrometer RFS 100/S (Bruker Optik, Ettlingen, Germany)

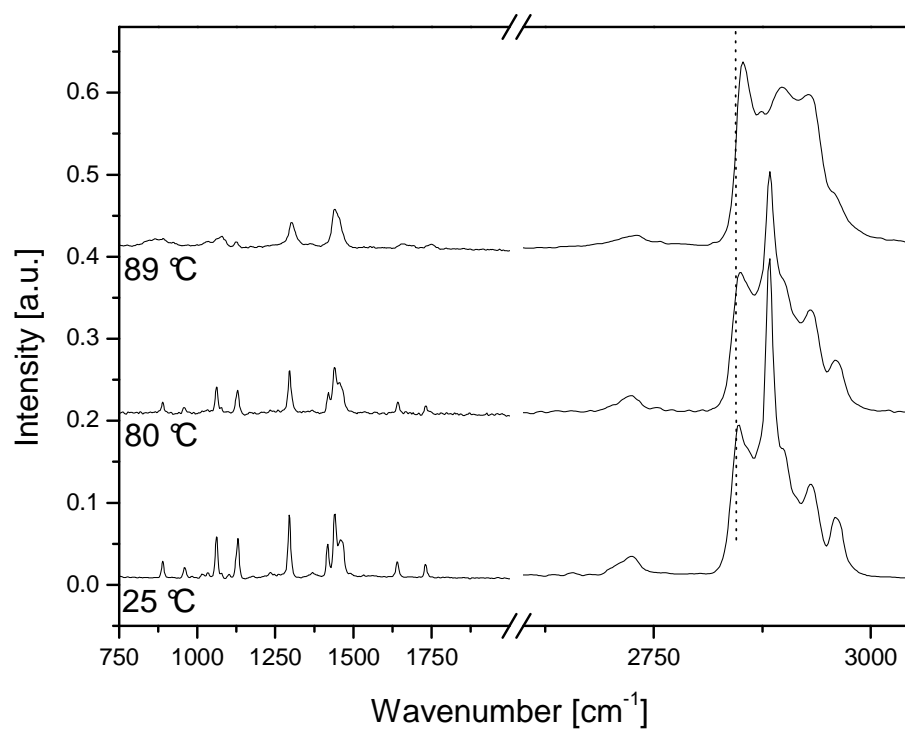
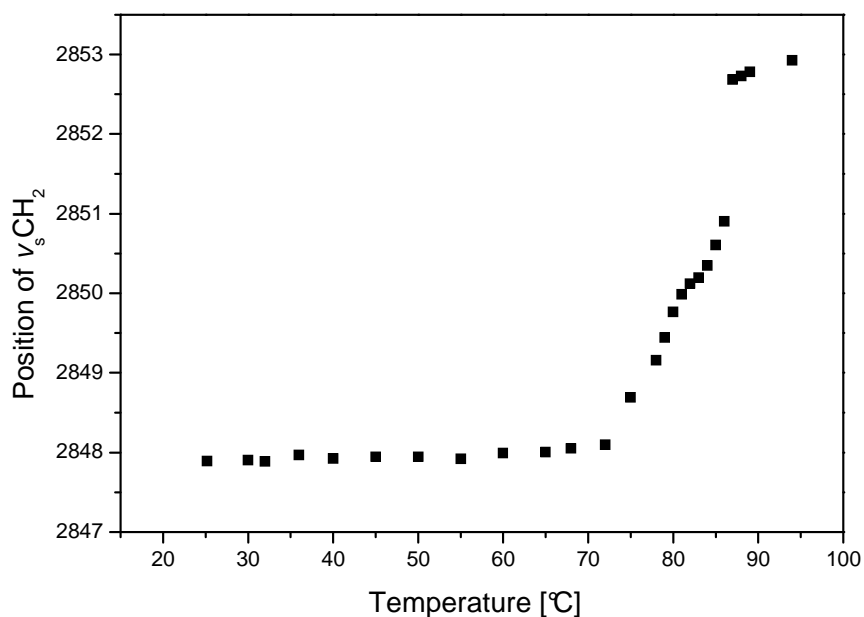


Fig. C2 Raman spectra of neat 12G12 measured at 25, 80, and 89 °C.

Table C1 Band assignment of 12G12.

Band position [cm ⁻¹]		Band assignment
20 °C	86 °C	
889		$\delta(\text{CH}_3)$ rocking, tt-chain end conformation
	873	$\delta(\text{CH}_3)$ rocking, tg or gt-chain end conformation
1062		$\nu_{\text{as}}(\text{C-C})$, 3 or more trans conformations in sequence
	1078	$\nu(\text{C-C})$, disordered structure
1130		$\nu_{\text{s}}(\text{C-C})$, 3 or more trans conformation in sequence
1295	1302	$\delta(\text{CH}_2)$ twisting
1417		$\delta(\text{CH}_2)$ scissoring, factor group splitting
1440	1440	
1458		
1640	1663	$\nu_{\text{C=O}}$ of the amid structure
1731	1747	$\nu_{\text{C=O}}$ of the ester structure
2848	2853	$\nu_{\text{s}}(\text{CH}_2)$
2883	2897	$\nu_{\text{as}}(\text{CH}_2)$
2931		Fermiresonanz und overtones of (CH_2) -scissoring modes
2959		$\nu_{\text{a}}(\text{CH}_3)$

**Fig. C3** Temperature dependence of the symmetrical stretching CH_2 mode of 12G12 during heating.

ACKNOWLEDGEMENTS

I would like to thank all people who contributed to this work, in particular to:

- **Prof. Dr. Reinhard Neubert** for the opportunity to participate in such an interesting research topic as well as for his interest and attentive support in the elaboration of this thesis.
- **Prof. Dr. Siegfried Wartewig** for many fruitful discussions and consultations of theoretical backgrounds of the thesis.
- **Dr. Mikhail Kiselev** for the opportunity to take part in his beam-times at various institutes, for the calculations of the neutron scattering length density profiles, and for his assistance in the measurements, the data treatment and evaluation.
- **Dr. Vasil Garamus** (GKSS, Geesthacht), **Dr. Sergio Funari** (DESY, Hamburg), **Dr. Pierre Leseur** (LURE, Orsay), **Dr. Claudie Bourgaux** (LURE, Orsay), **Dr. Thomas Hauß** (HMI, Berlin), and **Dr. Laszlo Almasy** (KFKI, Budapest), who are responsible for the instruments where the measurements were carried out, for the kind welcome at their institutes and for their help with the technical part of the measurements and the data treatment.
- **Dr. Christoph Wagner** for his assistance with the X-ray pre-measurements.
- **Dr. Karel Palát** for the molar volumes calculations.
- **Mrs. Heike Rudolf** and **Mrs. Kerstin Schwarz** for the technical assistance with the Raman and DSC measurements, respectively.
- **Dr. Melkamu Getie** for language consulting.
- **Dr. Hany Farwanah** and **Ms. Karen Schirmig** for their kind assistance with the HP TLC and DLS analysis, respectively.
- **Dr. Kateřina Vávrová** and **Dr. Petra Fechner** for fruitful discussions and their friendly support.
- All the colleagues at the Institute for Pharmaceutical Technology and Biopharmacy at the Martin-Luther-University Halle-Wittenberg for the friendly atmosphere in their team.
- DESY, Hamburg; HMI, Berlin; LURE, Orsay; KFKI, Budapest and GKSS, Geesthacht for the accommodation and travel reimbursements.
- Cosmoferm/Degussa and Lipoid for the donated ceramides and phospholipids, respectively.
- The DAAD scholarship and the Anniversary Scholarship of the Federal State of Saxony-Anhalt for the financial assistance.
- My husband, my parents, my parents-in-law and my whole family for their support and patience throughout my study period.

CURRICULUM VITAE

Name: **Mgr. Jarmila Zbytovská**
Maiden name: Neumannová
Born: 17 September 1976, Prague, Czechoslovakia
Nationality: Czech Republic
Marital Status: Married

Education:

1983-1990 **Primary School Pod Marjánkou, Prague**
class focused on foreign languages (German, Russian)

1990-1995 **Jan Neruda Grammar School, Prague**
specialization: foreign languages (German, English)
special courses in chemistry, biology and physics

Sept 1995: student training in Düsseldorf (Germany), experience in a medical facility

1995-2000 **Faculty of Pharmacy, Charles University in Prague**
graduate studies

1999-2000 **Saarland University, Saarbrücken, Germany (Erasmus Scholarship)**
student residency, elaboration of the diploma thesis at the Dept. of Biopharmacy and Pharm. Technology at the Lab. of *Prof. C.-M. Lebr*

May 2000 diploma thesis defence
topic: *'Human Alveolar Cells as In Vitro Model for Pulmonal Application: Transport Studies of Model Compounds'* (written in German)

July 2000 graduation in the field of pharmacy at the Charles University, Prague and obtained degree Magister of Pharmacy (Mgr.)

Professional Experience:

since 2005 **Faculty of Pharmacy, Charles University in Prague**
Research and teaching assistant at the Department of Pharmaceutical Technology

2001-2004 **Martin-Luther-University Halle-Wittenberg, Germany**
PhD research and teaching at the Dept. of Pharm. Technology and Biopharmacy, under the leadership of *Prof. R. H. H. Neubert*.

2000-2001 **Faculty of Pharmacy, Charles University in Prague**
PhD studies at the Dept. of Pharm. Technology under the leadership of *Associated Prof. P. Doležal*

PUBLICATION LIST (to May 2006)**Research Articles:**

1. Hrabálek A, Doležal P, Vávrová K, Zbytovská J, Holas T, Klimentová J, Novotný J., 2006. Synthesis and enhancing effect of Transkarbam 12 on the transdermal delivery of theophylline, clotrimazole, flobufen, and griseofulvin. . Pharm. Res. 23, 912-919.
2. Holas T, Zbytovská J, Vávrová K, Berka P, Mádlová M, Klimentová J, Hrabálek A, 2006. Thermotropic phase behavior of long-chain alkylammonium-alkylcarbamates. Thermochim. Acta 441, 116-123.
3. Zbytovská J, Kiselev MA, Funari SS, Garamus VM, Wartewig S, Neubert R, 2005. Influence of phytosphingosine-type ceramides on the structure of DMPC membrane. Chem. Phys. Lipids 138 (1-2), 69-80.
4. Kiselev MA, Ryabova NY, Balagurov AM, Dante S, Hauss T, Zbytovská J, Wartewig S, Neubert RHH, 2005. New insights into the structure and hydration of a stratum corneum lipid model membrane by neutron diffraction. Eur. Biophys. J. 34, 1030-1040.
5. Kiselev MA, Zbytovská J, Matveev D, Wartewig S, Gapienko I.V., Perez J, Lesieur P, Hoel A, Neubert R, 2005. Influence of trehalose on the structure of unilamellar DMPC vesicles. Colloids and Surfaces A 256 (1), 1-7.
6. Zbytovská J, Raudenkolb S, Wartewig S, Hübner W, Rettig W, Pissis P, Hrabálek A, Doležal P, Neubert R, 2004. Phase behaviour of Transkarbam 12. Chem. Phys. Lipids 129, 97-109.
7. Vávrová K, Hrabálek A, Doležal P, Holas T, Zbytovská J, 2003. L-Serine and glycine based ceramide analogues as transdermal permeation enhancers: polar head size and hydrogen bonding. Bioorg. Med. Chem. Lett. 13 (14), 2351-2353.
8. Vávrová K, Hrabálek A, Doležal P, Šámalová L, Palát K, Zbytovská J, Holas T, Klimentová J, 2003. Synthetic ceramide analogues as skin permeation enhancers: structure – activity relationships. Bioorg. Med. Chem., 11 (24), 5381-5390.
9. Vávrová K, Zbytovská J, Holas T, Klimentová J, Hrabálek A, Doležal P, 2003. Novel ceramide analogue based on L-serine is effective for skin barrier repair in vitro. J. Invest. Dermatol. 121 (5), 1261.

Reviews:

1. Vávrová K, Zbytovská J, Hrabálek A, 2005. Amphiphilic transdermal permeation enhancers: Structure-activity relationships. Curr. Med. Chem., 12 (19), 2273-2291.

Important abstracts and research reports:

Zbytovská J, Kiselev MA, Hauss T, Garamus VM, Wartewig S, Neubert R: Neutron scattering techniques in characterizing stratum corneum lipid model membranes. *Pespectives in Percutaneous Penetration* Vol. 10a, 2006 Edited by Brain, KR and Walters KA, 104.

Zbytovská J, Funari SS, Neubert R, Rube A, Wartewig S, Kiselev MA: Small-Angle X-ray diffraction studies on stratum corneum model lipid membranes. *Annual HASYLAB Report*, 2004.

Zbytovská J, Garamus V, Neubert R, Wartewig S, Kiselev MA: Influence of ceramides on the DMPC membrane structure studied via small angle neutron scattering. *GKSS/GeNF Experimental Report*, 2004.

Zbytovská J, Garamus V, Neubert R, Wartewig S, Kiselev MA: Influence of cholesterol on the structure of SC model lipid membrane studied via small angle neutron scattering. *GKSS/GeNF Experimental Report*, 2004.

Neumannová (Zbytovská) J, Wartewig S, Hrabálek A, Huebner W, Rettig W, Doležal P and Neubert RHH: Studies of interactions between skin permeation enhancer transkarbam 12 and two model lipids. *Pespectives in Percutaneous Penetration* Vol. 8a, 2004 Edited by Brain, KR and Walters KA.

Neumannová (Zbytovská) J, Wartewig S, Neubert R, Hrabálek A, Doležal P: Phase behaviour of newly synthesised permeation enhancer. *Proceed. 1st Int. World Meeting on Pharm., Biopharm. and Pharm. Technol.* Florence, 4, 1169-1170 (2002).

Neumannová (Zbytovská) J, Fuchs S, Schäfer U, Lehr CM, 2000. Human Alveolar Monolayers in vitro: Transport Studies of Model Compounds. *Arch. Pharm. Pharm. Med. Chem.* 333, Supp. 1, 23.

DECLARATION

I, the undersigned, declare that this dissertation is solely my own work and no part of it has been submitted to other Universities or Higher Learning Institutions. In addition, all sources of materials used in this dissertation have been duly acknowledged.

Halle/Saale

Jarmila Zbytovská